HALLOYSITE NANOTUBE COATINGS FOR SELECTIN-MEDIATED CAPTURE OF RARE CELLS FROM PERIPHERAL BLOOD

A Dissertation

Presented to the Faculty of the Graduate School

of Cornell University

In Partial Fulfillment of the Requirements for the Degree of

Doctor of Philosophy

by

Andrew David Hughes

February 2016

HALLOYSITE NANOTUBE COATINGS FOR SELECTIN-MEDIATED CAPTURE OF RARE CELLS FROM PERIPHERAL BLOOD

Andrew David Hughes, Ph. D.

Cornell University 2016

Recent years have seen the emergence of a number of devices designed to separate specific cells of interest from background cells and particulate. Applications range from the isolation of stem and bone marrow cells from bone marrow aspirates to the detection of abnormal and malignant cells from spinal and pleural fluids. Of particular interest have been microfluidic devices, due to their ability to process relatively large volumes on a small surface area, and the favorable fluidics within. Attempts at improving the interaction between flowing cells and the adhesive wall have been carried out with the incorporation of wall features that create microvortices and with the introduction of obstacles that span the flow regime. Significant drawbacks of these technologies include the need for complex and sophisticated microfabrication techniques and difficulties removing captured. The focus of this research is to investigate the utility of cell capture in a relatively simple microfluidic device that is enhanced by the modulation of surface roughness through the addition of a coating of naturally-occurring halloysite nanotubes. This nanotube coating is characterized thoroughly and shown to create significant advantages in the capture of viable target cells, and its utility proven in the ability to capture primary circulating tumor cells from peripheral blood samples of cancer patients.

Comparison to today's gold standard for circulating tumor cells enumeration demonstrates the advantages offered by this device. Finally, it is established that enhancements in the purity of the captured cell population is achieved due to the remarkable activity of the halloysite nanotube coating in reducing the capture of and preventing the spreading of contaminating leukocytes within the device.

BIOGRAPHICAL SKETCH

Andrew Hughes was born on the 3rd of September, 1986, in the city of Livingston, New Jersey to Peter and Susan Hughes. He has two younger sisters, Claire and Jackie. He attended Glen Ridge High School and then went on to Lehigh University in Bethlehem, Pennsylvania and achieved a Bachelor of Science degree in Chemical Engineering, completed in the summer of 2008. From there the author pursued a Master's of Engineering degree in Biomedical Engineering at Cornell University, which he achieved in the fall of 2009. Having completed the Master's degree the author worked in the laboratory of Professor Michael R. King and the following year matriculated in the PhD program at Cornell University where he continued to work under the mentorship and guidance of Professor King. He was awarded a National Science Foundation Graduate Research Fellowship in 2010, which was completed in 2014. During the course of this fellowship he published three primary research papers and two review papers as first author. Subsequently, in the summer of 2014 Andrew began medical school at the University of Pittsburgh School of Medicine, at which he was accepted into the Physician Scientist Training Program. He was awarded a pre-doctoral scholarship by the American Society of Transplantation for research conducted in the laboratory of Dr. Fadi Lakkis in the summer of 2015.

PUBLICATIONS & PATENTS

Hughes, A.D. and King, M.R. (2010). "Use of naturally occurring halloysite nanotubes for enhanced capture of flowing cells," Langmuir 26:12155-64.

Hughes, A.D. and King, M.R. (2012). "Nanobiotechnology for the capture and manipulation of circulating tumor cells," Wiley Interdisciplinary Reviews in Nanomedicine and Nanobiotechnology 4:291-309.

Hughes, A.D., Mattison, J., Western, L.T., Powderly, J.D., Greene, B.T., King, M.R. (2012). "Microtube device for selectin-mediated capture of viable circulating tumor cells from blood," Clinical Chemistry 58:846-53.

Mitchell, M.J., Chen, C.S., Ponmudi, V., Hughes, A.D., King, M.R. (2012). "E-selectin liposomal and nanotube-targeted delivery of doxorubicin to circulating tumor cells," Journal of Controlled Release 160(3):609-17.

Hughes, A.D., Mattison, J., Powderly, J.D., Greene, B.T., King, M.R. (2012). "Rapid isolation of viable circulating tumor cells from patient samples," Journal of Visualized Experiments Jun 15;(64):e4248

Greene, B.T.*, Hughes, A.D.*, King, M.R. (2012). "Circulating tumor cells: the substrate of personalized medicine?" Frontiers in Oncology 2:69.

King, M.R. and Hughes, A.D. "Fluid Flow Device Containing Nanotubes and Method for Cell Trafficking Using Same." U.S. Patent Application No. 13/500,476, filed April 5, 2012.

Geng, Y., Chandrasekaran, S., Hsu, J.W., Gidwani, M., Hughes, A.D., King, M.R. "Phenotypic Switch in Blood: Effects of Pro-Inflammatory Cytokines on Breast Cancer Cell Aggregation and Adhesion," PLoS ONE 8(1): e54959.

Hughes, A.D.*, Marshall, J.R.*, Keller, E., Powderly, J.D., Greene, B.T., King, M.R. (2014). "Differential drug responses of circulating tumor cells within patient blood," Cancer Letters 352(1):28-35.

Hedges, E.A.*, Hughes, A.D.*, Liesveld, J.L., King, M.R. (2014). "Modulation of seletin-mediated adhesion of flowing lymphoma and bone marrow cells by immobilized SDF-1," International Journal of Molecular Sciences 15,15061-72.

To my parents - Susan and Peter Hughes

ACKNOWLEDGMENTS

First and foremost I would like to thank my advisor Professor Michael R. King, not only for giving me the opportunity to explore this exciting work, but also for his guidance, patience, support, and education. Professor King has been a mentor in every sense of the word and an invaluable role model at the formative phase of my career. He always had his eye on the big picture, could find a solution to any problem, and remained calm and collected at all times. I will strive to do the same. The King Laboratory is an ideal place to work, with an environment that is both professional and nurturing and filled with intelligent, driven, and collaborative people.

I would also like to thank my committee members, Professor Susan Daniel and Professor David Nanus for not only taking the time to be my minor advisors but also for their guidance and advice. They have pushed me to expand my knowledge and consideration, and I am grateful to them for helping me grow.

Every member of the King Lab has been a pleasure to work with. I would like to acknowledge the wonderful King Lab members, all of whom helped and challenged me along the way: Jocelyn Marshall, Dr. Kuldeepsinh Rana, Dr. Jiahe Li, Jeffrey Mattison, Carissa Ball, Dr. Siddarth Chandrasekaran, Dr. WeiWei Wang, Dr. Michael Mitchell, Dr. Yue Geng, Thong Cao, Kevin Anderson, Dr. Hsu Jong-Wei, Anne Rocheleau, Nerymar Ortiz-Otero, Elizabeth Hedges, James Messing, and Carlos Castellanos.

I would also like to thank the Cornell Nanobiotechnology Center and Cornell Nanofabrication Facility, and in particular Dr. Teresa Porri and John Grazul for their teaching and patience. Finally, I would like to thank Dr. Bryan Greene and Dr. John

Powderly of BioCytics, Inc. and the Carolina BioOncology Institute for their excellent collaboration, as well as their patients for donating their blood samples and making so much of this work possible.

TABLE OF CONTENTS

LIST OF FIGURES

LIST OF TABLES

CHAPTER 1 – BACKGROUND & INTRODUCTION:

Nanobiotechnology for the capture and manipulation of circulating tumor cells

This section is adapted from the following publication: AD Hughes and MR King, Nanobiotechnology for the capture and manipulation of circulating tumor cells. *WIRES Nanomedicine and Nanobiotechnology*, **2011**, 4(3):291-309.

Cancer is the second leading cause of death in the developed world. More specifically, the dissemination of cancer cells and subsequent seeding of secondary tumors in distant organs is the second leading cause of death, in that approximately 90% of cancer deaths are due to metastasis (*1*). Studies have reported greater than one million cancer cells can detach from the primary tumor per gram of tumor per day (*2, 3*) in a temporally heterogeneous manner (*4*), and invade surrounding tissue in search of a distant site which will support growth of a secondary tumor. The majority of dispersed cancer cells do not survive, however those that do clearly pose the most significant threat to the host organism (*5*). A large body of experimental evidence makes the case that the primary route for metastatic dissemination is the circulatory system, wherein cancer cells travel throughout the body as circulating tumor cells (CTC) (*6, 7*). Indeed, studies utilizing in vivo video microscopy have visualized cancer cell intravasation and describe it as a robust step in the metastasis process (*8, 9*). While it is true that lymphatic invasion occurs and is a criterion for poor diagnosis, there are generally no direct lymphatic routes to distant organs where metastases propagate. Therefore cancer cells must subsequently enter the bloodstream before seeding a secondary tumor (*6*). Studies have found that unique adhesive properties of the luminal surface of particular organ vasculature are sufficient to explain the habitual homing of certain cancers to specific secondary tissues (*6, 10-13*). Thus, it is evident that the presence of CTC in the circulatory system is a

necessary phenomenon in cancer progression, and researchers and physicians have recently begun to recognize the relevance and use of CTC for diagnosis and treatment (*14*).

Detection of CTC in the peripheral blood of patients has led to the realization that the quantity of CTC corresponds closely to disease severity, and CTC count is currently used as a prognostic tool and to track treatment efficacy (*15-21*). Studies have shown that the concentration of CTC in the blood of cancer patients is on the order of one in a billion healthy blood cells (*16*), or one in a million leukocytes (*17, 22*). Considering the prevalence of CTC, the detection or isolation technique must be able to analyze large sample volumes and achieve high sensitivities and purities. Many technologies have emerged in recent years to detect CTC, all with their inherent advantages and disadvantages. Consequently it is imperative to note that the current state of knowledge of CTC is still evolving, as it is dependent on the technologies available to identify them. It is increasingly apparent that micro- and nanobiotechnology are the most likely routes to the ideal CTC capture device due to the ability to recognize and exploit unique molecular-level features that distinguish CTC from normal cells, and also due to the unsurpassed degree of control that is afforded.

Devices for utilizing CTC to assist the clinical treatment of cancer patients can be categorized into three separate classes, based on the intended purpose of the technology. The first class consists of devices that are primarily concerned with the quantification of CTC. This class contains the inceptive technologies as well as those that are currently used in the clinic, and are meant to be used primarily as diagnostic tools (Figure 1.1a). A second class focuses on further characterization of CTC beyond enumeration. As easily

accessible samples of individual patients' malignant tissue, isolated CTC can be studied in vitro to detail the characteristics of each particular cancer and rapidly identify the optimal course of therapy. Thus, this class of technologies aims to isolate or detect CTC in such a way that cell viability is not compromised so that CTC can be subsequently utilized to improve therapy strategies (Figure 1.1a,b). The third class of devices addresses the objective of manipulating CTC directly in vivo as a therapy (Figure 1.1c).

1.1 Circulating Tumor Cell Detection Assays

Researchers have theorized that rare primary tumor cells are programmed early on to be able to metastasize (*23-25*), indeed studies have shown that metastatic dissemination of cancer cells into the bloodstream can occur very early in the disease lifetime, before symptoms present or the primary tumor can be detected by conventional methods (*26*). Consequently, many groups have endeavored to create technologies for detecting and enumerating CTC from patient blood samples.

The current gold standard is the CellSearch system (Veridex, Raritan, NJ). CellSearch is currently the only FDA-approved device for CTC detection (*21*). In practice, patient blood samples are first processed via Ficoll density gradient centrifugation to separate nucleated cells, including CTC and leukocytes (the so-called "buffy coat"), from the remainder of blood components. Immunomagnetic precipitation is then performed using magnetic nanoparticles functionalized with antibodies specific to epithelial cell adhesion molecule (EpCAM) (*17*). Nanoparticle-bound cells are then separated in a magnetic field. To make detection more specific, isolated cells are subsequently permeabilized and stained for epithelial markers such as cytokeratin, as well

as for CD45 to exclude contaminating leukocytes. CellSearch has been shown to be sensitive down to 1 CTC per 0.5 mL blood (*4*), and has successfully been used to predict patient survival following treatment in a multicenter study (*27*). The CellSearch system, along with many of the alternative devices described below, relies on epithelial markers and therein lies an inherent limitation in that studies have shown a lack of EpCAM expression in approximately 30% of cancer cells (*28*). In addition, the epithelial to mesenchymal transition (EMT) phenotype switch that occurs in many metastatic cells is known to coincide with the loss of epithelial markers such as cytokeratins (*29, 30*).

Arguably the most commonly used methods for detecting CTC involve reverse transcriptase polymerase chain reaction (RT-PCR) techniques to recognize and amplify messenger RNA (mRNA) for individual genes linked to malignant cells. Trials have been conducted to detect CTC based on a variety of cancer-specific genes, such as epithelial growth factor receptor 2 (EGFR), carcinoembryonic antigen (CEA), cytokeratin 19 and 20, human epithelial growth factor receptor (HER-2), mucin-1 (MUC-1), and mammaglobin (h-MAM), to name a few. While there have been several tumor-specific genes identified, not one has been found to be expressed in 100% of CTC (*31, 32*). RT-PCR methods provide high sensitivities, routinely down to 1 CTC per mL (*4*), however the increase in sensitivity comes at the cost of a few drawbacks. First, CTC are necessarily destroyed in the process of harvesting the mRNA, making it difficult to enumerate and impossible to study live CTC. Second, the level of sensitivity afforded by RT-PCR techniques requires rigorous negative controls to avoid false-positive detection (*4*). Finally, low levels of epithelial marker gene-expressing cells have been reported in the blood of healthy individuals (*33, 34*). To address the challenge of false-positive

detection researchers have started using quantitative RT-PCR (qRT-PCR), which allows for thresholding of outputs using negative controls of healthy blood cells (*32*). A high-throughput method has been developed to attempt to eliminate the challenge of expression heterogeneity within cancer cell populations whereby four mRNA markers are detected simultaneously by qRT-PCR and results are determined using an alkaline phosphatase colorimetric membrane-array. To screen patients for gastric cancer researchers have concurrently screened for human telomerase reverse transcriptase (hTERT), cytokeratin 19 (CK-19), CEA, and MUC-1 and report sensitivities of 5 CTC per mL, with a specificity of 91.3% (*35*).

The AdnaTest BreastCancerSelect system (AdnaGen, Lagenhagen, Germany) is a CTC detection system that utilizes semiquantitative RT-PCR along with CTC isolation using immunomagnetic nanoparticles. The AdnaTest system works by first treating patient blood samples with magnetic nanoparticles functionalized with a mixture of three separate antibodies to different epithelial cell surface markers (the specific markers are proprietary), and then isolated CTC are lysed and PCR is performed for HER-2, MUC-1, and GA733-2 (*36*). The makers of the AdnaTest report that they are able to achieve greater sensitivity than the CellSearch system (*37*). A recent study has been performed comparing simultaneous RT-PCR of CK-19 and h-MAM with CellSearch and AdnaTest using blood samples from 76 metastatic breast cancer patients, and report a notable amount of discordance between the three techniques (*38*). While the authors report that the RT-PCR technique detects significantly more CTC than CellSearch or AdnaTest, the number of CTC detected with AdnaTest was much lower than what has been reported by

other studies, highlighting the need for rigorous standardization requirements between laboratories as well as a large-scale multicenter study.

One exciting new technique is the use of green fluorescent protein-expressing attenuated adenovirus (GFP-AAV, designated OBP-401) to infect CTC and make them fluoresce. CTC-specificity is achieved by making AAV replication only possible in the presence of telomerase. As telomerase activity is required for AAV replication, only viable CTC will be able to support AAV replication and become fluorescent (*39*). To perform this assay, patient peripheral blood samples are drawn and red blood cell lysis is performed. Following centrifugation, OBP-401 is introduced into the cell pellet containing leukocytes and rare CTC and incubated for 24 h. Finally, the entire cell sample is placed on a slide and scanned by automated fluorescence microscopy to detect fluorescent CTC. As telomerase activity has been identified as a relevant marker of cancer cells (*40-42*), this is an attractive technology because it does not rely on epithelial markers. However, one challenge of this technique is that modest telomerase activity has been reported in hematopoietic stem and progenitor cells as well as in activated lymphocytes (*43*), both of which can be found in peripheral blood. This could therefore lead to false-positive detection.

An interesting technology was recently developed for the detection of single CTC in patient blood samples using antibody-functionalized single-walled carbon nanotube (SWCNT) field effect transistors (*44*). The device works based on the change in electrical conduction through SWCNT from the stress imposed by an antigen binding to an SWCNT-bound antibody. 10-20 nm diameter SWCNT are secured between electrodes and then functionalized with antibodies specific to insulin-like growth factor 1 receptor

(IGF1R) or HER-2 to detect breast cancer cells (*45*). The authors demonstrate the extremely high sensitivity of the device and speculate on the ability to create arrays of SWCNT transistors functionalized with a range of antibodies specific to different cell markers, however in the current state the device is only able to detect the presence of CTC and significant modifications are necessary to be able to enumerate CTC.

Another technique for detecting CTC is the EPISPOT (for epithelial immunospot) assay. EPISPOT is performed by isolating the buffy coat of a blood sample and then performing a CD45 negative selection treatment using anti-CD45 magnetic nanoparticles to remove leukocytes. Residual CD45- cells are incubated for 24 to 48 h and then the media is analyzed for secreted factors using an enzyme-linked immunosorbent assay (ELISA) technique. CTC are then enumerated based on the number of colored spots, and the type of secreted protein can be identified by the color of the spot (*46*). In a proof of concept study, one MCF7 breast cancer cell was detected in 5 mL blood based on its secretion of cathepsin D and MUC-1 (*47*). An advantage of this assay is that CTC detection is not dependent on a surface marker such as EpCAM, which may introduce a bias and result in false-negative results. In addition, only viable cells are detected because only viable cells will produce and secrete protein (*32*), however the requirement for a cancer-specific secreted marker protein constrains its applicability. Additionally, the amount of sample pretreatment required poses a risk of CTC loss, and since CTC can be extremely rare this could result in false-negative readouts.

Laser scanning cytometry (Compucyte, Cambridge, MA) is a slide-based procedure, essentially flow cytometry on an immobilized sample, that has been developed for CTC detection (*48, 49*). Cell samples are pretreated via Ficoll density

centrifugation or red blood cell lysis and then deposited on a microscope slide were they can be fluorescently stained for a number of different markers, such as EpCAM or human epithelial antigen (HEA), as well as CD45 to exclude leukocytes. A collimated laser beam is then rapidly scanned over the slide to analyze each cell for fluorescence (*50*). Laser scanning cytometry (LSC) has been shown to be sensitive to one positive event in 10^5 negative events (*51*), and has demonstrated good correlation between CTC count and therapeutic success in a recent clinical study (*52*). A strong advantage of LSC is that x,y coordinates of each event are recorded along with the fluorescent emission data, allowing the user to return to specific events and perform additional analysis, such as verify positive events and eliminate false-positives (*49, 50*). One notable drawback to LSC is the sample size: only 100,000 cells can be analyzed per sample (*48*). A similar technology, termed fiber-optic array scanning technology (FAST), is able to scan and analyze up to $3x10^5$ fluorescently labeled cells per second using laser-printing optical technology. Automated digital microscopy (ADM) is a fluorescence microscopy system in which a computed scans an entire sample in the X, Y direction while automatically focusing, and records the fluorescence data of each event it detects. ADM has been shown previously to accomplish high sensitivity and accuracy (*53*). The FAST system has reported a sensitivity of >90% of the 500-fold slower ADM while maintaining a specificity of one false positive in approximately 70,000 negative events for CTC stained with a pan-cytokeratin antibody (*54-56*).

In an effort to avoid using antibodies against a single epithelial cell surface marker to identify cancer cells, one group has adapted the systematic evolution of ligands for exponential enrichment (SELEX) process to whole cells (cell-SELEX) to screen large

aptamer libraries for a panel of target cell-specific aptamers. Aptamers are short DNA or RNA probes that exhibit high specificity with lower affinities for their molecular targets and a relatively small signal when fluorescently labeled. To capitalize on the specificity of cell-specific aptamer panels and overcome their binding and signal limitations, researchers have constructed 12 nm x 56 nm gold-silver nanorods that are decorated with up to 80 fluorescently labeled aptamers. The result is a 26-fold greater affinity for target cells together with a 300-fold greater fluorescent signal compared to cells labeled with soluble aptamers (*57*). This technology has potential for a broad range of applications as many CTC-detection devices rely on fluorescent staining of target cell surfaces for identification or verification.

1.2 Detection + Manipulation Techniques

The utility of devices for enumerating CTC has been demonstrated to a significant extent to track disease progression and predict therapeutic outcome. However, the technologies mentioned above do not allow for subsequent employment of CTC to advance cancer research and therapy development due to the destruction of the CTC in the detection procedure.

1.2.1 Function-Based Methods

CTC extravasation is necessarily preceded by CTC arrest in a vessel. This can occur either by size restriction in small capillaries or molecular adhesion to the vessel surface. The latter is more likely due to the observation that CTC arrest in vessels that are larger than the CTC diameter (*6*). There is substantial experimental evidence that make the case that CTC adhere to endothelium in a manner analogous to leukocyte adhesion in

the inflammatory cascade; specifically, CTC may use selectin binding as the initial step in diapedesis (*11, 12, 58-63*). As such, we have performed a number of studies that have focused on capturing CTC on selectin molecules to mimic physiological conditions, with the intention of capturing the CTC population that is able to take the first step in extravasation, comprising the relevant population for detection and study. Cells captured on selectin-coated surfaces can be gently removed by introducing ethylenediaminetetraacetic acid (EDTA) to chelate the divalent cation Ca^{2+} which is required for the activation of selectin molecules. Thus captured cells remain viable and can be subsequently analyzed in the laboratory. Initial studies were performed in which the lumen of MicroRenathane (MRE) microtubes, with an inner diameter of 300 μm, were coated with P-selectin to capture the CD34+ population of hematopoietic stem and progenitor cells (HSPC) from the peripheral circulation of rats (*64*) and human bone marrow aspirates (*65, 66*). As CTC likewise adhere to selectin proteins, the application of this device for CTC capture is possible. Importantly, selectin-mediated adhesion of flowing cells is a physiological process and thus is not expected to impact viability. Furthermore, the success in capturing CD34+ HSPC suggests a potential application in selecting for and capturing rare primary cancer stem cells (*67, 68*).

The selectin-functionalized microtube device has been successfully used by our group to capture CTC from blood, and experiments describe a 50% capture efficiency in cancer cell spiking experiments when the microtube is additionally coated with antibodies specific to cancer cells to help retain captured cells in the device (Figure 1.2) (*69*). Subsequent work has been performed to alter the nanoscale properties of the inner surface of the device to augment capture. In one study, a monolayer nanoparticle coating

of colloidal silica (10-15 nm) was deposited on the inner surface of the device using either a thin layer of poly L-lysine or titanium (IV) butoxide as an adhesive and experiments showed an increase in P-selectin adsorption, and consequently as CTC were perfused through the device at physiological flow rates significantly more cells were captured (Figure 1.3). In addition, rolling velocity values were diminished, indicating that the strength of adhesion of captured cells was greater on the nanoparticle coating compared to control (*70*).

1.2.2 Non Function-Based Techniques

Several devices have been developed involving arrays of antibody-coated microposts for the capture of viable CTC. The "CTC-chip" is a constructed using deep reactive ion etching (DRIE) in silicon to create 78,000 posts in a staggered arrangement with 50 μm gaps between posts (*71*). The microposts are coated with antibodies against EpCAM, and blood samples are pumped through at a flow rate of 1 mL/h to maintain a shear stress below 0.4 dyn/cm^2. Such a low shear stress is necessary to provide enough time for the relatively slow antibody bonds to form, and CTC capture efficiency drops below 20% at 3 mL/h (*71*). Such low flow rates would seem to make the processing of patient samples to capture viable CTC for subsequent study appear somewhat unfeasible due to the amount of time required to process several mililiters. Nevertheless, the CTC-chip has demonstrated >60% capture efficiency in whole blood spiking experiments with model blood samples containing as few as 50 CTC per mL. Additionally, the CTC-chip was able to captured viable CTC from 115 out of 116 blood samples from patients suffering from a variety of metastatic carcinomas. CTC comprised ~50% of the captured

primary cells, and 98% of captured cells were viable based on inspection of membrane integrity by confocal microscopy (*71*). However, a notable limitation of the CTC-chip is equivalent to that of the CellSearch and other antibody-based systems, in that only portions of primary CTC populations express the surface makers that antibodies target, such as EpCAM, and the subpopulations that would be excluded by an antibody device may be those that are the most aggressively metastatic (*28-30*).

An updated version of the CTC-chip is a microfluidic chip consisting of a 50 μm-high channel with 45 μm-deep chevron-shaped grooves in the upper surface, termed the "Herringbone-Chip" (*72*). The Herringbone-Chip is designed to induce vortices in the fluid streamlines to break up the laminar flow profile and promote collisions between perfused cells and the antibody-coated walls. The Herringbone-chip demonstrates a capture efficiency of 92% at a flow rate of 1.2 mL/h in cancer cell spiking experiments, compared to 66% in the CTC-chip at 1.0 mL/h. In addition, experimental evidence suggests that flow rates as high as 4.8 mL/h can be utilized while achieving a capture efficiency of >40%. This represents a significant improvement over the CTC-chip. Another improvement over the CTC-chip micropost concept applies microfluidic modeling of the movement of cells around microposts. This mathematical model is used to maximize the collision rate of cancer cells with antibody-coated microposts while minimizing the collisions of healthy leukocytes with microposts, and works on the observation that CTC are often larger than leukocytes. This device has been labeled geometrically enhanced differential immunocapture (GEDI), is composed of 5000 posts in a 8 mm x 25 mm channel that is 100 μm high, and is functionalized with an antibody against prostate-specific membrane antigen (PSMA) (*73*). The GEDI device is operated

at 1mL/h and has attained 85% capture efficiency and 68% purity in blood spiking experiments. In processing blood samples of patients known to have metastatic cancer, CTC were detected in 18 out of 20 samples (*73*). An important feature of these antibody-functionalized fluidic devices is that introduction of the soluble antibody or ligand, or a commercially available protease such as trypsin, will release captured cells from the device without compromising viability.

A further advancement of a microfluidic platform for capture of CTC is the high throughput microsampling unit (HTMSU) device, which consists of high aspect ratio sinusoidal channels (35 μm x 150 μm) in poly(methyl methacrylate) (PMMA) that are coated with anti-EpCAM antibodies. 51 channels were cast in parallel to create a device that is able to process blood samples at a rate of approximately 2 mL per hour. Spiking experiments reported excellent capture efficiency (>97%) due to the channel dimensions. An intriguing feature of this device is that a conductivity sensor is integrated at the output to enumerate unlabeled CTC after they are released by trypsin and pumped out of the chip. The conductivity sensor is able to distinguish between CTC and contaminating leukocytes and erythrocytes based on size, a feature that allows for the prevention of false-positive detection (*74*). A more recent study by the same group utilized anti-PSMA instead of anti-EpCAM antibodies to detect LNCaP prostate cancer cells spiked into whole blood and reported a capture efficiency of 90% (*75*).

A new approach to viable CTC capture endeavors to enhance interactions between an antibody-coated surface and a cell using substrates with nanoscale surface features to promote local topological interactions. This device is composed of a silicon nanopillar array coating with anti-EpCAM or antibodies. The nanopillars are 100 to 200

nm in diameter and lengths can be controllably varied between 1 and 20 μm depending on etching times. The rationale for this device lies in the extensive observations that substrate topography can influence cellular behavior, particularly cellular adhesion. Preliminary blood spiking experiments were performed in which stained MCF7 breast cancer cells or PC3 prostate cancer cells were suspended in blood samples which were then incubated over the device with 10 μm-long pillars for 45 min. Results indicate greater than 40% improvement in capture efficiency compared to CellSearch (*76*).

1.3 In Vivo CTC Manipulation Techniques

The observation that cancer cells are shed from primary tumors at rates that vary sporadically, or even in a discontinuous manner (*4*), means that extraction of a volume of blood from a cancer patient represents only a snapshot of the bigger picture of the disease. As described above, many studies have identified a correlation between CTC count and disease severity, indicating that these snapshots are often reliable, at least on the whole. However, continuous monitoring in vivo would be an improvement over discrete time points. A further motivation for continuous monitoring of the circulation is evident considering the prevalence of CTC: reports have identified as few as 1 CTC per 7.5 mL patient sample (*4*). Based on this estimate there is a low probably of capturing any CTC in a single blood sample of a few milliliters (*14*). A device that would allow for screening of the entire circulation would minimize the chance of CTC evading the device. One such device is an implantable microtube that, when incorporated into the circulatory system as a shunt, will continuously screen for CTC via selectin-mediated adhesion. Studies have been performed in which a vascular shunt device was functionalized with P-

selectin and anti-CD34 antibodies, and inserted into the vasculature of rat to successfully capture viable HSPC (*64*). In a subsequent study directed at CTC capture and depletion, a vascular shunt device designed for implantation was functionalized with E-selectin and tumor necrosis factor (TNF) related apoptosis-inducing ligand (TRAIL, also known as Apo2).(*77*) TRAIL is a protein that induces apoptosis in malignant cells via the caspase pathway (*78*), however systemic delivery to eliminate cancer cells is precluded by reports of apoptosis induction in healthy hepatocytes (*79*), keratinocytes (*80*), and brain cells (*81*). Thus a device that localizes TRAIL delivery to the peripheral bloodstream would provide limited side effects while specifically targeting CTC, reducing metastatic load. This device, once implanted, would first act as a functional screen for cells that have the ability to extravasate (via selectin adhesion) by inducing them to roll over E-selectin on the device surface and sample the surface as they would along the endothelium. On the device surface, immobilized TRAIL molecules induce apoptosis in rolling CTC (Figure 1.4), while rolling leukocytes (TRAIL-insensitive) pass out of the device unaltered. Experiments performed in a validation study achieve a 30% kill rate for CTC pumped through the device for 1 h at physiological flow rates, while no impact on the viability of identically-treated primary leukocytes was observed (Figure 1.4) (*77*). Studies manipulating the nanoscale topography of the device to achieve enhanced kill rates have been successfully carried out and are ongoing.

The implantable selectin-based vascular shunt has been utilized in a separate study to accomplish delivery of genetic therapeutics to rolling cells (*82*). In this technique, liposomes (150 nm diameter) were covalently coated with P-selectin and polyethylene glycol (PEG), with small interfering RNA (siRNA) encapsulated within.

Liposomes were then adsorbed onto the inner surface of a microfluidic device at high surface densities. Validation experiments showed efficient delivery of siRNA to greater than 90% of target HL60 leukemic cells, with approximately 70% reduction in target gene expression across the cell population (Figure 1.5) (*82*). We have previously shown that CTC can be preferentially induced to roll on P-selectin (*65*), making this an exciting device for direct treatment of CTC in vivo.

A novel technology that has been under recent development for noninvasive enumeration and elimination of CTC in circulation is photoacoustic flow cytometry (PAFC). One study was performed primarily for the detection and eradication of unlabeled melanoma CTC (*83*). Melanoma cells are unique in that they overexpress melanin, which forms endogenous melanin nanoparticles (30 to 50 nm in diameter) within the cell, and these melanin nanopaticles can be used as spectrally-specific markers for photoacoustic detection. In PAFC, incident photons from a laser are absorbed by the nanoparticles and converted into thermal energy. The heated nanoparticles expand and generate acoustic waves in the surrounding medium, and an ultrasonic transducer detects these acoustic waves. Depending on the laser intensity, it is possible to either detect or ablate flowing CTC. Using this technology, acoustic signals from melanoma CTC were detected as they flow in the blood vessel of a mouse. The authors describe this technology as sensitive to 1 CTC per mL and effective to depths of 4 mm into skin (*83*). This technique could be applied to CTC that aren't themselves spectrally-unique using gold plated carbon nanotubes, shown to be good contrast agents for photoacoustic and photothermal excitation by a diode laser (*84, 85*). Challenges may arise for this technique in that the gold plated carbon nanotubes have to be targeted specifically to CTC and

administered for the duration of the detection/eradication procedure. Furthermore, CTC shedding into the circulation is a chronic process, as evidenced by the experimental observation that photothermal CTC ablation in tumor-bearing mice for 1 h resulted in a reduction in CTC count that was only temporary as new CTC were shed into the bloodstream (*83*). It remains to be seen how this technology could be utilized for long-term treatment to prevent metastasis. Nevertheless, the noninvasive, direct eradication of CTC in vivo is an intriguing concept, warranting further development.

1.4 Conclusions from CTC capture technology

Since the first identification of circulating tumor cells in the bloodstream of a patient with metastatic cancer in 1869 (*86*) significant advances have been made in the characterization and utility of CTC. To date, the most important clinical application of CTC technology has been the real-time monitoring of CTC counts in patients undergoing treatment to track disease progress along with treatment efficacy and outcome prediction (*4, 27, 87*). This class of CTC technology, while undoubtedly useful and beneficial to the patient, serves a passive role in cancer therapeutics and may not realize the full potential of CTC. Patient blood samples have the potential to be used as liquid biopsies, both to develop treatment schemes on a patient-to-patient basis and to study the nature of cancer metastasis to identify better drug targets. The ideal detection system would be one that is singularly specific and sensitive, but does not preclude further study by compromising cell viability. However, the molecular target (or targets) to accomplish sufficient specificity have yet to be identified and will only come from a better understanding of the metastatic cascade. Steps have been taken in the right direction; observations into the

mechanisms used by CTC to transmigrate from the bloodstream to a secondary tissue have distinguished selectins as utilitarian molecules for identification and capture of those CTC that pose the greatest threat to metastasize. Direct manipulation of CTC in vivo is another compelling direction for CTC technology, representing a potential means to reduce metastatic load and even block metastasis while the primary tumor is addressed, as well as a means to overcome some of the greatest challenges in CTC detection: temporal heterogeneity of dissemination and sample size limitations for in vitro techniques. Ultimately, the concepts and technologies described in this review represent true potential advances in cancer therapy. There can be no question that the future of CTC detection and manipulation lies unquestionably in the application of micro- and nanotechnology to achieve acute control with atomic-level accuracy and sensitivity.

1.5 Halloysite nanotube coatings

Previous work by Han et al. explored the incorporation of nanoparticles onto the surface of the inner lumen of the MRE microtube in an attempt to enhance the capture of perfused cells (*70*). Silica oxide nanoparticles of diameter 10-15 μm were coated onto the inner lumen of the surface using a thin layer of organic poly-L-lysine or inorganic titanium(IV) butoxide as adhesives. The authors were able to show that up to 35% more P-selectin was adsorbed on the surface. Atomic force microscopy verified that the nanotube-coated surface was sufficiently rougher than the uncoated surface, correlating roughness with increased protein deposition. These results resulted in significantly improved capture of CD34+ HSPC as well as human leukemic cell line HL60 cells. Capture was enhanced both in terms of the number of cells captured, and in the strength

with which cells were adhered to the surface. Cell rolling velocity in shear flow is directly related to the number of selectin-mediated bonds with the surface (*88*), and as expected the same shear rates produced reduced rolling velocities of cells on the nanoroughened surfaces.

Halloysite nanotubes are naturally occurring alluminosilicate minerals that are uncharacteristically large for nanoparticles: typically 500 nm to 1.2 μm in length and 40 to 200 nm in diameter. Nanotubes coated with release-delaying polymer have been investigated as a novel platform for drug delivery, and have shown the ability to sustain tetracycline HCl release for up to six weeks *in vivo* (*89-91*). Dynamic light scattering of halloystie nanotubes has reported an average size of 796±7 nm and a net-negative charge of -35.0±0.5 mV (unpublished data). As such, the combination of relatively large, charged surface features on the inner lumen of the MRE microtubes may have enhancing effects on cell capture due to increased surface area as well as more subtle effects due to changes in the fluid dynamics at the surface and charge.

1.6 Leukocyte adhesion to nanostructured surfaces

Numerous biomedical devices involve the handling of blood or blood components. The ability to remain inert to these components is often a requirement to avoid fouling and retain functionality. Leukocytes are a major contributor to fouling because they will actively bind to a biomaterial and then firmly adhere, spread on the surface, and can promote inflammation. Progress has been made to avoid this biofouling by altering the roughness or charge of the surfaces of biomaterials. Cell response to nanostructured surfaces varies widely, depending on cell type, surface composition,

surface feature dimensions, orientation, and organization. The modes of action are unclear (*92, 93*). Studies into the behavior of macrophages on microstructured surfaces have shown both increased spreading (*94*) and decreased spreading (*95*). A review of studies into the interaction of immune cells and nanostructured surfaces has concluded that materials with altered nanotopographies can generally be less inflammatory than planar surfaces (*96*). Clearly, the results are conflicting, depending on cell type, surface composition, surface feature orientation, dimension, and orientation. This makes the design of biomaterials to obtain predictable cellular behavior difficult. Computational models of leukocyte adhesion have been built in an attempt to understand this process. These models are based on the roughness of both the cell surface and the biomaterial surface, as well as ligand localization and prevalence on the cell surface (*97, 98*). When ligands are localized to their correct areas on the cell surface, such as L-selectin and selectin glycoprotein ligands to the ridges of membranous folds and microvilli tips, and β_2-integrins to the valleys of folds, the forces involved in leukocyte adhesion and membrane deformation can begin to be modeled and understood.

1.7 Specific Aims

Specific Aim 1: Investigation of the impact of halloysite nanotubes on the capture of flowing cells

The King lab has previously developed a microtube device that can be functionalized with target cell-specific proteins for cell isolation. A notable feature of the device is the incorporation of selectin proteins that have distinct adhesion behaviors that allow for transient capture of fast flowing cells. Techniques for creating a reproducible

coating of halloysite nanotubes will be evaluated. Enhancements in cell capture will be investigated using a non-adherent leukemic cell line as a model for flowing cells. Capture improvements will be evaluated both in terms of the strength with which cells adhere to the surface, as well as the number of cells that adhere under flow. Mechanisms of capture enhancement will be investigated to determine the role of protein adsorption, surface area, and microfluidic considerations.

Specific Aim 2: Capture of circulating tumor cells from blood using a halloysite nanotube-enhanced selectin-functionalized device

The halloysite nanotube coating will be applied to a microtube device designed for the capture of circulating tumor cells (CTC) from the blood of patients diagnosed with metastatic disease. The device will be validated with model samples of cell line cells spiked into normal blood. Several patient samples will be processed and captured cells will be analyzed for CTC count and purity. Matched patient samples will be processed by the gold-standard technology, CellSearch, for comparison.

Specific Aim 3: Investigation of the adhesion of leukocytes on halloysite nanotube coatings

Leukocyte adhesion is modulated by surface features such as roughness. Leukocyte adhesion and subsequent spreading is considered a form of biofouling in microfluidic cell isolation devices because it leads to reduced target cell capture. The nanotube coating will be utilized to tune the surface of selectin-functionalized surfaces, creating a range of surface roughnesses. Leukocyte adhesion will be evaluated in terms of

adhesive area as well as the number of adherent cells. The nanotube coatings will be evaluated for roughness and charge by various criteria.

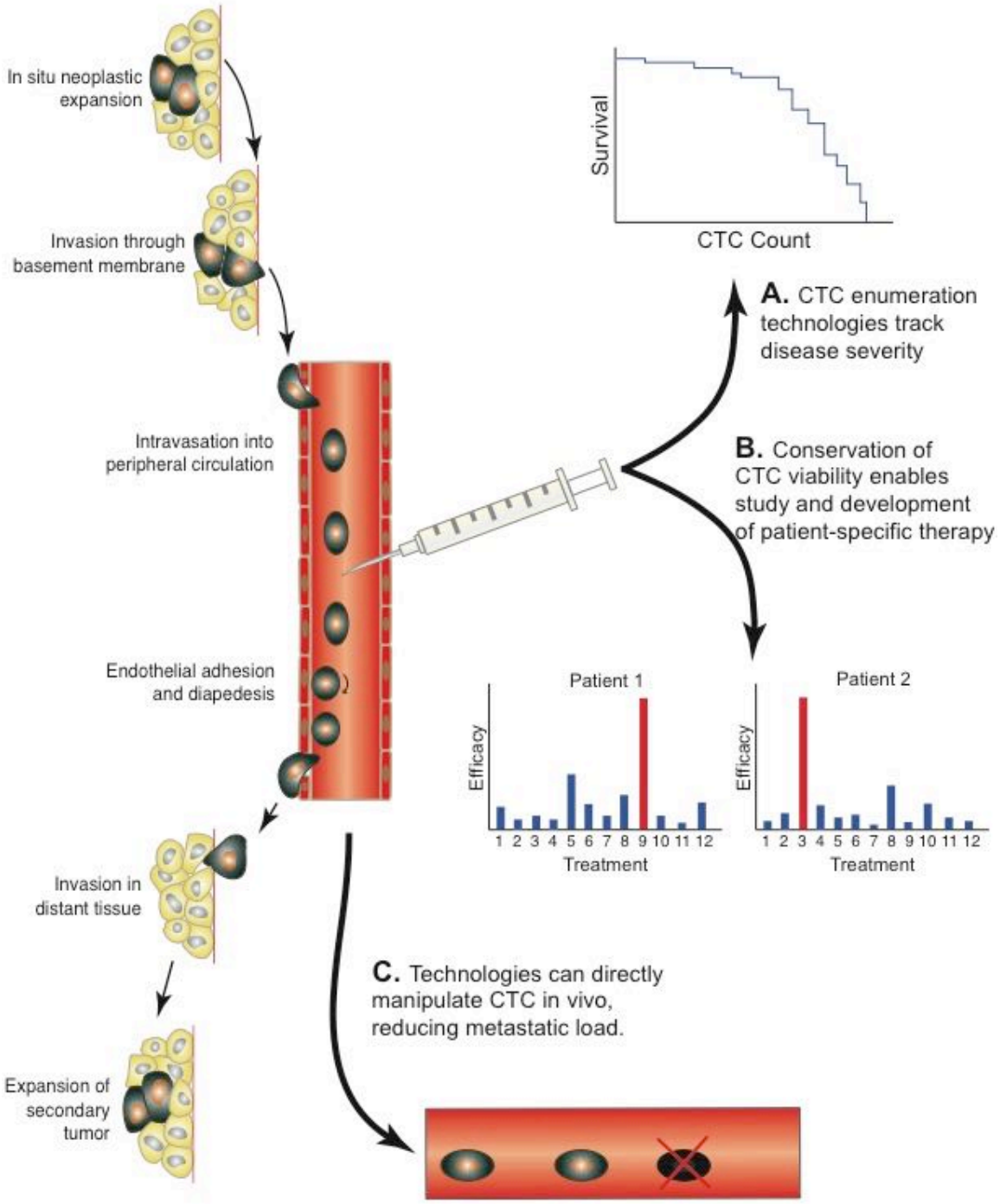

Figure 1.1. Schematic describing the utility of the three major classes of technologies for capture and/or manipulation of circulating tumor cells.

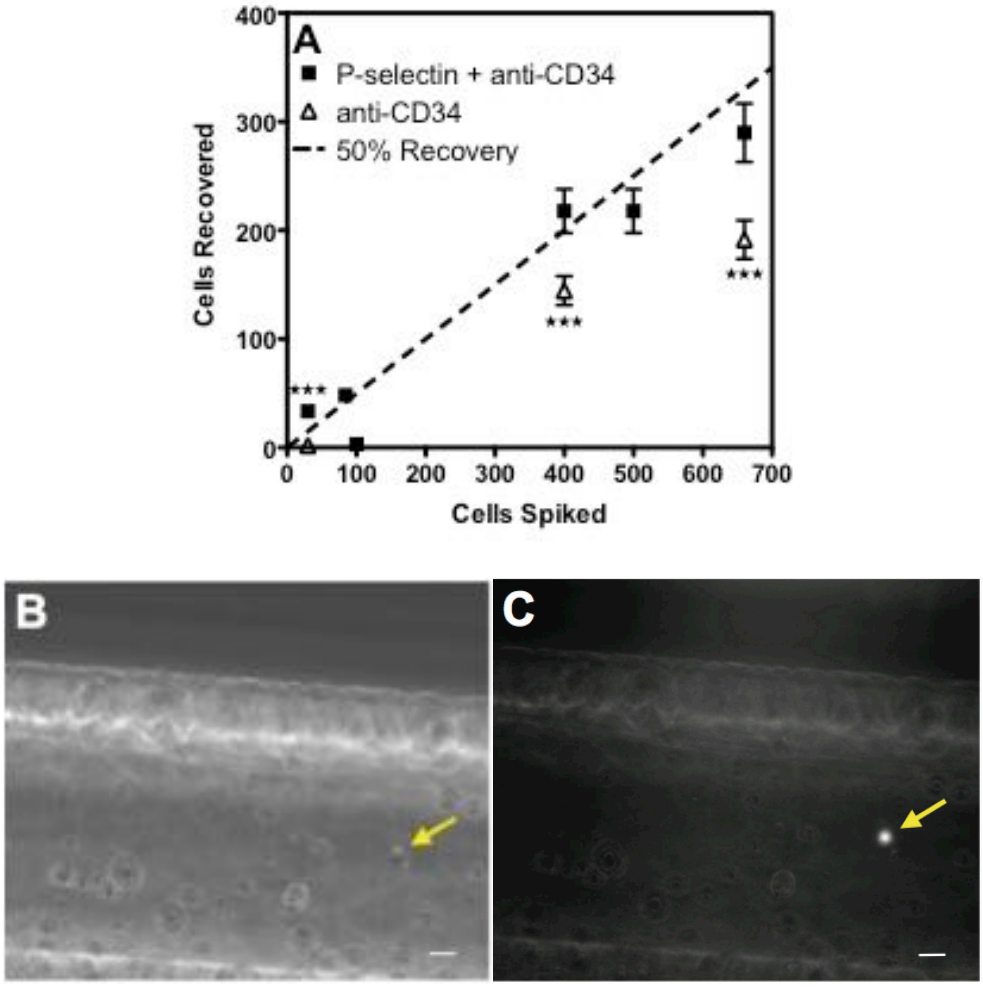

Figure 1.2. CTC capture from blood in a selectin-functionalized microtube. A. Various numbers of KG1a acute myeloid leukemia cells were spiked into blood. Samples were perfused through MRE tubes coated with either 50 μg/mL anti-CD34 alone or coated with both 50 μg/mL anti-CD34 and 0.5 μg/mL P-selectin. Approximately 50% of KG1a cells spiked into blood samples were recovered on the bimolecular-coated MRE tube. B. Representative low-intensity bright field micrograph of cells captured in a bimolecular-coated MRE tube. C. Fluorescent KG1a cell captured in bimolecular-coated MRE tube. 84 fluorescently-labeled KG1a cells were spiked into 4 mL blood. Scale bars are 20 μm.

(Data is adapted and micrographs are reproduced with permission from Ref. 67. Copyright 2009 Elsevier Ltd)

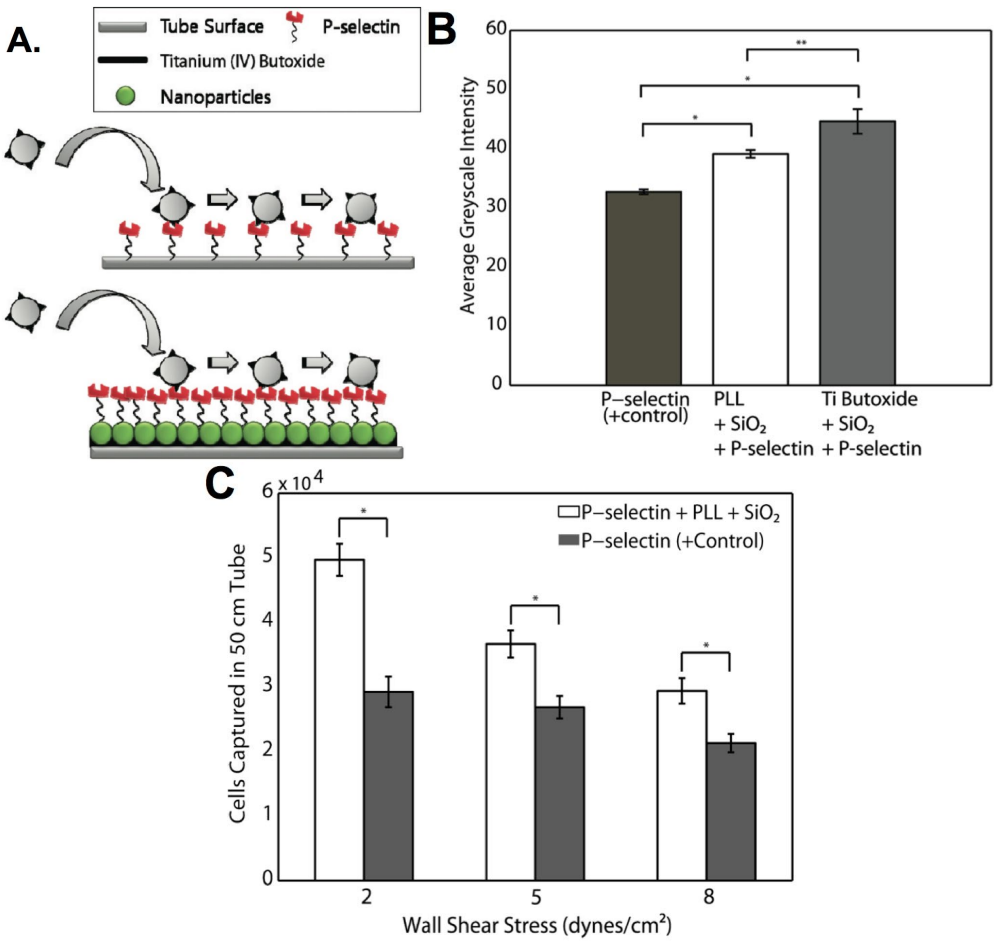

Figure 1.3. Silica (SiO_2) nanoparticle (10-15 nm) coatings augment cell capture in a selectin-functionalized device. A. Schematic of nanoparticle coating shows the impact on P-selectin adsorption. B. Silica nanoparticles were coated onto the device surface using two different adhesives and P-selectin adsorption was significantly enhanced using both methods. Adsorption quantification was determined using fluorescent antibodies against P-selectin. C. The number of cells captured was greater using the silica nanoparticle coating over the physiological range of shear stresses compared to the smooth surface. (Figures are reproduced with permission from Ref. 68. Copyright 2010 American Chemical Society)

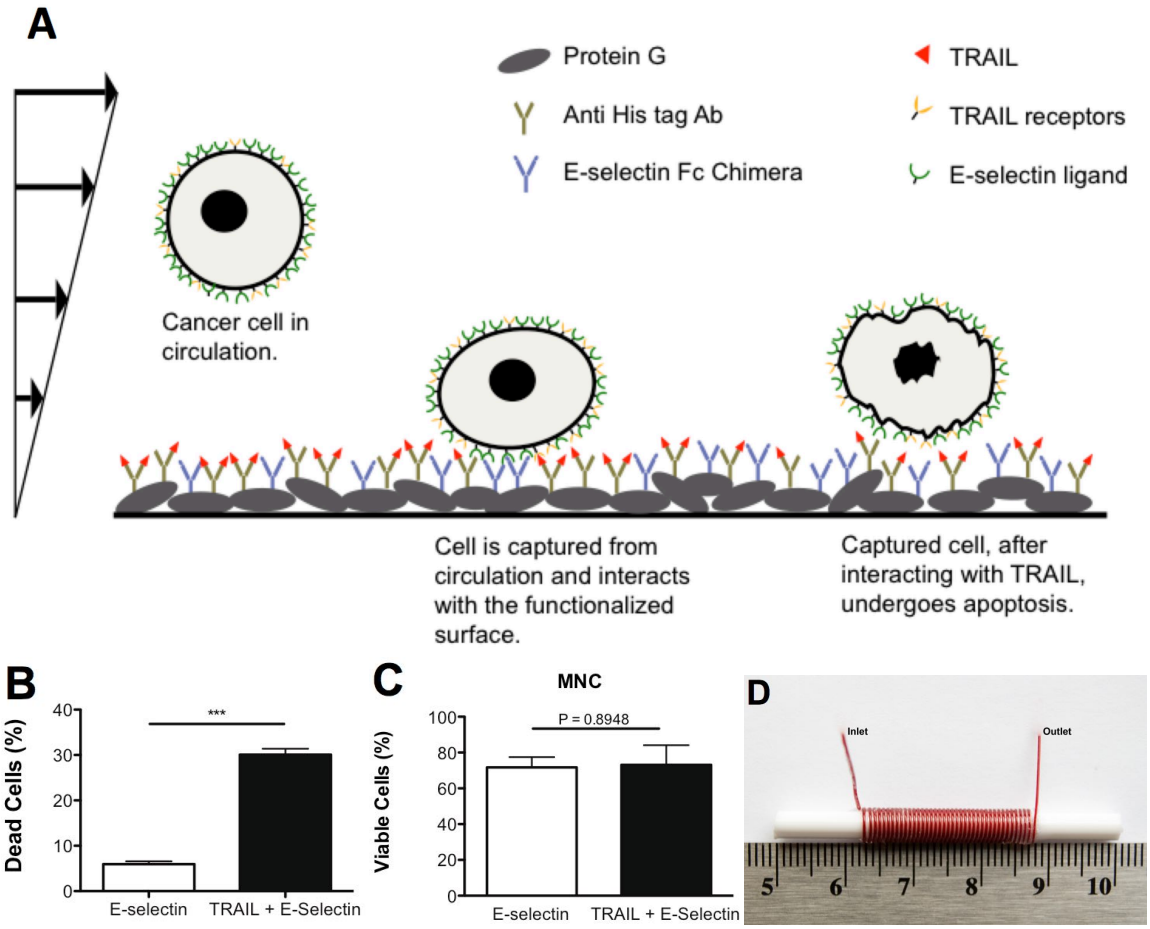

Figure 1.4. Schematic of the implantable shunt device for inducing apoptosis in CTC in vivo using E-selectin for capture and TRAIL to deliver the death signal. B. HL60 leukemic cells are eliminated by approximately 30% following perfusion through the devices coated with both E-selectin and TRAIL. C. Viability of normal mononuclear cells is not effected by the TRAIL-coating, confirming the specificity of TRAIL for malignant cells. D. Image showing the size of a compact shunt device for implantation. (Figures A-C are reproduced from Ref. 78 and figure D is reproduced from Ref. 67 with permission. Ref. 78 is Copyright 2008 Wiley Periodicals, Inc.)

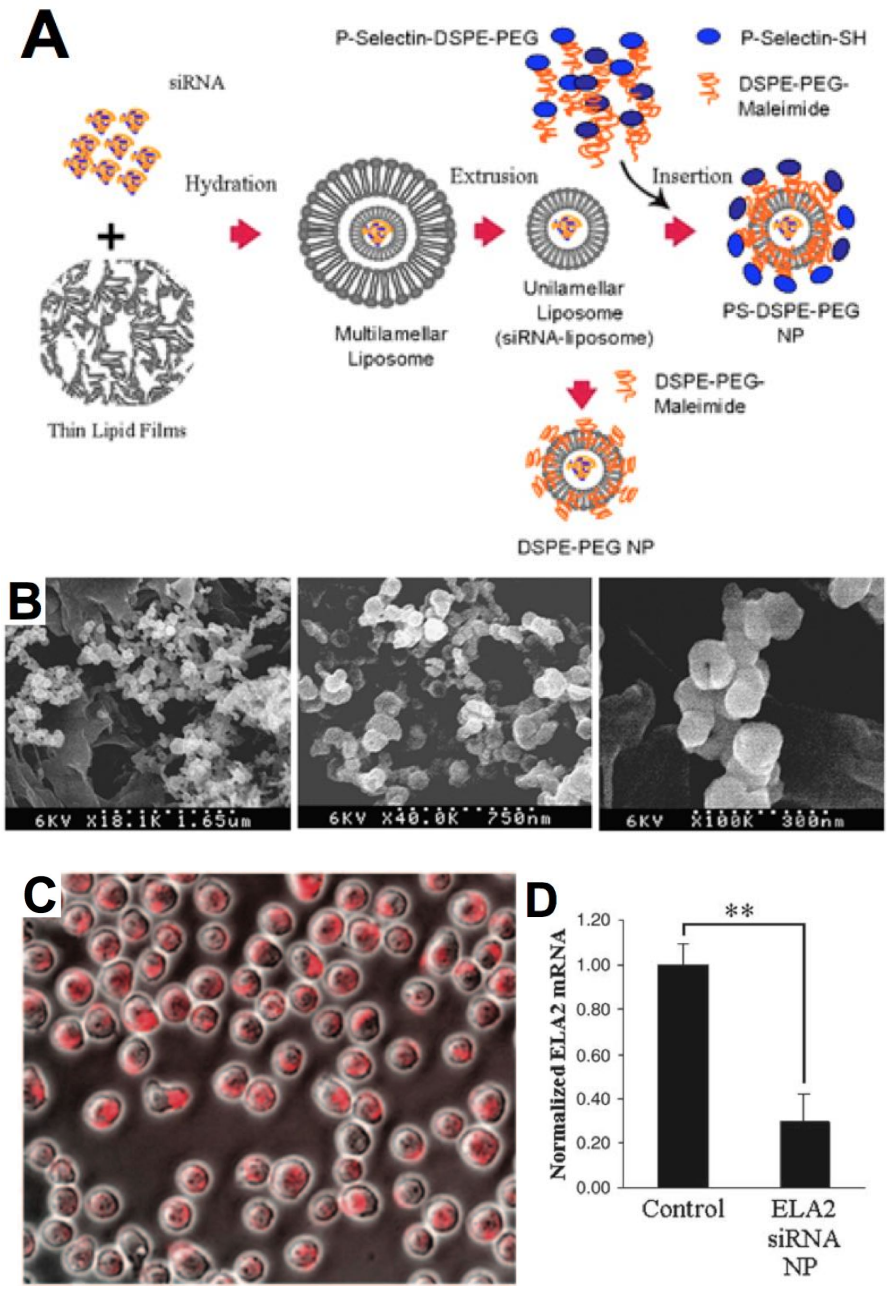

Figure 1.5. Efficient delivery of siRNA using P-selectin targeted liposomes coated in an implantable shunt device. A. Liposomes are encapsulated with siRNA and covalently coated with P-selectin and polyethylene glycol (PEG). B. Scanning electron microscopy shows the size and shape of the encapsulated liposomes. The average diameter was found to be approximately 150 nm. C. Red fluorescent RNA encapsulated within the liposomes

was efficiently delivered to HL60 cells perfused through the liposome-coated shunt device. D. Significant ELA2 gene knockdown is shown using real-time quantitative-PCR to indicate the effectiveness of this siRNA delivery technique. (Figures are reproduced with permission from Ref. 83. Copyright 2009 Macmillan Publishers Ltd)

Table 1.1. Characteristics of several devices for therapeutic utilization of CTC (continued on following page)

Class	Device/ Technique	Molecular Target	Description	Sensitivity	Development Stage
I	CellSearch	EpCAM	CTC are immunoprecipitated from buffy coat samples using magnetic nanoparticles coated with anti-EpCAM antibody. Subsequent staining is employed to improve detection specificity. CellSearch is currently the only FDA-approved device for CTC detection.	1 CTC in 0.5 mL blood	FDA approved
I	RT-PCR	Cancer-specific mRNA	Cells are lysed and PCR is used to detect the expression of a cancer-specific gene (e.g., EGFR, CEA, CK-19, CK-20, HER-2, MUC-1, h-MAM).	1 CTC per mL blood	Trials with primary patient samples
I	qRT-PCR	Cancer-specific mRNA	qRT-PCR eliminates some false-positive detection by thresholding results when detecting the expression of cancer-specific genes (e.g., hTERT, CK-19, CEA, MUC-1).	5 CTC per mL blood	Trials with primary patient samples
I	AdnaTest	Three epithelial cell surface markers + HER-2, MUC-1, and GA733-2 mRNA	Immunoprecipitation of CTC using antibody-coated magnetic nanoparticles, followed by semiquantitative RT-PCR to detect the expression of cancer-specific genes.	2 CTC per 5 mL blood	Clinically approved
I	OBP-401 (TelomeScan)	Active telomerase	A GFP-expressing AAV was developed that has telomerase-dependent replication. This virus is used to infect all the cells in a blood sample and telomerase-expressing CTC will become fluorescent.	1 CTC per 5 mL blood	Experiments with cancer cell lines
I	SWCNT field effect transistors	IGF1R, HER-2	SWCNTs are arranged across electrodes and coated with antibodies. The binding of a single CTC to a CNT alters the electrical conductivity between the electrodes, providing CTC detection.	Not evaluated	Experiments with cancer cell lines
I	ELISPOT	Cell-secreted cathepsin D and MUC-1	CD45-negative buffy coat cells are incubated for 24–48 h and the cell-conditioned media are analyzed for secreted factors using an ELISA array technique.	1 CTC in 5 mL blood	Trials with primary patient samples
I	Laser scanning cytometry (LSC)	EpCAM, HEA	Cells are deposited onto a slide in a monolayer and then fluorescently stained. A computer-driven microscope then scans over the slide and records the fluorescence of each event.	1 CTC in 100,000 cells	Trials with primary patient samples
I	FAST	CK	FAST is similar to LSC in that cells are deposited on a slide and scanned by computer-driven optics. FAST utilizes laser-printing technology to scan samples very rapidly: 300,000 cells/s.	1 CTC in 100,000 cells	Trials with primary patient samples
I	Fluorescent aptamer-coated nanorods	Various cell surface markers	Aptamer libraries are screened for affinity to the target cell using cell-SELEX. Up to 80 fluorescently labeled target cell-specific aptamers are then coated onto gold-silver nanorods and used for detection via flow cytometry.	Not evaluated	Trials with primary patient samples

Table 1.1 (continued)

Class	Device/ Technique	Molecular Target	Description	Sensitivity	Development Stage
II	Selectin-functionalized microtube	Selectin-binding proteins (e.g., PSGL-1, ESL-1, CD44)	Patient buffy coat is perfused through a polymeric microtube coated with adhesive E-selectin protein, and isolated in viable form.	30 CTC in 4 mL blood	Trials with primary patient samples
II	CTC-chip	EpCAM	A microfluidic chip with staggered posts coated with anti-EpCAM antibodies. This arrangement provides a high surface area for antibody–CTC interaction.	Not directly evaluated	Trials with primary patient samples
II	Herringbone-Chip	EpCAM	A microfluidic chip with chevron-shaped grooves, coated with anti-EpCAM antibodies. The chevron grooves induce vortices which promote cell-to-surface contact.	10 CTC per mL	Trials with primary patient samples
II	GEDI	PSMA	A microfluidic chip with posts that are arranged according to a mathematical model used to maximize cell-to-post contact probability.	Not directly evaluated	Trials with primary patient samples
II	HTMSU	PSMA, EpCAM	A microfluidic chip with parallel sinusoidal channels coated with antibodies. A conductivity sensor mounted at the chip outlet is able to detect CTC as they are eluted from the chip.	Not directly evaluated	Experiments with cancer cell lines
II	Nanopillar array	EpCAM	A silicon surface is etched to have 100–200-nm-wide pillars that enhance cellular adhesion.	5–20 CTC per mL blood	Experiments with cancer cell lines
III	TRAIL/selecin vascular shunt	Selectin-binding proteins	The inner surface of a microtube is coated with selectin protein and TRAIL. Once implanted as a shunt in a vessel, CTC that flow through are induced to roll on the surface of the tube where apoptosis is induced by TRAIL.	Not directly evaluated	Experiments with cancer cell lines
III	siRNA/ selectin vascular shunt	Selectin-binding proteins	The inner surface of a microtube is coated with liposomes decorated with selectin protein and containing siRNA for gene therapy. Cells flowing through the implanted microtube rapidly bind to the liposomes and subsequently internalize the siRNA.	Not directly evaluated	Experiments with cancer cell lines
III	Photoacoustic flow cytometry	Spectrally specific markers (e.g., melanosomes, targeted gold NPs)	Enumeration or ablation of CTC in peripheral vessels is achieved using a laser that induces vibration in endogenous or exogenous nanoparticles.	1 CTC per mL blood	Animal trials with cancer cell lines

Abbreviations: AAV, attenuated adenovirus; CEA, carcinoembryonic antigen; CK, cytokeratin; CNT, carbon nanotube; CTC, circulating tumor cell; EGFR, epidermal growth factor receptor; ELISA, enzyme-linked immunosorbent assay; ELISPOT, enzyme-linked ImmunoSpot; EpCAM, epithelial cell adhesion molecule; ESL-1, E-selectin ligand-1; FAST, fiber-optic array scanning technology; FDA, Food and Drug Administration; GEDI, geometrically enhanced differential immunocapture; GFP, green fluorescent protein; HEA, human epithelial antigen; HER-2, human epithelial growth factor receptor-2; h-MAM, human mammaglobin; hTERT, human telomerase reverse transcriptase; HTMSU, high-throughput microsampling unit; IGF1R, insulin-like growth factor 1 receptor; LNCaP, an androgen-sensitive human prostate adenocarcinoma cell line; mRNA, messenger RNA; MUC-1, mucin-1; NP, nanoparticle; PCR, polymerase chain reaction; PSGL-1, P-selectin glycoprotein ligand-1; PSMA, prostate-specific membrane antigen; qRT-PCR, quantitative RT-PCR; RT-PCR, reverse transcriptase polymerase chain reaction; SELEX, systematic evolution of ligands for exponential enrichment; siRNA, small interfering RNA; SWCNT, single-walled carbon nanotube; TRAIL, tumor necrosis factor-related apoptosis-inducing ligand.

1.8 References

1. C. Wittekind, M. Neid, Cancer invasion and metastasis. *Oncology* **69 Suppl 1**, 14-16 (2005).
2. Y. S. Chang *et al.*, Mosaic blood vessels in tumors: frequency of cancer cells in contact with flowing blood. *Proc Natl Acad Sci U S A* **97**, 14608-14613 (2000).
3. T. P. Butler, P. M. Gullino, Quantitation of cell shedding into efferent blood of mammary adenocarcinoma. *Cancer Res* **35**, 512-516 (1975).
4. P. Paterlini-Brechot, N. L. Benali, Circulating tumor cells (CTC) detection: clinical impact and future directions. *Cancer Lett* **253**, 180-204 (2007).
5. P. Gassmann, A. Enns, J. Haier, Role of tumor cell adhesion and migration in organ-specific metastasis formation. *Onkologie* **27**, 577-582 (2004).
6. A. F. Chambers, A. C. Groom, I. C. MacDonald, Dissemination and growth of cancer cells in metastatic sites. *Nat Rev Cancer* **2**, 563-572 (2002).
7. A. B. Al-Mehdi *et al.*, Intravascular origin of metastasis from the proliferation of endothelium-attached tumor cells: a new model for metastasis. *Nat Med* **6**, 100-102 (2000).
8. M. D. Cameron *et al.*, Temporal progression of metastasis in lung: cell survival, dormancy, and location dependence of metastatic inefficiency. *Cancer Res* **60**, 2541-2546 (2000).
9. G. N. Naumov *et al.*, Persistence of solitary mammary carcinoma cells in a secondary site: a possible contributor to dormancy. *Cancer Res* **62**, 2162-2168 (2002).

10. D. X. Nguyen, P. D. Bos, J. Massague, Metastasis: from dissemination to organ-specific colonization. *Nat Rev Cancer* **9**, 274-284 (2009).

11. F. W. Orr, H. H. Wang, R. M. Lafrenie, S. Scherbarth, D. M. Nance, Interactions between cancer cells and the endothelium in metastasis. *J Pathol* **190**, 310-329 (2000).

12. S. Gout, P. L. Tremblay, J. Huot, Selectins and selectin ligands in extravasation of cancer cells and organ selectivity of metastasis. *Clin Exp Metastasis* **25**, 335-344 (2008).

13. G. P. Gupta, J. Massague, Cancer metastasis: building a framework. *Cell* **127**, 679-695 (2006).

14. B. Panchapakesan *et al.*, Micro- and nanotechnology approaches for capturing circulating tumor cells. *Cancer Nanotechnology* **1**, 3-11 (2010).

15. U. De Giorgi *et al.*, 18F-FDG PET/CT findings and circulating tumor cell counts in the monitoring of systemic therapies for bone metastases from breast cancer. *J Nucl Med* **51**, 1213-1218 (2010).

16. S. Maheswaran, D. A. Haber, Circulating tumor cells: a window into cancer biology and metastasis. *Curr Opin Genet Dev* **20**, 96-99 (2010).

17. W. J. Allard *et al.*, Tumor cells circulate in the peripheral blood of all major carcinomas but not in healthy subjects or patients with nonmalignant diseases. *Clin Cancer Res* **10**, 6897-6904 (2004).

18. J. G. Moreno *et al.*, Circulating tumor cells predict survival in patients with metastatic prostate cancer. *Urology* **65**, 713-718 (2005).

19. D. C. Danila *et al.*, Circulating tumor cell number and prognosis in progressive castration-resistant prostate cancer. *Clin Cancer Res* **13**, 7053-7058 (2007).

20. J. S. de Bono *et al.*, Circulating tumor cells predict survival benefit from treatment in metastatic castration-resistant prostate cancer. *Clin Cancer Res* **14**, 6302-6309 (2008).

21. M. C. Miller, G. V. Doyle, L. W. Terstappen, Significance of Circulating Tumor Cells Detected by the CellSearch System in Patients with Metastatic Breast Colorectal and Prostate Cancer. *J Oncol* **2010**, 617421 (2010).

22. P. C. Tong *et al.*, White blood cell count is associated with macro- and microvascular complications in chinese patients with type 2 diabetes. *Diabetes Care* **27**, 216-222 (2004).

23. R. Bernards, R. A. Weinberg, A progression puzzle. *Nature* **418**, 823 (2002).

24. J. W. Gray, Evidence emerges for early metastasis and parallel evolution of primary and metastatic tumors. *Cancer Cell* **4**, 4-6 (2003).

25. S. Ramaswamy, K. N. Ross, E. S. Lander, T. R. Golub, A molecular signature of metastasis in primary solid tumors. *Nat Genet* **33**, 49-54 (2003).

26. E. C. Kohn, L. A. Liotta, Molecular insights into cancer invasion: strategies for prevention and intervention. *Cancer Res* **55**, 1856-1862 (1995).

27. M. Cristofanilli *et al.*, Circulating tumor cells, disease progression, and survival in metastatic breast cancer. *N Engl J Med* **351**, 781-791 (2004).

28. P. T. Went *et al.*, Frequent EpCam protein expression in human carcinomas. *Hum Pathol* **35**, 122-128 (2004).

29. M. Zeisberg, E. G. Neilson, Biomarkers for epithelial-mesenchymal transitions. *J Clin Invest* **119**, 1429-1437 (2009).

30. B. Willipinski-Stapelfeldt *et al.*, Changes in cytoskeletal protein composition indicative of an epithelial-mesenchymal transition in human micrometastatic and primary breast carcinoma cells. *Clin Cancer Res* **11**, 8006-8014 (2005).

31. V. Zieglschmid, C. Hollmann, O. Bocher, Detection of disseminated tumor cells in peripheral blood. *Crit Rev Clin Lab Sci* **42**, 155-196 (2005).

32. K. Pantel, R. H. Brakenhoff, B. Brandt, Detection, clinical relevance and specific biological properties of disseminating tumour cells. *Nat Rev Cancer* **8**, 329-340 (2008).

33. M. Novaes, I. Bendit, B. Garicochea, A. del Giglio, Reverse transcriptase-polymerase chain reaction analysis of cytokeratin 19 expression in the peripheral blood mononuclear cells of normal female blood donors. *Mol Pathol* **50**, 209-211 (1997).

34. P. J. Bostick *et al.*, Limitations of specific reverse-transcriptase polymerase chain reaction markers in the detection of metastases in the lymph nodes and blood of breast cancer patients. *J Clin Oncol* **16**, 2632-2640 (1998).

35. C. H. Wu *et al.*, Development of a high-throughput membrane-array method for molecular diagnosis of circulating tumor cells in patients with gastric cancers. *Int J Cancer* **119**, 373-379 (2006).

36. M. Tewes *et al.*, Molecular profiling and predictive value of circulating tumor cells in patients with metastatic breast cancer: an option for monitoring response to breast cancer related therapies. *Breast Cancer Res Treat* **115**, 581-590 (2009).

37. J. S. Ross, E. A. Slodkowska, Circulating and disseminated tumor cells in the management of breast cancer. *Am J Clin Pathol* **132**, 237-245 (2009).

38. I. Van der Auwera *et al.*, Circulating tumour cell detection: a direct comparison between the CellSearch System, the AdnaTest and CK-19/mammaglobin RT-PCR in patients with metastatic breast cancer. *Br J Cancer* **102**, 276-284 (2010).

39. T. Kojima *et al.*, A simple biological imaging system for detecting viable human circulating tumor cells. *J Clin Invest* **119**, 3172-3181 (2009).

40. P. Marchetti *et al.*, The novel retinoid 6-[3-(1-adamantyl)-4-hydroxyphenyl]-2-naphtalene carboxylic acid can trigger apoptosis through a mitochondrial pathway independent of the nucleus. *Cancer Res* **59**, 6257-6266 (1999).

41. E. Hiyama *et al.*, Telomerase activity as a marker of breast carcinoma in fine-needle aspirated samples. *Cancer* **90**, 235-238 (2000).

42. J. W. Shay, S. Bacchetti, A survey of telomerase activity in human cancer. *Eur J Cancer* **33**, 787-791 (1997).

43. S. E. Artandi, R. A. DePinho, Telomeres and telomerase in cancer. *Carcinogenesis* **31**, 9-18 (2010).

44. B. Panchapakesan, G. Cesarone, S. Liu, K. Teker, E. Wickstrom, Single-wall carbon nanotubes with adsorbed antibodies detect live breast cancer cells. *NanoBioTechnology* **1**, 353-360 (2005).

45. N. Shao, E. Wickstrom, B. Panchapakesan, Nanotube-antibody biosensor arrays for the detection of circulating breast cancer cells. *Nanotechnology* **19**, - (2008).

46. C. Alix-Panabieres *et al.*, Detection and characterization of putative metastatic precursor cells in cancer patients. *Clin Chem* **53**, 537-539 (2007).

47. C. Alix-Panabieres *et al.*, Characterization and enumeration of cells secreting tumor markers in the peripheral blood of breast cancer patients. *J Immunol Methods* **299**, 177-188 (2005).

48. K. Pachmann *et al.*, Standardized quantification of circulating peripheral tumor cells from lung and breast cancer. *Clin Chem Lab Med* **43**, 617-627 (2005).

49. S. J. Zoog *et al.*, Measurement of conatumumab-induced apoptotic activity in tumors by fine needle aspirate sampling. *Cytometry A* **77**, 849-860 (2010).

50. M. M. Harnett, Laser scanning cytometry: understanding the immune system in situ. *Nat Rev Immunol* **7**, 897-904 (2007).

51. K. Pachmann, P. Heiss, U. Demel, G. Tilz, Detection and quantification of small numbers of circulating tumour cells in peripheral blood using laser scanning cytometer (LSC). *Clin Chem Lab Med* **39**, 811-817 (2001).

52. K. Pachmann *et al.*, Monitoring the response of circulating epithelial tumor cells to adjuvant chemotherapy in breast cancer allows detection of patients at risk of early relapse. *J Clin Oncol* **26**, 1208-1215 (2008).

53. K. D. Bauer *et al.*, Reliable and sensitive analysis of occult bone marrow metastases using automated cellular imaging. *Clin Cancer Res* **6**, 3552-3559 (2000).

54. R. T. Krivacic *et al.*, A rare-cell detector for cancer. *Proc Natl Acad Sci U S A* **101**, 10501-10504 (2004).

55. H. B. Hsieh *et al.*, High speed detection of circulating tumor cells. *Biosens Bioelectron* **21**, 1893-1899 (2006).

56. D. Marrinucci *et al.*, Case study of the morphologic variation of circulating tumor cells. *Hum Pathol* **38**, 514-519 (2007).

57. Y. F. Huang, H. T. Chang, W. Tan, Cancer cell targeting using multiple aptamers conjugated on nanorods. *Anal Chem* **80**, 567-572 (2008).

58. L. M. Coussens, Z. Werb, Inflammation and cancer. *Nature* **420**, 860-867 (2002).

59. Y. J. Kim, L. Borsig, H. L. Han, N. M. Varki, A. Varki, Distinct selectin ligands on colon carcinoma mucins can mediate pathological interactions among platelets, leukocytes, and endothelium. *Am J Pathol* **155**, 461-472 (1999).

60. F. W. Orr, H. H. Wang, Tumor cell interactions with the microvasculature: a rate-limiting step in metastasis. *Surg Oncol Clin N Am* **10**, 357-381, ix-x (2001).

61. B. McDonald *et al.*, Systemic inflammation increases cancer cell adhesion to hepatic sinusoids by neutrophil mediated mechanisms. *Int J Cancer* **125**, 1298-1305 (2009).

62. S. Kohler, S. Ullrich, U. Richter, U. Schumacher, E-/P-selectins and colon carcinoma metastasis: first in vivo evidence for their crucial role in a clinically relevant model of spontaneous metastasis formation in the lung. *Br J Cancer* **102**, 602-609 (2010).

63. T. M. van Ginhoven, J. W. van den Berg, W. A. Dik, J. N. M. Ijzermans, R. W. F. de Bruin, Preoperative dietary restriction reduces hepatic tumor load by reduced E-selectin-mediated adhesion in mice. *Journal of Surgical Oncology* **102**, 348-353 (2010).

64. J. C. Wojciechowski *et al.*, Capture and enrichment of CD34-positive haematopoietic stem and progenitor cells from blood circulation using P-selectin in an implantable device. *Br J Haematol* **140**, 673-681 (2008).

65. N. Charles, J. L. Liesveld, M. R. King, Investigating the feasibility of stem cell enrichment mediated by immobilized selectins. *Biotechnol Prog* **23**, 1463-1472 (2007).

66. S. D. Narasipura, J. C. Wojciechowski, N. Charles, J. L. Liesveld, M. R. King, P-Selectin coated microtube for enrichment of CD34+ hematopoietic stem and progenitor cells from human bone marrow. *Clin Chem* **54**, 77-85 (2008).

67. B. J. Huntly, D. G. Gilliland, Leukaemia stem cells and the evolution of cancer-stem-cell research. *Nat Rev Cancer* **5**, 311-321 (2005).

68. D. Bonnet, J. E. Dick, Human acute myeloid leukemia is organized as a hierarchy that originates from a primitive hematopoietic cell. *Nat Med* **3**, 730-737 (1997).

69. M. R. King, L. T. Western, K. Rana, J. L. Liesveld, Biomolecular Surfaces for the Capture and Reprogramming of Circulating Tumor Cells. *Journal of Bionic Engineering* **6**, 311-317 (2009).

70. W. Han, B. A. Allio, D. G. Foster, M. R. King, Nanoparticle coatings for enhanced capture of flowing cells in microtubes. *ACS Nano* **4**, 174-180 (2010).

71. S. Nagrath *et al.*, Isolation of rare circulating tumour cells in cancer patients by microchip technology. *Nature* **450**, 1235-1239 (2007).

72. S. L. Stott *et al.*, Isolation of circulating tumor cells using a microvortex-generating herringbone-chip. *Proc Natl Acad Sci U S A* **107**, 18392-18397 (2010).

73. J. P. Gleghorn *et al.*, Capture of circulating tumor cells from whole blood of prostate cancer patients using geometrically enhanced differential immunocapture (GEDI) and a prostate-specific antibody. *Lab Chip* **10**, 27-29 (2010).

74. A. A. Adams *et al.*, Highly efficient circulating tumor cell isolation from whole blood and label-free enumeration using polymer-based microfluidics with an integrated conductivity sensor. *J Am Chem Soc* **130**, 8633-8641 (2008).

75. U. Dharmasiri *et al.*, Highly efficient capture and enumeration of low abundance prostate cancer cells using prostate-specific membrane antigen aptamers immobilized to a polymeric microfluidic device. *Electrophoresis* **30**, 3289-3300 (2009).

76. S. Wang *et al.*, Three-dimensional nanostructured substrates toward efficient capture of circulating tumor cells. *Angew Chem Int Ed Engl* **48**, 8970-8973 (2009).

77. K. Rana, J. L. Liesveld, M. R. King, Delivery of apoptotic signal to rolling cancer cells: a novel biomimetic technique using immobilized TRAIL and E-selectin. *Biotechnol Bioeng* **102**, 1692-1702 (2009).

78. M. Plasilova *et al.*, TRAIL (Apo2L) suppresses growth of primary human leukemia and myelodysplasia progenitors. *Leukemia* **16**, 67-73 (2002).

79. M. Jo *et al.*, Apoptosis induced in normal human hepatocytes by tumor necrosis factor-related apoptosis-inducing ligand. *Nat Med* **6**, 564-567 (2000).

80. M. Leverkus *et al.*, Regulation of tumor necrosis factor-related apoptosis-inducing ligand sensitivity in primary and transformed human keratinocytes. *Cancer Res* **60**, 553-559 (2000).

81. R. Nitsch *et al.*, Human brain-cell death induced by tumour-necrosis-factor-related apoptosis-inducing ligand (TRAIL). *Lancet* **356**, 827-828 (2000).

82. Z. Huang, M. R. King, An immobilized nanoparticle-based platform for efficient gene knockdown of targeted cells in the circulation. *Gene Ther* **16**, 1271-1282 (2009).

83. E. I. Galanzha, E. V. Shashkov, P. M. Spring, J. Y. Suen, V. P. Zharov, In vivo, noninvasive, label-free detection and eradication of circulating metastatic melanoma cells using two-color photoacoustic flow cytometry with a diode laser. *Cancer Res* **69**, 7926-7934 (2009).

84. J. W. Kim, E. I. Galanzha, E. V. Shashkov, H. M. Moon, V. P. Zharov, Golden carbon nanotubes as multimodal photoacoustic and photothermal high-contrast molecular agents. *Nat Nanotechnol* **4**, 688-694 (2009).

85. E. I. Galanzha *et al.*, In vivo magnetic enrichment and multiplex photoacoustic detection of circulating tumour cells. *Nat Nanotechnol* **4**, 855-860 (2009).

86. T. R. Ashworth, A case of cancer in which cells similar to those in the tumors were seen in the blood after death. *Aust Med J* **14**, 146-147 (1869).

87. S. Riethdorf, H. Wikman, K. Pantel, Review: Biological relevance of disseminated tumor cells in cancer patients. *Int J Cancer* **123**, 1991-2006 (2008).

88. D. A. Hammer, S. M. Apte, Simulation of cell rolling and adhesion on surfaces in shear flow: general results and analysis of selectin-mediated neutrophil adhesion. *Biophys J* **63**, 35-57 (1992).

89. S. R. Levis, P. B. Deasy, Characterisation of halloysite for use as a microtubular drug delivery system. *Int J Pharm* **243**, 125-134 (2002).

90. R. R. Price, B. P. Gaber, Y. Lvov, In-vitro release characteristics of tetracycline HCl, khellin and nicotinamide adenine dineculeotide from halloysite; a cylindrical mineral. *J Microencapsul* **18**, 713-722 (2001).

91. H. M. Kelly, P. B. Deasy, E. Ziaka, N. Claffey, Formulation and preliminary in vivo dog studies of a novel drug delivery system for the treatment of periodontitis. *Int J Pharm* **274**, 167-183 (2004).

92. E. K. Yim, K. W. Leong, Significance of synthetic nanostructures in dictating cellular response. *Nanomedicine* **1**, 10-21 (2005).

93. J. Y. Lim, H. J. Donahue, Cell sensing and response to micro- and nanostructured surfaces produced by chemical and topographic patterning. *Tissue Eng* **13**, 1879-1891 (2007).

94. B. Wojciak-Stothard, Z. Madeja, W. Korohoda, A. Curtis, C. Wilkinson, Activation of macrophage-like cells by multiple grooved substrata. Topographical control of cell behaviour. *Cell Biol Int* **19**, 485-490 (1995).

95. J. A. Schmidt, A. F. von Recum, Macrophage response to microtextured silicone. *Biomaterials* **13**, 1059-1069 (1992).

96. K. M. Ainslie *et al.*, In vitro inflammatory response of nanostructured titania, silicon oxide, and polycaprolactone. *J Biomed Mater Res A* **91**, 647-655 (2009).

97. S. A. Hocde, O. Hyrien, R. E. Waugh, Cell adhesion molecule distribution relative to neutrophil surface topography assessed by TIRFM. *Biophys J* **97**, 379-387 (2009).

98. S. A. Hocde, O. Hyrien, R. E. Waugh, Molecular accessibility in relation to cell surface topography and compression against a flat substrate. *Biophys J* **97**, 369-378 (2009).

CHAPTER 2 – NATURALLY OCURRING HALLOYSITE NANOTUBES FOR ENHANCED CAPTURE OF FLOWING CELLS

This section has been adapted from the following publication: AD Hughes and MR King, Use of Naturally occurring halloysite nanotubes for enhanced capture of flowing cells. *Langmuir*, **2010**, 26(14) 12155-64.

2.0 Abstract

The development of individualized treatments for cancer can be facilitated by more efficient methods for separating cancer cells from patient blood in such a way that they remain viable for live cell assays. It has previously been shown by the King group that immobilized P-selectin protein can be used on the inner surface of a microscale flow system to induce leukemic cells and leukocytes to roll at different velocities and relative fluxes, thereby creating a means for rapid cell fractionation without inflicting cellular damage. In this study I explore a method to more efficiently capture leukemic and epithelial cancer cells from flow by altering the nanoscale topography of the inner surface of P selectin-coated microtubes. This functionalized topography is achieved by attaching naturally occurring halloysite nanotubes to the microtube surface via a monolayer of poly L-lysine, followed by functionalization with recombinant human selectin protein. I have found that halloysite nanotube coatings promote increased capture of leukemic cells and have determined the key parameters for controlling cell capture under flow: halloysite content and selectin density. Ultimately, selectin-functionalized nanotube coatings should provide a means for enhanced cancer cell isolation from whole blood and other mixtures of cells.

2.1 Introduction

The ability to capture rare circulating tumor cells from the blood of cancer patients provides a significant advance in cancer study, diagnosis, and treatment on a patient-to-patient basis (*99*). The King Lab has previously displayed the ability to selectively target and isolate live circulating tumor cells (CTC) from flow using a novel microfluidic device using immobilized selectin molecules (*100*), and the focus of the present study is to use a nanoparticle coating to enhance the efficiency and selectivity of this approach.

Cancer is the second leading cause of death in the United States, with approximately 90% of these deaths being caused by the formation of metastases by invasive transformed cells (*101*). Experimental models have shown that up to one million cancer cells per gram of tumor can be released into systemic circulation every day (*102*). Metastasis is a highly inefficient process, however, due to the low survival rate of epithelial cells in circulation (*103*), and the concentration of CTC in blood has been reported to be as little as 1 to 84 per 7.5 mL (*104*) compared to the normal concentration of WBC of 3.5-12.5 x 10^6 per mL (*105*). The detection and capture of CTC is further complicated by the fact that the much more prevalent leukocytes are similar in size.

Several methods are currently in use for the identification of CTC in blood (*99, 106*). Most methods involve Ficoll density centrifugation to separate CTC and leukocytes from erythrocytes, platelets, and plasma, and subsequent separation of CTC based on epithelial cell markers. One method, now called CellSearch, separates CTC from leukocytes by immunoprecipitation; magnetic beads coated with antibodies specific

to epithelial cellular adhesion molecule (EpCAM) bind to CTC which express EpCAM (*104*). Another approach commonly used for CTC detection is to lyse the CTC and leukocytes separated by Ficoll centrifugation, and perform reverse transcriptase polymerase chain reaction (RT-PCR) on the isolated mRNA to amplify mRNA for epithelial markers. A significant drawback to these techniques is evident due to the lack of epithelial markers on 30% of CTC (*107*). A further drawback to these techniques is that CTC are destroyed in the process of detecting them, precluding further characterization. The ability to rapidly screen large volumes of blood for rare CTC and specifically capture the CTC while maintaining cell viability, would not only provide individualized disease prognosis, but also provide a means for simultaneous in vitro analyses of multiple treatment schemes to efficiently determine the most effective treatment for each patient.

The novel device that has previously been developed by our group has successfully been used to capture both viable hematopoietic stem and progenitor cells from bone marrow (*108-110*) and viable CTC from blood (*111*). The device is characterized by the immobilization of selectin molecules onto the inner surface of polyurethane microtubes (300 μm ID) and is designed to mimic a post-capillary venule in which the endothelial cells are stimulated by an inflammatory stimulus. In the inflammatory cascade, stimulated epithelial cells express selectin proteins on their luminal surface and flowing leukocytes are able to transiently bind to several selectins, producing a slow rolling interaction. When appropriately stimulated, rolling leukocytes then firmly adhere to the vessel surface through integrin bonds and eventually cross through the endothelium into the inflamed tissue (*112*). It has been shown that CTC

follow similar steps in the early stages of metastasis (*113-117*), therefore, the device mimics a natural process occurring in the post-capillary venules. CTC have exhibited stronger rolling adhesion on selectins then healthy blood cells, thus providing a straightforward and rapid method for CTC enrichment.

Halloysite nanotubes are naturally occurring alluminosilicate minerals that are characteristically large for nanoparticles: typically 500 nm to 1.2 μm in length and 40 to 200 nm in diameter. Halloysite nanotubes have been investigated as a novel platform for drug delivery, and have shown the ability to sustain tetracycline HCl release for up to six weeks *in vivo* (*118-120*). In this study, I functionalize the inner surface of microtubes with halloysite nanotubes to investigate the impact on cell capture as quantified by the rolling velocity and the number of adherent cells. I hypothesize that halloysite will not only increase the surface area of the inner surface of microtubes, but will also affect cell behavior because of the physical dimensions of the particles, resulting in enhanced CTC capture and purity.

2.2 Materials and Methods

2.2.1 Reagents and Antibodies

RPMI 1640 cell culture media, fetal bovine serum, penicillin-streptomycin, phosphate buffered saline (PBS), Hank's balanced salt solution (HBSS), and 1x trypsin were purchased from Invitrogen (Grand Island, NY). Recombinant P-selectin-IgG chimera, and recombinant E-selectin-IgG chimer were obtained from R&D Systems (Minneapolis, MN). Halloysite nanotubes in water (6.6% by weight) was provided by NaturalNano (Rochester, NY). Trypan blue stain (0.4%) was obtained from Lonza

(Wilkersville, MD). Poly-L-lysine (0.1% w/v in water) was obtained from Sigma-Aldrich (St. Louis, MO). Blotting grade blocker non-fat dry milk was obtained from Bio-Rad Laboratories (Hercules, CA). Mouse anti-human CD62P (P-selectin) monoclonal IgG was obtained from eBioscience (San Diego, CA). Alexa Fluor 546 donkey anti-mouse IgG (H+L) antibody was obtained from Invitrogen (Carlsbad, CA).

2.2.2 Cell Lines and Cell Culture

Acute myeloid leukemic KG1a cell line (ATCC number CCL-264.1) and colon cancer Colo205 cell line (ATCC number CCL-222) were obtained from ATCC (Manassas, VA). These cell lines were cultured in RPMI 1640 media supplemented with 2 mM L-glutamine, 25 mM HEPES, 10% (v/v) fetal bovine serum, and 100 U/mL penicillin-streptomycin (complete media) at 37°C and 5% CO_2 under humidified conditions.

2.2.3 Preparation of Cells for Rolling Experiments

Colo205 cells, an adherent cell line, were trypsinized for 5 min and then allowed to incubate for up to 5 h before use to ensure normal surface receptor expression. Both KG1a and Colo205 cells were washed twice with 1x PBS at 1,100 rpm in an Allegra X-22 refrigerated centrifuge at 4°C and resuspended in the flow buffer at a concentration of 10^6 cells/mL. The flow buffer was composed of PBS containing Mg^{2+} and saturated with Ca^{2+}. At least 90% viability of cells was confirmed by trypan blue stain.

2.2.4 Preparation of Halloysite Nanotube Solution

Stock halloysite solution was treated to break up and remove large aggregates. Stock solution was vigorously mixed and subjected to a sonic dismembrator obtained from Fischer Scientific (Pittsburgh, PA). The resulting solution was then filtered through a 0.45 μm pore size PVDF membrane syringe filter (Pall Life Sciences, Port Washington, NY).

2.2.5 Preparation of Surfaces

Recombinant human P- or E-selectin-IgG chimeric protein was dissolved in PBS to 20 μg/mL. The surface was first washed with 75% ethanol and then distilled water. Control surfaces were incubated for 2 h with P- or E-selectin-IgG diluted to concentrations of 2.5 – 10 μg/mL, then incubated with 5% milk protein in PBS for 1 h. Finally, the immobilized selectin molecules were activated by incubation with calcium-containing flow buffer for 10 min. Nanotube-coated surfaces were incubated with 2:8 poly-L lysine solution (0.02% w/v) for 5 min and then treated nanotube solution was incubated for 3 min. The nanotube-coated surfaces were then coated with P- or E-selectin-IgG and milk protein in the same manner as the control surfaces. All incubations were carried out at room temperature.

2.2.6 Rolling Experiments

Micro-Renathane microtubing (300 μm ID) was obtained from Braintree Scientific (Braintree, MA), cut to a length of 50 cm, and secured to the stage of the Olympus IX81 motorized inverted research microscope (Olympus America, Melville,

NY) after surface functionalization as described above. A CCD camera (Hitachi, Tokyo, Japan) and DVD recorder (Sony Electronics) were used to record experiments for offline analysis. Flow of cell suspension containing cells at a concentration of 10^6 cells/mL in flow buffer through the microtubes was controlled by a syringe pump (KDS 230, IITC Life Science, Woodland Hills, CA). Cells were loaded in the microtubes at a shear stress of 2.5 dyne/cm^2 for 5 min prior to performing flow experiments. Shear stress values of 2.5 to 4.5 dyne/cm2 were then initiated and flow was allowed to establish for 1 min prior to data collection.

2.2.7 Viability Assays

Viability assays were performed on KG1a and Colo205 cells in triplicate in which treated cells were incubated for 72 hours in media containing 10% treated halloysite nanotube solution. Viability counts were performed at the beginning and end of the 72 hour period on a hemacytometer (Hausser Scientific, Horsham, PA) using trypan blue stain. Cells were initially diluted to a concentration of 2.5 x 10^5 cells/mL

2.2.8 Atomic Force Microscopy

Flat samples of halloysite nanotube-coated surfaces were prepared for atomic force microscopy by coating glass cover slips following the same method used to coat the microtubes. Surfaces were prepared using nanotube solutions before and after being treated by the methods described above. New tubes were sectioned into planar substrates for imaging of the inner surface. Samples were then imaged using a Veeco DI-3000 AFM. 10 μm x 10 μm images were recorded at five random locations on each sample

and surface topography as well as phase shift data were recorded and analyzed off line using Image SXM 189 software for Mac OS. Three images each of the flat nanotube-coated samples and untreated tube samples were analyzed in Image SXM to inspect the surface height profiles. This was done across the entire image at 20 random positions per image.

2.2.9 Antibody Blocking Experiments

Nanotube-coated and control surfaces were prepared as described above. P-selectin-IgG was diluted to 2.5 μg/mL in PBS- and incubated inside the microtube for 2 h at room temperature (RT). The microtube was then blocked with 5% milk protein solution in PBS- for 1 h at RT. The P-selectin in the microtube was activated by incubation with PBS+ saturated with Ca^{2+} for 15 min. Mouse anti-human CD62P (P-selectin) AK-4 monoclonal antibody was diluted to 100 μg/mL in PBS+ and incubated inside the microtube for 2 h at RT. Cell suspension containing KG1a cells at a concentration of 10^6 cells/mL in flow buffer was then perfused through the microtube at low shear (2.5 dyne/cm^2) and cellular behavior under flow was observed by video microscopy.

2.2.10 Ca^{2+} Chelation Experiments

Nanotube-coated and control surfaces were prepared in the same manner as those prepared for rolling experiments, with an incubating concentration of P-selectin-IgG protein of 2.5 μg/mL in PBS- (2 h) and blocked with 5% milk protein (1 h). After activation of P-selectin with PBS+ saturated with Ca^{2+}, KG1a cell suspension at a

concentration of 10^6 cells/mL was perfused through the tubes at a shear stress of 2.5 dyne/cm^2 for 5 minutes. Flow was then stopped and the syringes in the syringe pump used to withdraw the cell suspension from the cell source through the tubes was replaced with syringes containing 5 mM EDTA (VWR Inc., West Chester, PA) in PBS-. The syringe pump was switched from withdraw to infuse and a tube volume was pumped slowly through each tube. The EDTA solution was allowed to sit in the tubes for 10 minutes and then another tube volume of EDTA solution was pumped slowly through the tubes to clear unbound cells. The tubes were then scanned using video microscopy for the presence of adherent cells.

2.2.11 P-selectin Surface Density Measurements

Eight tubes were cut to a length of 20 cm. Four tubes were coated with halloysite nanotubes, and four were left uncoated as control tubes. Three nanotube-coated tubes and three control tubes were coated with varying concentrations of P-selectin-IgG in PBS- for two hours and then blocked for one hour with 5% milk protein. The remaining nanotube-coated tube and control tube were incubated with PBS- for 2 h and then blocked with 5% milk protein for 1 h. All tubes were then incubated with PBS+ saturated with Ca^{2+} to activate the adsorbed P-selectin and then with 100 μg/mL mouse anti-human CD62P (P-selectin) IgG in PBS+ for 2 h. The tubes were then washed thoroughly with PBS+ and then a solution of 200 μg/mL donkey anti-mouse IgG in PBS+ was incubated in all of the tubes for 2 h protected from light. The tubes were then washed thoroughly with PBS+. One tube at a time was placed on the microscope stage to avoid unequal photobleaching, and prior to being placed on the microscope, either end of

the tube was sealed using surgical clamps. Fluorescence micrographs were taken using a 4x objective so that a large area of background could be observed along with a large area of tube. Fifteen micrographs were collected at random locations along the length of each tube per tube. The exposure time for each image was set to 300 ms. Micrographs were analyzed off-line in ImageJ, with the regions of interest outlined and histograms of the brightness intensity within the regions of interest quantified. Mean intensity was determined from the histograms along with standard deviation. Individual micrographs were analyzed by subtracting the intensity of the regions outside the tube. Relative fluorescence intensity values were then corrected by the mean brightness values observed in the tubes that were not coated with P-selectin.

2.2.12 Pressure Drop Experiments

A 50 cm tube was coated with halloysite nanotubes as described above and compared with 50 cm uncoated control tubes. A 75 mL reservoir was connected to a tube and initially suspended using a ring stand so that the tube outlet reached the bench top. The vertical distance between the tube outlet at the bench top and the 75 mL mark in the reservoir was initially set at 84 cm. The reservoir was then filled to the 75 mL mark with water and this water level was manually maintained throughout the experiment. The tube outlet was placed in a dry weigh boat as a stop watch was simultaneously started and flow effluent was collected for 5 min, after which the tube outlet was immediately removed from the weight boat and the weigh boat was weighed to determine the volume of water that flowed through the tube. This was repeated three times for each tube at each of four heights: 84, 74, 64, and 49 cm.

2.2.13 Microsphere Perfusion Experiments

Nanotube-coated and control tubes were prepared as described above, coated with 2.5 μg/mL for two hours, and blocked for one hour. Fluorescent microspheres with mean diameter of 1.9 μm and an emission wavelength of 520 nm (Bangs Inc., Fishers, IN) were suspended in flow buffer at a concentration of 5 x 10^5 microspheres/mL and perfused through the tubes at various flow rates. For each flow rate, a location along either tube was chosen at random and the surface was brought into focus on the using a 20x objective with a 1.6x magnification changer engaged. Epifluorescence mode was then used to take 100 time lapse micrographs for times ranging from 10 to 75 ms, with 500 ms intervals between each micrograph, using a TRITC filter set. This was repeated so that 100 micrographs were recorded at three random locations along the length of each tube for each of the four flow rates examined: 0.03, 0.06, 0.095, and 0.13 mL/min. Microsphere velocity was determined by measuring the length of the in-focus streaks made by translating microspheres that were close to the tube surface. Measurements were taken using ImageJ and the scale was determined using a slide micrometer (Olympus, Tokyo, Japan).

2.2.14 Data Analysis

Rolling velocity was calculated by measuring the distance a rolling cell traveled over a 30 second interval. Rolling cells were defined as cells travelling in the direction of flow at an average velocity less than 50% of the hydrodynamic free stream velocity. Videos of rolling cells were taken at three random locations along the microtube. The

quantity of cells adherent to the surface was determined by recording micrographs at 30 random locations along the microtube. All errors are reported as standard error of the mean, and statistical significance was determined by unpaired t test using GraphPad Prism (GraphPad Software, San Diego, CA).

2.3 Results

2.3.1 Halloysite nanotube coating reduces cancer cell rolling velocity

Cell suspensions containing KG1a cells in flow buffer were perfused through capillary tubes at a range of flow rates imparting known shear stresses on the inner surface of the tubes. Tubes coated with halloysite nanotubes coated with P-selectin were compared to tubes coated with P-selectin alone, for a P-selectin incubating solution concentration of 2.5 μg/mL. The average rolling velocity of KG1a cells in the nanotube-coated tubes was significantly reduced, when compared to control tubes, across the range of shear stresses (Figure 2.1a).

2.3.2 Reduction of rolling velocity caused by nanotube coating attenuates with increased P-selectin surface density

The average rolling velocity of KG1a cells on the nanotube-coated surfaces was compared to that on control surfaces for a range of P-selectin surface densities. It was determined that the average velocity of rolling cells on the nanotube-coated surfaces was consistently lower than on the control surfaces, however the degree to which the average rolling velocity is reduced decreases as the surface density of P-selectin is increased.

This was seen at both lower and higher shear stress (Figures 2.1b and 2.1c, respectively). It was also determined that increasing the surface density of P-selectin significantly affected rolling velocity on the control surface, but had little effect on rolling velocity on the halloysite-coated surface at both lower and higher shear stress.

2.3.3 Halloysite nanotube coating increases the number of captured cells

The number of cells both rolling and statically adhered to the tube surface is a useful indication of the effectiveness of the surface at capturing target cell populations. The number of cells adhered to the inner surface of the tubes was analyzed as a function of shear stress as well as P-selectin surface density. A significant increase in the number of cells captured on the nanotube-coated surface was discovered (Figure 2.2a and b) for all P-selectin surface densities at both lower and higher shear stress (Figures 2.2c and 2.2d, respectively). Interestingly, the effect of the nanotube coating was found to be insensitive to the surface density of P-selectin.

2.3.4 Epithelial CTC exhibit similar behaviors on nanotube-coated surfaces

Colo205 colon carcinoma cells were perfused through tubes coated with halloysite nanotubes and E-selectin as well as tubes coated with E-selectin alone, and their behavior was compared over a range of shear stresses. Colo205 cells were used as a model of epithelial cancer CTC. For these experiments, the concentration of the E-selectin incubating solution was held constant at 2.5 μg/mL. The reduction in both the average rolling velocity as well as the increase in the number of adherent cells due to the

halloysite nanotube coating for Colo205 cells was found to be similar to those of KG1a cells (Figures 2.3a and b, respectively).

2.3.5 Halloysite nanotubes do not affect cell viability

Cells were cultured with and without halloysite nanotubes dispersed in their media, and cell viability was measured after 72 hours of incubation at 37°C and 5% CO_2, at humidified conditions. Treated cells were those cultured in 10% nanotube solution and 90% media, while untreated cells were cultured in 10% distilled water and 90% media. As shown in Figure 2.4, after 72 hour incubation neither KG1a nor Colo205 cells were affected by the presence of nanotubes in the media.

2.3.6 AFM shows nanotubes extend above surface

Atomic force microscopy images taken of nanotubes coated on a thin layer of poly-L lysine show that nanotubes are oriented in such a way that they extend above the surface a distance of hundreds of nanometers up to a micrometer. AFM images were taken of untreated nanotubes (Figure 2.5b) as well as treated nanotubes (Figure 2.5c), and it was found that the treatment procedure was effective at breaking up and removing large aggregates, however the height to which the nanotubes extended above the surface was largely preserved.

2.3.7 Immunofluorescence labeling shows increased P-selectin adsorption on nanotube coating

Fluorescence microscopy of tagged antibodies specific to P-selectin shows that the surface density of P-selectin adsorbed onto the nanotube-coated surfaces is significantly greater than on control tubes (Figure 2.6a). The relative difference in P-selectin surface density due to the nanotube coating attenuates as the concentration of the incubating P-selectin solution is increased. Representative micrographs are shown in Figures 2.6b and 2.6c. The fluorescence intensity value from each image was calculated relative to background brightness and mean fluorescence values for the tubes were subsequently corrected by the small amount of fluorescence seen due to tube autofluorescence or nonspecific antibody binding.

2.3.8 Specificity of selectin-mediated cell capture

In one set of experiments, tubes were prepared in an identical manner to the other rolling experiments and then incubated with a blocking anti-P-selectin antibody. A negligible number of cells were adherent in both the control or nanotube-coated tube (Figure 2.7). In another set of experiments, nanotube-coated and control tubes were prepared for rolling experiments and cells were allowed to adhere and roll. EDTA was then introduced to chelate all divalent ions in solution, thereby inactivating the P-selectin protein. After the tubes were gently washed to remove all unbound cells, no cells were observed to remain adhered in the tubes (Figure 2.8).

2.3.9 Halloysite nanotube coating does not alter the macroscale fluid dynamics

50 cm tubes in the presence or absence of a nanotube-coating were subjected to a constant hydrostatic pressure drop. At four different reservoir heights, the flow rate

through each tube was determined by weighing the fluid collected at the tube outlet over a 5 min period. The flow rates in the nanotube-coated and control tubes were calculated and the mean flow rates were found to differ by only 0.18% at a reservoir position of 84 cm, 0.71% at 74 cm, 0.77% at 64 cm, and 2.1% at 49 cm. Theoretical flow rates were calculated using the Hagen-Poiseuille equation, and the experimental values were shown to agree very well with theory (Figure 2.9a).

2.3.10 Halloysite nanotube coating alters surface separation distance of flowing particles

Fluorescent microspheres were perfused through nanotube-coated and control tubes at varying flow rates in order to obtain a local measurement of fluid velocity and wall shear rate. Time lapse fluorescence microscopy enabled calculation of individual microsphere velocities. Mean microsphere velocity was found to be significantly higher in the nanotube-coated tube than in the control tube, and the rate of increase of microsphere velocity seen with the increasing perfusion rate was found to be greater in the nanotube-coated tube (Figure 2.9b).

Several AFM images of nanotube-coated surfaces and untreated tube surfaces were analyzed to characterize their nanoscale topography (Figure 2.9c). The maximum surface feature height was evaluated in 20 random slices of the AFM images, and the mean maximum surface feature in the control tube was found to be ~30 nm, while the mean maximum feature height on the nanotube-coated surface was found to be ~505 nm. Since microspheres cannot flow any closer to the tube surface than the tallest roughness elements on the surface (*121*), the mean maximum feature height can be employed as limiting surface-to-surface separation parameters. The theoretical velocity of a

microsphere translating at a specified separation distance from a plane wall can be calculated based on the Stokes' flow solution for a sphere near a wall in shear flow

$$\frac{U}{hS} \sim \frac{0.7431}{0.6376 - 0.200\ln(\delta/a)} \tag{2.1}$$

where U is the microsphere velocity, h is the distance between the center of the microsphere and the wall, S is the shear rate, δ is the distance between the microsphere surface and the wall (the separation distance), and a is the microsphere radius (*122*) (Figure 2.9b). Prediction of the microsphere velocity based on the measured surface roughness agreed well with experimental observations with no adjustable parameters. This suggests that the microspheres translating over the nanotube-coated surface are translating in the same velocity field as those flowing over the control surface, however they are on a different streamline as forced by the larger roughness elements.

2.4 Discussion

In this study, I demonstrate that halloysite nanotube coatings can significantly enhance selectin-mediated cell adhesion to a microtube surface under flow, and that the cellular adhesion is mediated specifically by selectin binding (supplementary figures 1 and 2). Results were consistent with previous findings, specifically that rolling velocity was found to increase and the number of cells captured was found to decrease with increased shear stress. This is consistent with our intuitive understanding of cell adhesion via selectin molecules because increased shear stress imparts more force acting against the bonds between selectin molecules and its cell surface ligand as a cell rolls along a surface (*123*). Interestingly, rolling velocity profiles were found to have a close correlation to the nanotube coating concentration, shifting to faster velocities as the

nanotube coating was increasingly diluted (data not shown). Additionally, a steep decline in cell capture was observed for P-selectin concentrations below 2.5 μg/mL (Figure 2.10).

It was found that at low surface densities of selectin protein, there was a large difference in the rolling velocity between nanotube-coated and control surfaces, and this difference in rolling velocity decreased as the selectin surface density increased (figures 1B and 1C). This phenomenon could be explained by a saturation effect on the nanotube coating. When the relatively large sized halloysite nanotubes adhere to a surface the total area of the surface is necessarily increased, providing more area onto which selectin molecules can absorb. Thus for a given incubation concentration of selectin, there would be a greater *macroscopic* surface density of selectin protein on the nanotube-coated surface. An increased surface density of selectin protein would then result in a decreased rolling velocity due to a greater average number of bonds per cell, and more bonds that must break for the cell to continue rolling. This effect has been seen previously with smaller silica nanoparticles, having an average diameter of 15 nm (*124*).

Immunofluorescent measurements support the hypothesis that P-selectin density is significantly higher on the nanoparticle-coated surfaces, and that this difference is attenuated at the highest P-selectin incubation concentrations (figure 6A). It is important to note that the P-selectin antibody used is specific to the carbohydrate-recognition domain (CRD) of P-selectin, the domain of P-selectin which binds to cells (*125*). Therefore the assay detects only those P-selectin molecules that are available for binding in the proper orientation (*126*).

The number of adherent cells on the surfaces was additionally investigated to characterize the impact of the nanotube coating. Significant enhancement in capture was

observed for all conditions. However, as the selectin surface density on the surfaces was increased, the effect of the nanotube coating was not found to attenuate as it did with rolling velocity. Consequently, the straightforward explanation of increased surface area caused by the nanotubes does not fully explain this trend because there is no saturation of the number of cells captured on the surfaces.

A likely explanation for the observed phenomena takes into account the reported dimensions of the nanotubes: nanotubes are situated such that they stick up off of the surface, presenting selectin molecules farther out into the flow profile (figure 5A). Due to hydrodynamic lubrication forces, the cell sedimentation time scale increases as $1/\delta$ (where δ is the surface-to-surface separation distance) as it approaches the wall (*121*). Thus, a conceptual explanation is that selectin molecules are presented into this lubrication region close to the surface, and flowing cells that would otherwise require more sedimentation time to contact the surface are captured earlier and brought to the surface and proceed to roll. Therefore, as the selectin incubation concentration is increased, more selectin molecules are presented into the flow field and cells are captured at a higher rate. This phenomenon would not be produced by adding more selectin to a flat surface, thus the effect of halloysite on the number of cells captured does not diminish.

Atomic force microscopy was performed to investigate the orientation of nanotubes on the surfaces and it was found that nanotubes indeed extend above the surface several hundred nm (Figure 2.5b). It was also found that the treatment procedure developed for the stock halloysite solution that was required to produce homologous solutions for all experiments did not significantly change the topography of the nanotube

coating, as those nanotubes were raised to a similar height above the surface with a comparable surface density of peaks (Figure 2.5c).

The effect that the nanotube coating has on the fluid dynamics within the microtubes was examined in two separate experiments designed to probe both the macroscopic and microscopic flow behavior. In one experiment, the flow rate was measured while pressure drop across the tube length was set to a constant value by maintaining the fluid level in a reservoir. The reservoir then moved to different heights to create different constant pressure drops. Negligible difference in the bulk flow rate was observed in the nanotube-coated and control tubes. A range of Reynolds numbers from 2 to 15 was studied, which extends beyond the range of flow rates used in the adhesion experiments. This is well within the laminar regime, and thus the friction factor is expected to be independent of surface roughness (*127*). It follows, then, that the Hagan-Poiseuille equation can be used to estimate the fluid flow rate in either tube, and comparison with experimental results confirms this (Figure 2.9a). The Hagan-Poiseuille equation for laminar flow of a viscous, incompressible fluid through a tube relates the pressure drop and volumetric flow rate as

$$\Delta P = \frac{8\mu LQ}{\pi r^4} \tag{2.2}$$

where ΔP is pressure drop, μ is the dynamic viscosity of the fluid, L is the tube length, Q is the volumetric flow rate, and r is the tube radius. Since ΔP, μ, and L are controlled in the experiment and Q was found to be identical between tubes, it may be concluded that the tubes have an equal hydraulic radius.

The microscale fluid dynamics was examined in nanotube-coated tubes and compared to those in control tubes. Time-lapse video microscopy of fluorescent

microspheres initially suggested that the fluid dynamics close to the tube surface is different, due to the observation that microspheres travel faster in nanotube-coated tubes than in control tubes. However, since it was previously determined that the bulk fluid flow corresponds to the same tube diameter with or without the nanotube coating, another explanation for this observation is that the microspheres in the nanotube-coated tube are translating on a streamline that is farther away from the tube surface.

A negatively buoyant particle flowing along a surface can only approach as close to the surface as the largest roughness features on the surface (*121*). This is evident when the sedimentation velocity of a microsphere close to a surface is considered. The sedimentation velocity can be calculated using Brenner's correction for Stokes' Law (*128*) as implemented by Smart and Leighton (*129*)

$$F = 6\pi\mu a^2 U_S \lambda \tag{2.3}$$

where U_S is the sphere sedimentation rate and λ is the correction term

$$\lambda = \frac{4}{3}\sinh(\alpha)\sum_{n=1}^{\infty}\left[\left(\frac{n(n+1)}{(2n-1)(2n+3)}\right)\left(\frac{2\sinh(2n+1)\alpha+(2n+1)\sinh(2\alpha)}{4\sinh^2\left(n+\frac{1}{2}\right)\alpha-(2n-1)^2\sinh^2(\alpha)}-1\right)\right] \tag{2.4}$$

$$\alpha = \cosh^{-1}(1+\delta) = \ln\left(1+\delta+\sqrt{\delta(2+\delta)}\right) \tag{2.5}$$

By performing a force balance on the microsphere, balancing the corrected drag force and the net buoyancy force $\frac{4}{3}\pi a^3 \Delta\rho g$, the sedimentation velocity is predicted to be $5\text{x}10^{-5}$ nm/s at δ = 505 nm and $3\text{x}10^{-6}$ nm/s at δ = 30 nm. Considering that the microspheres are translating on the order of 10^2-10^3 μm/s, and encountering roughness features on the order of one every 10 μm, the microspheres are expected to translate at a constant distance from the surface, with the distance defined by the tallest roughness features. The height of nanotubes sticking into the flow is sufficient to explain the separation distance

of microspheres flowing over them, providing further evidence that the fluid flow field in the tube is unaltered by the presence of the nanotube coating, whereas the particle/cell convection will be altered (Figure 2.9c). Therefore the shear rate in the tube, and the shear stress at the tube surface as predicted by Poiseuille Law, for a given flow rate is equivalent to smooth surfaces. Since the tube radius is about 150-fold larger than that of a microsphere, and about 150-fold larger than the characteristic δ, the error in assuming a planar geometry is negligible (*130*).

Previous studies have demonstrated that nanoparticles can be cytotoxic to cells (*131-135*). This, however, was not found to be the case with halloysite nanoparticles (Figure 2.4). This finding, coupled with the equally enhanced capture of leukemic and epithelial CTC, indicates that halloysite nanotube coatings provide an effective and practical method for enhancing cancer cell capture, and ultimately promises to advance the feasibility of individualized cancer treatment.

2.5 Conclusions

In this study, I demonstrate a novel method for enhancing the capture of viable CTC in a selectin-functionalized microtube by altering the surface topography with immobilized halloysite nanotubes. The effect of the nanotubes on cell adhesion was demonstrated by significant changes in the average cell rolling velocity and the number of CTC captured, and was explained by a conceptual model in which the nanotubes are oriented to extend above the surface and into the flow. This model was subsequently supported by atomic force microscopy and immunofluorescence quantification of P-selectin density, showing a straightforward engineering approach to an intrinsic physical

obstacle. The nanotube coating was analyzed in the device and found to have negligible effect on the macroscopic fluid dynamics, but alters the equilibrium streamline of convecting particles or cells. The device proposed in this study, characterized by a halloysite nanotube coating, provides a potential for successful capture of CTC from individual patients in a clinical setting, improving cancer detection and therapy.

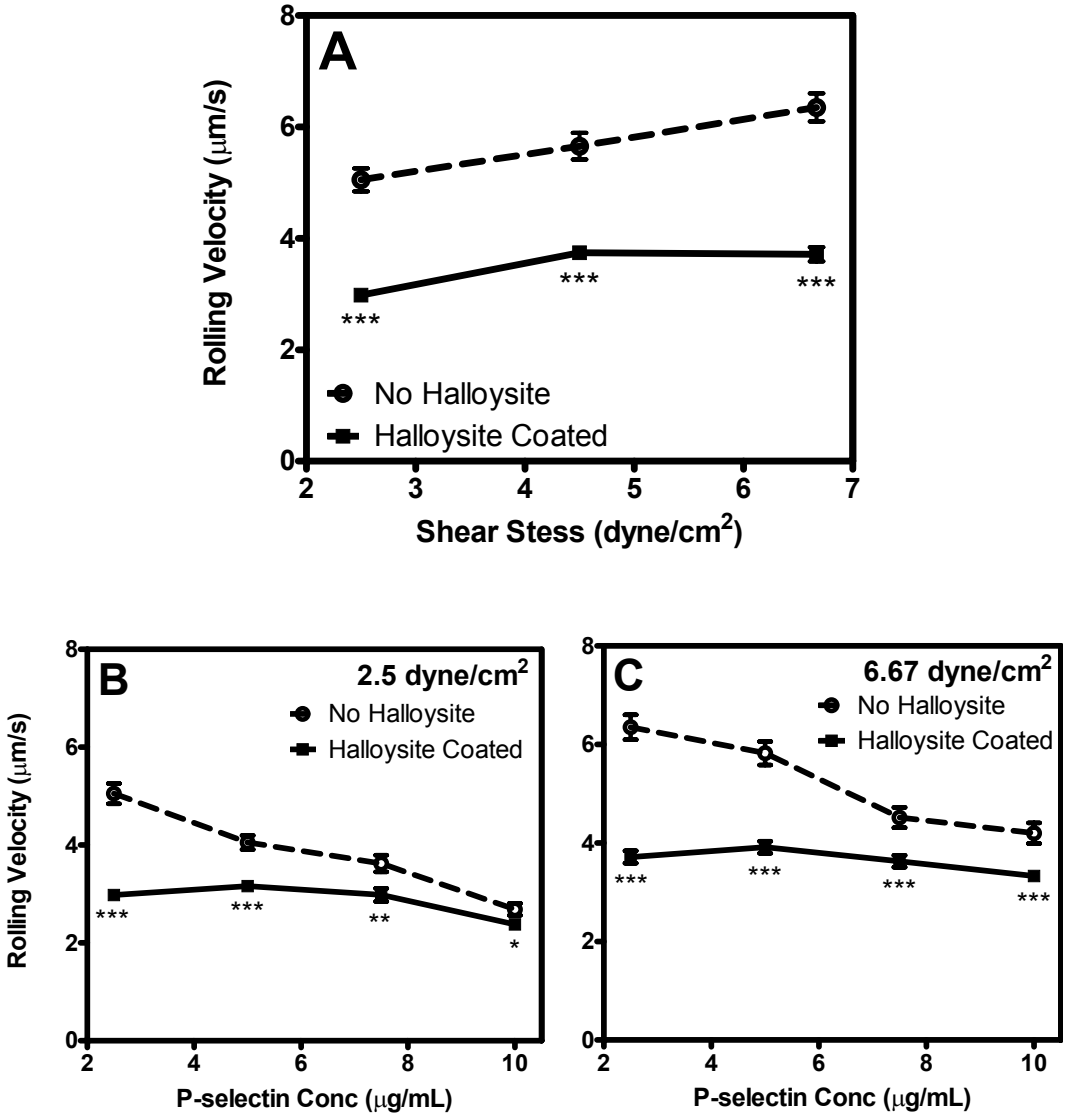

Figure 2.1. (A) Average rolling velocity of KG1a cells is reduced on halloysite nanotube-coated surface across the physiological range of shear stress. P-selectin was incubated at a concentration of 2.5 μg/mL. Average rolling velocity of KG1a cells as a function of the P-selectin incubation concentration at lower (B) or higher (C) shear stress. Errors are SEM (N=3), *** $P < 0.001$, ** $P < 0.01$, * $P < 0.05$.

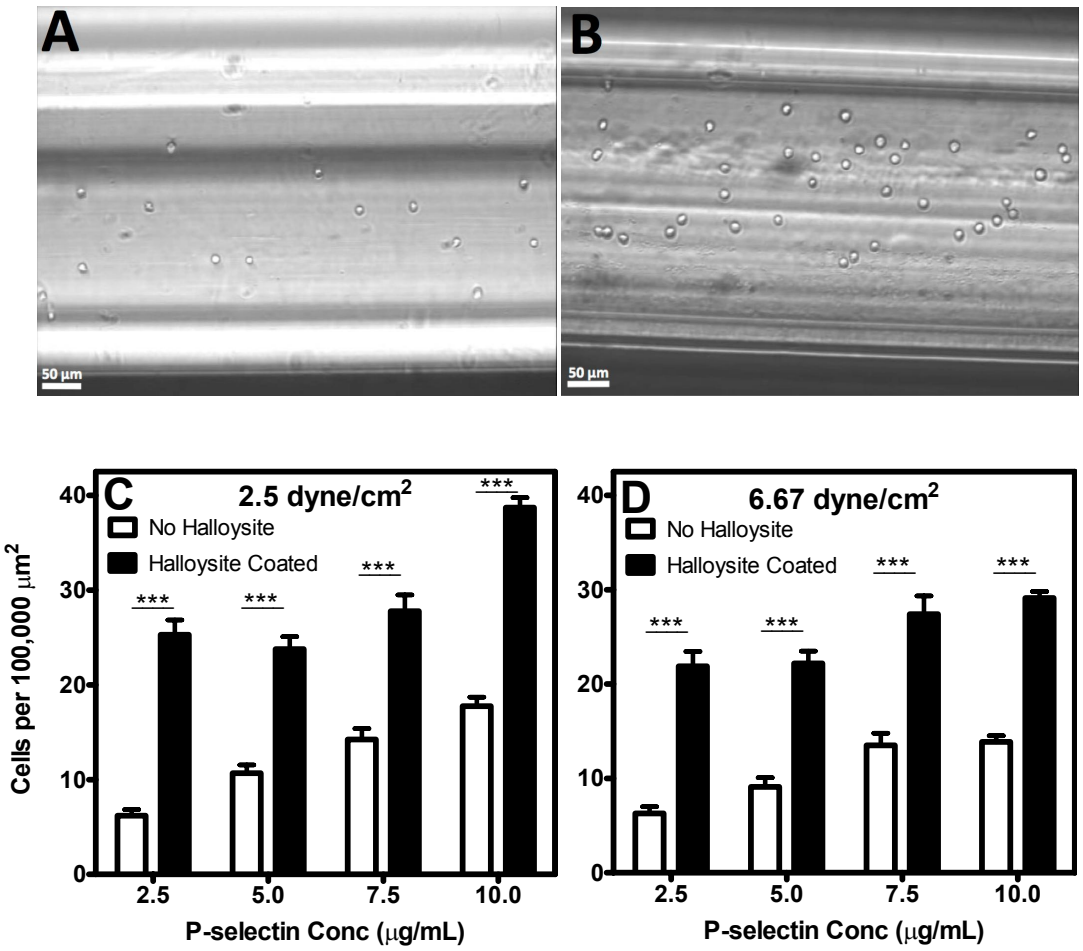

Figure 2.2. The number of cells captured is noticeably enhanced as seen in representative micrographs of cells rolling on control (A) and nanotube-coated (B) surfaces. Number of KG1a cells captured per area of surface as a function of the selectin incubation concentration at lower (C) or higher (D) shear stress. Errors are SEM (N=3), *** $P < 0.001$.

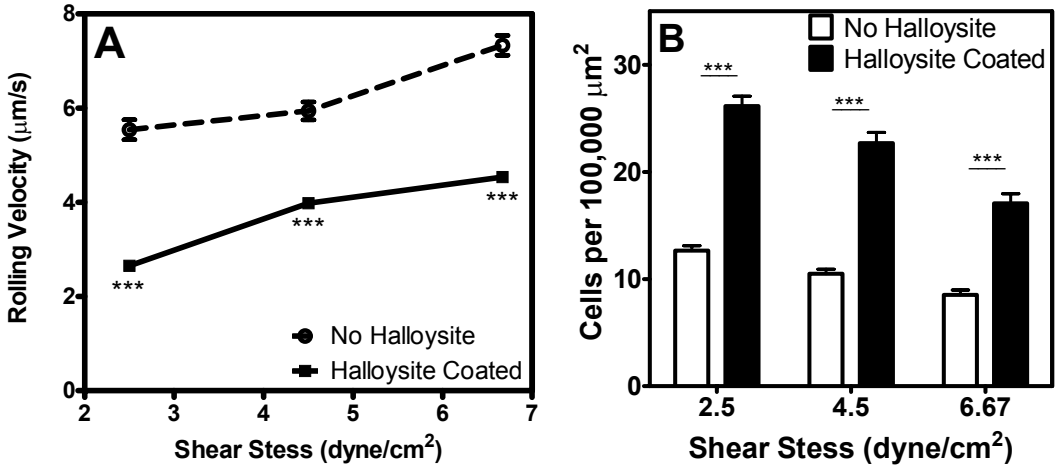

Figure 2.3. Halloysite nanotube coating on the inner surface of microtubes enhances Colo205 epithelial cancer cell capture as quantified by rolling velocity (A) and the number of cells captured per area of tube surface (B). Errors are SEM (N=3), *** $P < 0.001$.

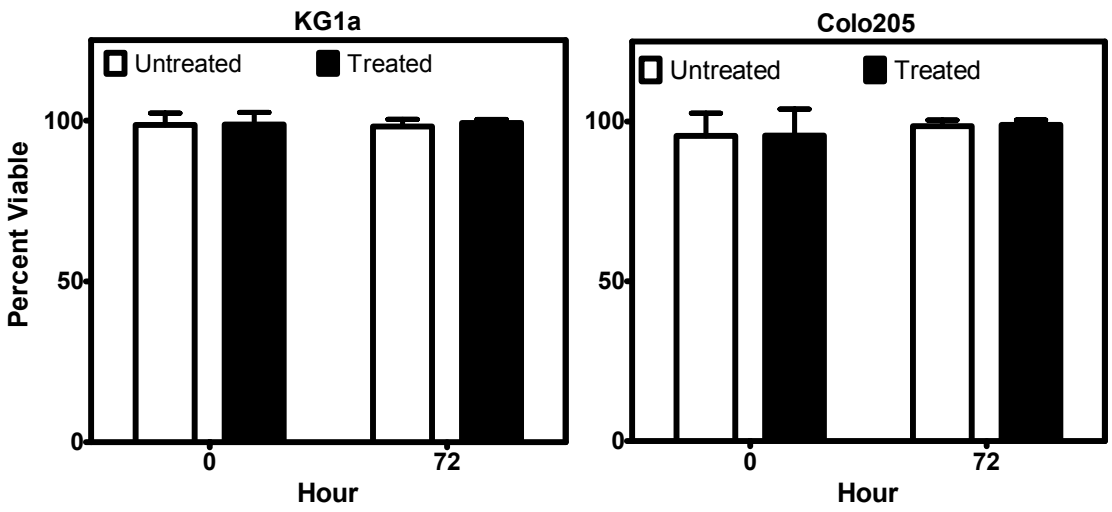

Figure 2.4. Incubation with nanotubes dispersed in media had no effect on the viability of KG1a or Colo205 cells over a 72-hour period. "Treated" bars represent the average viability of cells incubated in 10% halloysite nanotube and 90% media, while "untreated" bars represent cells incubated in 10% distilled water and 90% media. Errors are SEM (N=3), *** $P < 0.001$.

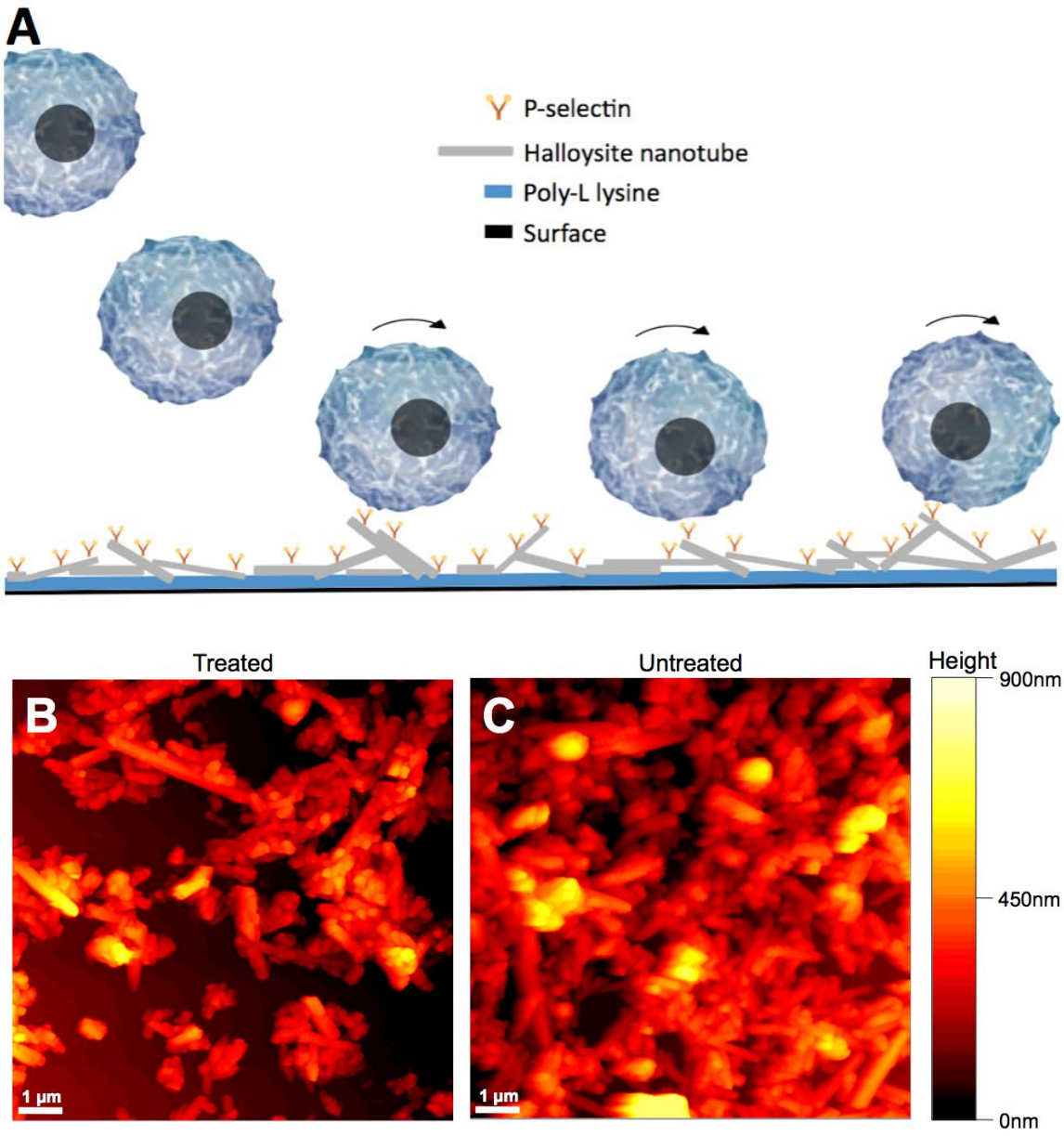

Figure 2.5. (A) Schematic of the hypothesized nanoscale surface topography in which individual nanotubes stick up off of the surface and facilitate early cell capture as cells sediment to the surface. Representative atomic force microscopy images of halloysite nanotubes immobilized on surfaces after (B) and before (C) treatment to break up and remove large aggregates. This treatment procedure was required to produce more reproducible cell adhesion behavior.

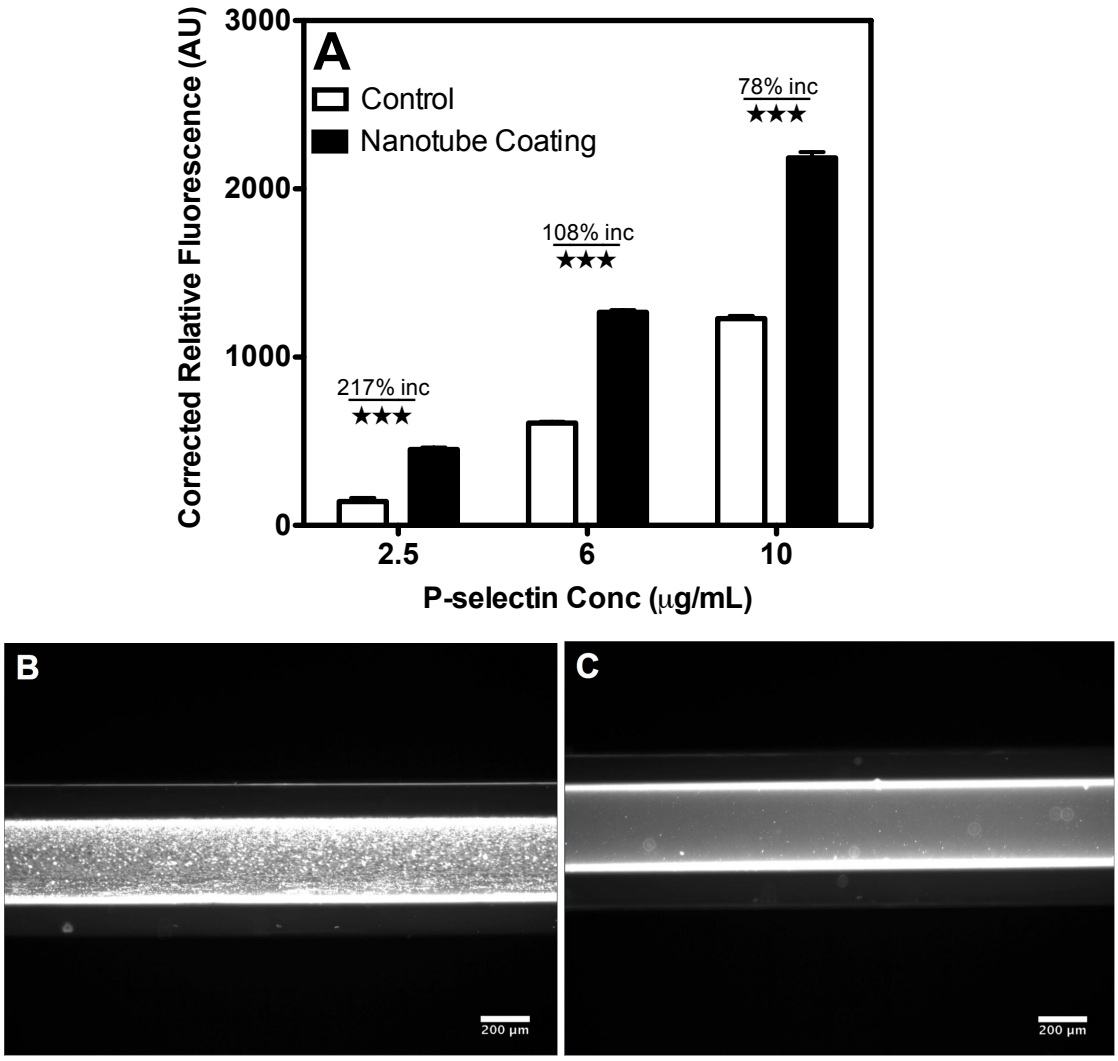

Figure 2.6. (A) Comparison of the immunofluorescence of nanotube-coated and control surfaces for a range of P-selectin incubating solution concentrations. Representative micrographs of a halloysite-coated tube (B) and control tube (C) both incubated with 10 μg/mL P-selectin solution. Errors are SEM, *** $P < 0.001$.

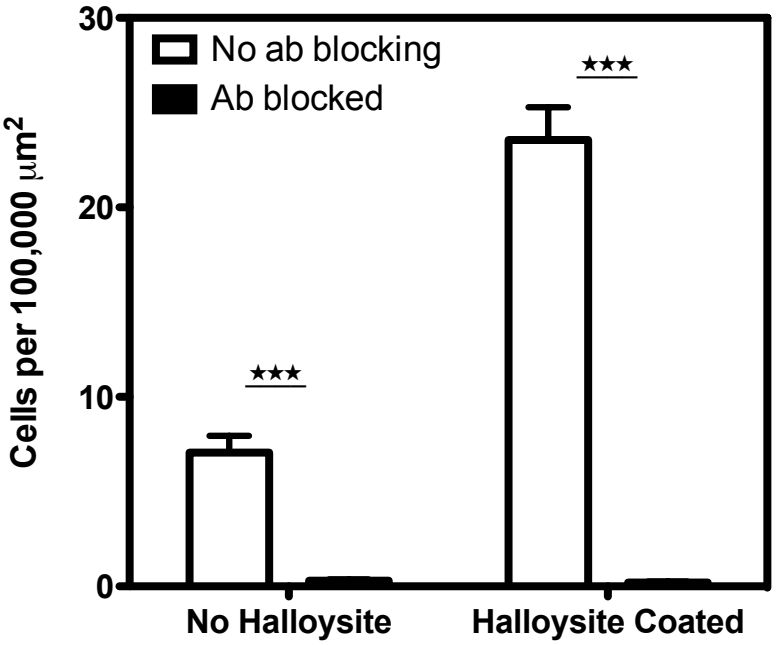

Figure 2.7. The number of cells captured in tubes with and without halloysite nanotube coating were compared to the number of cells captured in tubes that had been pre-incubated with an P-selectin blocking antibody. 2.5 μg/mL P-selectin was incubated in each tube and data was collected at a shear stress of 2.5 dyne/cm^2. Errors are SEM, ∗∗∗ $P < 0.001$.

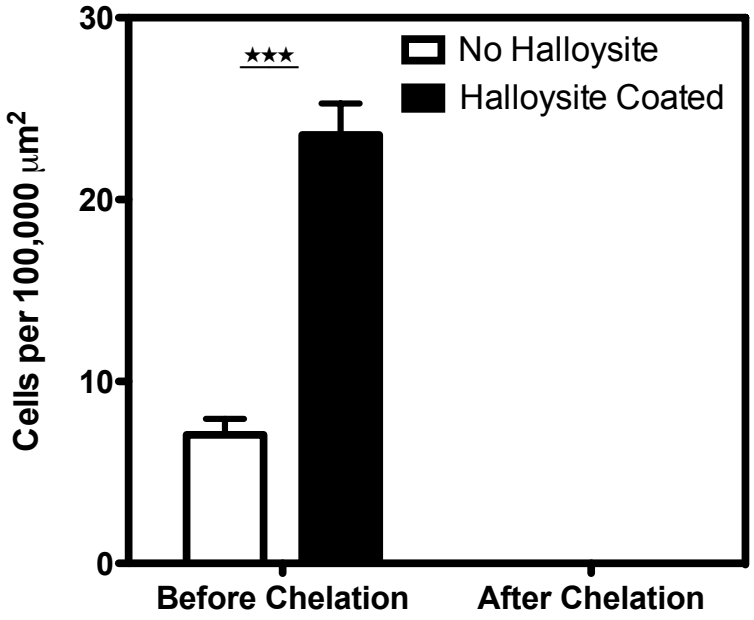

Figure 2.8. The number of cells captured in tubes with and without nanotube coating was assessed before and after chelation of Ca^{2+} by 5 mM EDTA. Ca^{2+} is required to activate P-selectin. All tubes were coated with 2.5 μg/mL P-selectin and data was collected at a shear stress of 2.5 dyne/cm^2. Errors are SEM, ∗∗∗ $P < 0.001$.

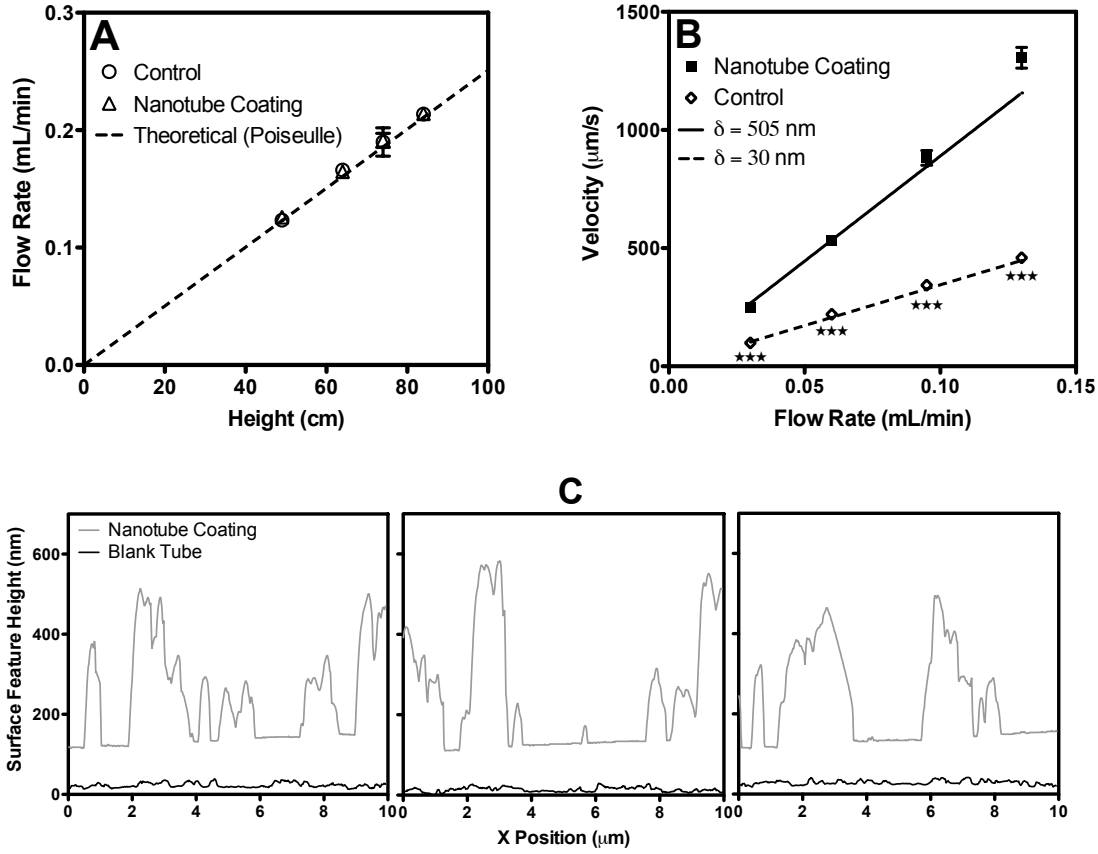

Figure 2.9. (A) The pressure drop across 50cm nanotube-coated and control tubes was held at a constant value and the resulting flow rate through either type of tube was calculated. The pressure drop was varied by changing the height of the fluid reservoir relative to the tube outlet, and the results were compared to theory with no adjustable parameters. (B) Fluorescent microspheres were perfused through tubes and the velocity of microspheres near the tube surface was determined as a function of flow rate. Maximum surface roughness heights were determined from AFM data, and the mean maxima were found to be 505 nm on the nanotube coating and 30 nm on the blank control surface. Theoretical microsphere velocities were calculated by equation 1 for surface-to-surface separation distances (δ) of 505 nm and 30 nm, and found to agree with experimental observations with no adjustable parameters. (C) Representative surface

features from AFM images. The nanotube coating profiles are shifted up 100 nm for ease of viewing. Errors are SEM, $***$ $P < 0.001$.

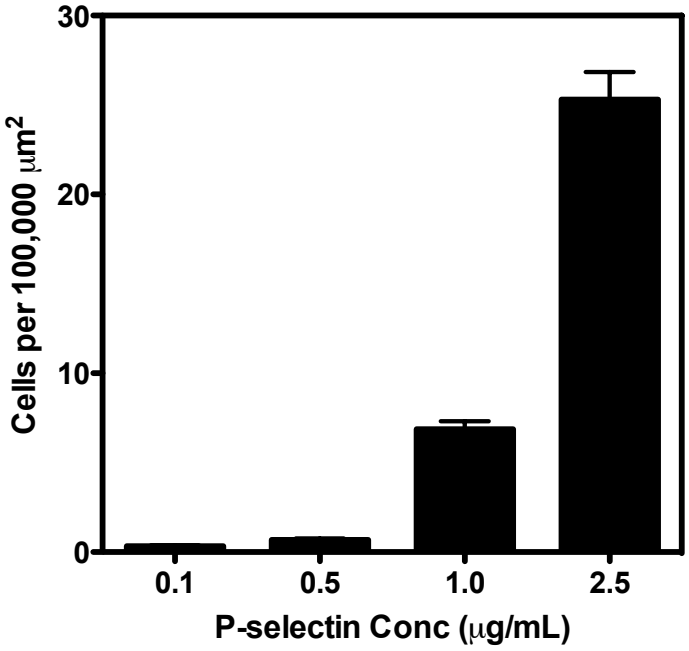

Figure 2.10. KG1a cells captured on low P-selectin concentrations at a shear stress of 2.5 dyne/cm^2 show that there is a steep decrease in cellular adhesion below the P-selectin concentration of 2.5 μg/mL. Errors are SEM.

2.6 References

99. P. Paterlini-Brechot, N. L. Benali, Circulating tumor cells (CTC) detection: clinical impact and future directions. *Cancer Lett* **253**, 180-204 (2007).

100. K. Rana, J. L. Liesveld, M. R. King, Delivery of apoptotic signal to rolling cancer cells: a novel biomimetic technique using immobilized TRAIL and E-selectin. *Biotechnol Bioeng* **102**, 1692-1702 (2009).

101. C. Wittekind, M. Neid, Cancer invasion and metastasis. *Oncology* **69 Suppl 1**, 14-16 (2005).

102. Y. S. Chang *et al.*, Mosaic blood vessels in tumors: frequency of cancer cells in contact with flowing blood. *Proc Natl Acad Sci U S A* **97**, 14608-14613 (2000).

103. P. Gassmann, A. Enns, J. Haier, Role of tumor cell adhesion and migration in organ-specific metastasis formation. *Onkologie* **27**, 577-582 (2004).

104. W. J. Allard *et al.*, Tumor cells circulate in the peripheral blood of all major carcinomas but not in healthy subjects or patients with nonmalignant diseases. *Clin Cancer Res* **10**, 6897-6904 (2004).

105. P. C. Tong *et al.*, White blood cell count is associated with macro- and microvascular complications in chinese patients with type 2 diabetes. *Diabetes Care* **27**, 216-222 (2004).

106. V. Zieglschmid, C. Hollmann, O. Bocher, Detection of disseminated tumor cells in peripheral blood. *Crit Rev Clin Lab Sci* **42**, 155-196 (2005).

107. P. T. Went *et al.*, Frequent EpCam protein expression in human carcinomas. *Hum Pathol* **35**, 122-128 (2004).

108. S. D. Narasipura, J. C. Wojciechowski, N. Charles, J. L. Liesveld, M. R. King, P-Selectin coated microtube for enrichment of CD34+ hematopoietic stem and progenitor cells from human bone marrow. *Clin Chem* **54**, 77-85 (2008).

109. J. C. Wojciechowski *et al.*, Capture and enrichment of CD34-positive haematopoietic stem and progenitor cells from blood circulation using P-selectin in an implantable device. *Br J Haematol* **140**, 673-681 (2008).

110. N. Charles, J. L. Liesveld, M. R. King, Investigating the feasibility of stem cell enrichment mediated by immobilized selectins. *Biotechnol Prog* **23**, 1463-1472 (2007).

111. M. R. King, L. Western, K. Rana, J. L. Liesveld, *J Bionic Engr.*, (in press).

112. H. F. Langer, T. Chavakis, Leukocyte-endothelial interactions in inflammation. *J Cell Mol Med* **13**, 1211-1220 (2009).

113. L. M. Coussens, Z. Werb, Inflammation and cancer. *Nature* **420**, 860-867 (2002).

114. D. J. Goetz, M. E. el-Sabban, D. A. Hammer, B. U. Pauli, Lu-ECAM-1-mediated adhesion of melanoma cells to endothelium under conditions of flow. *Int J Cancer* **65**, 192-199 (1996).

115. Y. J. Kim, L. Borsig, H. L. Han, N. M. Varki, A. Varki, Distinct selectin ligands on colon carcinoma mucins can mediate pathological interactions among platelets, leukocytes, and endothelium. *Am J Pathol* **155**, 461-472 (1999).

116. F. W. Orr, H. H. Wang, R. M. Lafrenie, S. Scherbarth, D. M. Nance, Interactions between cancer cells and the endothelium in metastasis. *J Pathol* **190**, 310-329 (2000).

117. F. W. Orr, H. H. Wang, Tumor cell interactions with the microvasculature: a rate-limiting step in metastasis. *Surg Oncol Clin N Am* **10**, 357-381, ix-x (2001).

118. S. R. Levis, P. B. Deasy, Characterisation of halloysite for use as a microtubular drug delivery system. *Int J Pharm* **243**, 125-134 (2002).

119. R. R. Price, B. P. Gaber, Y. Lvov, In-vitro release characteristics of tetracycline HCl, khellin and nicotinamide adenine dineculeotide from halloysite; a cylindrical mineral. *J Microencapsul* **18**, 713-722 (2001).

120. H. M. Kelly, P. B. Deasy, E. Ziaka, N. Claffey, Formulation and preliminary in vivo dog studies of a novel drug delivery system for the treatment of periodontitis. *Int J Pharm* **274**, 167-183 (2004).

121. M. R. King, D. T. Leighton, Measurement of the inertial lift on a moving sphere in contact with a plane wall in a shear flow. *Phys Fluids* **9**, 1248-1255 (1997).

122. A. J. Goldman, R. G. Cox, H. Brenner, Slow Viscous Motion of a Sphere Parallel to a Plane Wall .2. Couette Flow. *Chemical Engineering Science* **22**, 653-& (1967).

123. D. A. Hammer, S. M. Apte, Simulation of cell rolling and adhesion on surfaces in shear flow: general results and analysis of selectin-mediated neutrophil adhesion. *Biophys J* **63**, 35-57 (1992).

124. W. Han, B. A. Allio, D. G. Foster, M. R. King, *ACS Nano*, (in press).

125. D. Torgersen, N. P. Mullin, K. Drickamer, Mechanism of ligand binding to E- and P-selectin analyzed using selectin/mannose-binding protein chimeras. *J Biol Chem* **273**, 6254-6261 (1998).

126. D. Lee, M. R. King, Microcontact Printing of P-Selectin Increases the Rate of Neutrophil Recruitment Under Shear Flow. *Biotechnology Progress* **24**, 1052-1059 (2008).

127. S. G. Kandlikar, S. Garimella, D. Li, S. Colin, M. R. King, *Heat Transfer and Fluid Flow in Minichannels and Microchannels*. (Elsevier Ltd, ed. 1, 2006), vol. 1.

128. H. Brenner, The Slow Motion of a Sphere through a Viscous Fluid Towards a Plane Surface. *Chemical Engineering Science* **16**, 242-251 (1961).

129. J. R. Smart, D. T. Leighton, Measurement of the Hydrodynamic Surface-Roughness of Noncolloidal Spheres. *Physics of Fluids a-Fluid Dynamics* **1**, 52-60 (1989).

130. M. R. King, Cell-surface adhesive interactions in microchannels and microvessels. *Microscale Thermophysical Engineering* **9**, 255-264 (2005).

131. J. Zhao *et al.*, Titanium dioxide (TiO2) nanoparticles induce JB6 cell apoptosis through activation of the caspase-8/Bid and mitochondrial pathways. *J Toxicol Environ Health A* **72**, 1141-1149 (2009).

132. P. Wick *et al.*, The degree and kind of agglomeration affect carbon nanotube cytotoxicity. *Toxicol Lett* **168**, 121-131 (2007).

133. C. M. Sayes *et al.*, Functionalization density dependence of single-walled carbon nanotubes cytotoxicity in vitro. *Toxicol Lett* **161**, 135-142 (2006).

134. S. Kang, M. S. Mauter, M. Elimelech, Physicochemical determinants of multiwalled carbon nanotube bacterial cytotoxicity. *Environ Sci Technol* **42**, 7528-7534 (2008).

135. J. Chen *et al.*, Differential Cytotoxicity of Metal Oxide Nanoparticles. *J Experimental Nanoscience* **3**, 321-328 (2008).

CHAPTER 3 – MICROTUBE DEVICE FOR SELECTIN-MEDIATED CAPTURE OF VIABLE CIRCULATING TUMOR CELLS FROM BLOOD

This section is adapted from the following publication: AD Hughes, J Mattison, LT Western, JD Powderly, BT Greene, and MR King, Microtube device for selectin-mediated capture of viable circulating tumor cells from blood, *Clinical Chemistry* **2012**, 58(5):846-53.

3.0 Abstract

3.0.1 Background

Circulating tumor cells (CTC) can be used clinically to treat cancer. As a diagnostic tool the CTC count can be used to follow disease progression and as a treatment tool CTC can be used to rapidly develop personalized therapeutic strategies. To be effectively used, however, CTC must be isolated at high purity without inflicting cellular damage.

3.0.2 Methods

A microscale flow device was designed with a functionalized surface of E-selectin and antibody molecules against epithelial markers. The device was additionally enhanced using a halloysite nanotube coating. Model samples were created in which a known number of labeled CTC were suspended in healthy whole blood to determine device capture efficiency. Primary CTC were then isolated from buffy coat samples of patients diagnosed with metastatic cancer and cultured.

3.0.3 Results

Approximately 50% of CTC were captured from model samples. Samples from 12 metastatic cancer patients and 8 healthy participants were processed in nanotube-coated or smooth devices to isolate CTC. 20-704 viable CTC per 3.75 mL sample were isolated,

achieving purities of 18-80% CTC. The nanotube-coated surface achieved significantly higher capture purities ($p = 0.0004$). Experiments suggested that this increase in purity was due to suppression of leukocyte spreading.

3.0.4 Conclusions

The device successfully isolates viable CTC from both blood and buffy coat samples. The approximately 50% capture rate with purities >50% using the nanotube coating demonstrates the functionality of this device in a clinical setting and opens the door for personalized cancer therapies.

Keywords

Circulating tumor cell, E-selectin, halloysite nanotubes, cell isolation, shear stress.

3.1 Introduction

Cancer patient morbidity is highly congruent with metastatic dissemination of cancer cells. Many studies have led to the conclusion that the prevalence of circulating tumor cells (CTC) in peripheral blood correlates with disease severity (*136-139*). It follows, therefore, that the ability to capture CTC in peripheral blood would potentiate cancer study, diagnosis, and treatment on a patient-to-patient basis (*140*). The prevalence of CTC in blood is decidedly low, ranging from a few to several hundred CTC per 7.5 mL blood (*138*). Detection of rare CTC is complicated by the fact that similarly sized leukocytes are much more prevalent, ranging from 3.5 to 12.5 x 10^6 per mL (*141*).

Most current methods for CTC detection begin with Ficoll density centrifugation to separate leukocytes and CTC from the remainder of whole blood, and use of antibodies or PCR to identify CTC. CellSearch®, the only FDA-cleared system for CTC enumeration (*139*), separates CTC from leukocytes using magnetic beads coated with anti-epithelial cellular adhesion molecule (EpCAM) antibodies (*138*). In a separate approach, CTC and leukocytes separated by Ficoll centrifugation are lysed and RT-PCR is performed to detect mutated mRNA or epithelial markers. A result of both methods is that the CTC are destroyed. The ability to keep CTC viable would provide not only individualized disease prognosis, but also a means for rapid *in vitro* analyses of the efficacy of different therapies on a patient-to-patient basis.

Devices to capture viable CTC have been developed in recent years, generally involving microfluidic chips with CTC-specific antibodies coated onto the inner lumen. The first generation was the “CTC-chip”, which is a chip containing anti-EpCAM coated microposts (*142*). An improvement on the CTC-chip device is the “GEDI chip” wherein

the microposts are arranged in such a way as to maximize CTC-post collisions and minimize leukocyte-post collisions based cell size (*143*). The slow nature of EpCAM binding requires low flow rates for CTC capture, posing a challenge for feasible clinical use.

The microscale flow device previously developed by our group has been used to capture hematopoietic stem and progenitor cells as well as cultured tumor cells from flow without causing any cellular damage to the captured cells (Figure 3.1) (*144-146*). The device consists of a 300 μm I.D. microtube coated with selectins. In vivo, selectin binding is highly specific with rapid dynamics, allowing fast-flowing leukocytes to bind and roll on the endothelium. If appropriately stimulated while rolling, leukocytes will bind firmly to the endothelium via integrins and subsequently extravasate (*147*). CTC may utilize the same process to metastasize to new tissues (*148-154*). CTC exhibit stable rolling adhesion to a selectin-coated surface, providing a rapid method for CTC enrichment (*155*). CTC can be more specifically targeted using a bimolecular surface consisting of both selectin molecules to induce slow rolling and CTC-specific antibodies.

Recent work has examined naturally-occurring halloysite nanotubes, nanoparticles composed of an aluminosilicate mineral having a typical diameter of ~300nm, variable length that can be >1μm, and negative surface charge at neutral pH (*156*). Enhanced capture of cultured cancer cells in buffer is accomplished with the nanotube coating because of the ability of the rough surface to overcome innate physical limitations to the capture of cells in microfluidic devices (*157*). In this study I validated the utility of this device by first isolating cancer cells spiked into whole blood. I then demonstrated the potential for use in a clinical setting by isolating CTC in 14 blood

samples from 12 patients diagnosed with metastatic breast, prostate, lung, or ovarian cancer.

3.2 Materials and Methods

3.2.1 Reagents and Antibodies

RPMI 1640 cell culture media, fetal bovine serum albumin, penicillin-streptomycin, 1X phosphate buffered saline pH 7.4 (PBS), goat anti-mouse IgG Alexafluor 488, and DAPI were purchased from Invitrogen. Recombinant human E-selectin (rhE-selectin-IgG) and P-selectin (rhE-selectin-IgG) fused to IgG were obtained from R&D Systems. Mouse anti-human PSMA monoclonal IgG was purchased from Abcam. Halloysite nanotubes in water (6.6% wt.) was provided by NaturalNano. Protein-G was purchased from EMD Biosciences. Blotting grade blocker non-fat dry milk was obtained from Bio-Rad Laboratories.

3.2.2 Cell Capture from Spiked Blood

An independent calibration was developed by our laboratory to estimate the total number of cells in the microtube using the following technique: Cells in flow buffer were drawn into a 300μm i.d. Micro-Renathane microtube (Braintree Scientific) blocked with 5% milk protein and allowed to settle for 10 min. Twenty images were recorded at random locations along the length of the microtube, and the average number of cells per micrograph area was computed. All cells within the microtube were then eluted and the total number of cells was determined in triplicate using a hemacytometer. A calibration

factor to correlate the number of cells in a micrograph to the total number of cells in the microtube was thus calculated from the experimental data. The supplementation of fluorescent KG1a leukemic cells into whole blood and their subsequent capture on the selectin-functionalized microtube, determined previously (20), was used to estimate cancer cell capture efficiency.

3.2.3 Acquisition and Preparation of Primary Cells

After obtaining informed consent peripheral whole blood (7.5 mL) was collected by venipuncture at BioCytics Inc. (Huntersville, NC) from Stage IV cancer patients seen at Carolina BioOncology Institute, PLLC. Blood samples were from six breast cancer patients (designated Bre-1 through -6), three prostate cancer patients (designated Pro-1 through -3), two lung cancer patients (designated Lun-1 and -2), and one ovarian cancer patient (designated Ova-1). Two samples were collected from patient Pro-2, approximately 2 months apart (designated Pro-2(1) and (2)). In some cases, whole blood was collected in BD Vacutainer EDTA tubes (BD BioSciences) and these tubes were immediately shipped overnight at ambient temperature to Cornell for processing. For buffy coat isolated and frozen at BioCytics, whole blood was collected in BD Vacutainer CPT tubes (BD BioSciences). CPT tubes were centrifuged at room temperature for 20 min at 1500 x *g*. Plasma was discarded and isolated buffy coat was rinsed once with 1X PBS. After rinsing, buffy coat was frozen in freezing media (70% RPMI, 20% FBS, 10% DMSO) and transferred to liquid nitrogen until shipment. Frozen buffy coat was shipped to Cornell overnight on dry ice. Frozen samples were rapidly thawed to 37°C and treated with 20 μg/mL DNAse I. Cells were washed twice with RPMI media and then

resuspended in media and incubated at 37°C and 5% CO_2 under humidified conditions for 3 h.

3.2.4 Primary CTC Capture

Buffy coat samples were washed twice with PBS by centrifugation at 120 x *g* for 10 min to remove the culture media, and resuspended in PBS saturated with Ca^{2+}. MicroRenathane (MRE) microtubes were coated with one microtube volume (35.3 μL) of 10 μg/mL Protein G for 1.5 h, followed by one microtube volume of a solution containing 5 μg/mL E-selectin-IgG and 50 μg/mL antibodies (anti-PSMA for prostate cancer patient samples, anti-EpCAM for all other cancer types) in PBS. Heparin (1000 Units/mL) was then incubated for 1 h to block nonspecific adhesion. Introduction of the halloysite nanotube coating has been described previously (22).

Each primary cell suspension was perfused through the microtube system at a shear stress of 4 dyn/cm^2. Tubes were then washed with a few tube volumes of PBS saturated with Ca^{2+} at 1 dyn/cm^2 to remove unbound and loosely bound cells. Accutase was gently perfused into the microtube and allowed to incubate for 10 min to detach adherent cells. Media was perfused through the microtube and the cells were collected into one well of a tissue culture treated 96 well plate (Becton Dickinson). Media was changed on days 1 and 3 and the cells analyzed on day 5.

Cells were fixed by incubation with 2% paraformaldehyde in PBS for 20 min. After gentle washing twice with PBS, cells were incubated with 10 μg/mL anti-EpCAM for breast, lung, and ovarian cancer samples, and 10 μg/mL anti-PSMA for prostate cancer samples for 30 min on ice, then washed with PBS. Goat anti-mouse IgG

conjugated to an Alexafluor 488 dye was subsequently incubated for 30 min on ice. DAPI nucleus stain was simultaneously incubated with the secondary antibody to stain the nucleus. Cells were then washed twice with PBS and analyzed for fluorescence by video microscopy. CTC in culture were defined as being positive for an epithelial marker (EpCAM or PSMA), positive for DAPI, and between 10 and 25 μm in diameter.

3.2.5 Processing of healthy blood samples

After informed consent peripheral whole blood (7.5 mL) was drawn from 8 healthy volunteers and processed in a similar manner as that of samples from patients diagnosed with metastatic cancer. Briefly, the buffy coat was isolated by Ficoll density gradient and left at room temperature for 24 h. Each buffy coat sample was then halved and perfused through a smooth tube and a nanotube coated tube, identically coated with single microtube volumes of 5 μg/mL E-selectin and 50 μg/mL epithelial antibody (anti-EpCAM or anti-PSMA). The buffy coat sample from Norm-6 was processed through a smooth tube coated with anti-PSMA antibody. Samples from participants Norm-1 through -5 were perfused through EpCAM-coated tubes while samples from participants Norm-7 and -8 were processed in both EpCAM- and PSMA-coated tubes. Captured cells were then harvested from each tube and placed in an incubator. The number of viable cells was assessed on day 5.

3.2.6 CTC enumeration using CellSearch®

At the same time blood was collected for shipping to Cornell, an additional tube of blood was collected in a CellSave tube. CellSave tubes were processed within 96

hours at BioCytics, Inc. using the CellSearch® Autoprep system and the CellSearch® CTC IVD kit according to standard operating procedures developed by the manufacturer (Veridex).

3.2.7 Analysis of leukocyte spreading

Planar nanotube-coated surfaces were prepared in a manner identical to that used for coating microtubes. E-selectin at a concentration of 7.5 μg/mL was incubated on nanotube-coated and smooth surfaces for 2 h followed by blocking with 5% milk protein for 1. Whole blood was drawn from three healthy volunteers after informed consent and the buffy coat isolated using density gradient centrifugation with 1-Step Polymorphs (Accurate Chemical & Scientific). 10^5 cells were allowed to settle and contact each surface for 10 min. Surfaces were washed off from the surfaces and remaining cells were immediately fixed with 4% paraformaldehyde. Cell membranes were stained with octadecyl rhodamine B (Invitrogen) or CellMask Deep Red (Invitrogen) according to manufacturer's instructions. Cell nuclei were then stained with DAPI (Vectashield Mounting Media, Vector Laboratories) and the interface between the surface and an adherent cell was imaged with a Zeiss 710 confocal microscope. The area of a cell that was in contact with the surface was measured using MetaMorph software (Universal Imaging). Statistical significance was determined using a paired nondirectional t-test.

3.2.8 Data Analysis

50-150 micrographs of each well were recorded at random locations, and total cell counts were recorded along with CTC counts as described above. Cell counts were

normalized by the total well area and the uncertainty in total cell count estimate was represented by the standard error of the mean. Statistical significance was determined by unpaired nondirectional t-test using GraphPad Prism. Purity values were calculated as the fraction of cells that were CTC-positive (EpCAM- or PSMA-positive and DAPI-positive) compared to the total number of cells that were DAPI-positive. Errors are reported as standard error of the mean (SEM), and statistical significance determined by unpaired nondirectional t-test using Prism, unless specified otherwise. P-values were compared to a significance level of a = 0.05. Data sets with sufficiently small numbers of positive observations were evaluated by bootstrap sampling with replacement to create 10 sets of data from the experimental data.

3.3 Results

3.3.1 Isolation of hematopoietic cancer cells from model blood samples

Known numbers of KG1a cells were supplemented into 1:1 diluted whole blood. Blood samples were perfused through microtubes at a flow rate of 4.8 mL/h. The mean number of KG1a cells observed as a function of surface area was converted to the total number of KG1a cells in each microtube based on independent calibration. Tubes coated with P-selectin in addition to anti-CD34 antibody performed significantly better than those coated with anti-CD34 alone. Recovery of approximately 50% was accomplished for the range of spiked samples (Figure 3.2).

3.3.2 Capture of primary CTC on smooth surfaces

Isolated buffy coat samples from cancer patients were perfused through functionalized microtubes. Captured cells were removed from the microtubes and cultured for 5 days. Viable CTC enumeration in culture was accomplished by counting cells that were DAPI-positive in addition to EpCAM- or PSMA-positive. 20 to 703 (mean 172 ± 47) viable CTC were captured, with a mean purity of 0.372 ± 0.030 (Figure 3.3). Reproducibility of the device was evaluated by dividing sample Bre-3 into two identical samples and processing in separate devices, and a high degree of congruency was observed (Figure 3.4).

3.3.3 Capture of primary CTC on halloysite nanotube-coated surfaces

Microtube devices were coated with halloysite nanotubes and then functionalized in the identical manner to the experiments described in the previous section. Samples from six patients were halved into two identical samples for parallel processing through nanotube-coated and smooth surfaces. Significant enhancements in the purity of processed samples were achieved for each trial (Figure 3.5). Despite variability between patient samples, the purities of the cell populations captured on the nanotube coating were consistently greater. Specifically, the mean purity of captured primary CTC samples was 0.660 ± 0.039 on the nanotube surface and 0.372 ± 0.030 on the smooth surface, demonstrating a significant benefit provided by the nanotube coating (Figure 3.6). A representative micrograph of captured CTC after 5 days in culture is included (Figure 3.7).

3.3.4 Capture of cells from healthy blood

Peripheral blood from healthy participants was processed in a manner identical to that of the metastatic cancer samples. Of the samples collected from 8 different healthy participants, two contained cells that were identified as CTC based on positive EpCAM staining on day 5. Norm-4 returned 11.6 (median 9.68, range 19.4) positive cells using both the smooth device and the nanotube-coated device, Norm-6 contained 7.75 (median 5.81, range 15.5) positive cells, and Norm-7 contained 3.87 (median 3.87, range 11.6) positive cells when processed through a nanotube-coated tube coated with EpCAM (Figure 3.8). The number of positive cells samples was significantly less than the number of positive cells recovered in any of the metastatic cancer samples for all samples except for Bre-5 processed through a smooth tube. The mean number of positive cells recovered in the healthy blood samples was 1.9 using the smooth tube and 1.7 using the nanotube-coated tube.

3.3.5 CellSearch® CTC Enumeration

The CellSearch® test was employed on identical samples as 12 of the 13 samples processed in the selectin-functionalized device. CTC counts ranged from 0 to 218 per 7.5 mL (median 1, range 218). Less than 2 CTC per sample were found in 8 out of the 12 samples. For appropriate comparison to the selectin-functionalized samples, in which half of the 7.5 mL sample was processed through the smooth device and the other half through the nanotube-coated tube, the CTC counts reported by CellSearch® were appropriately normalized (Figure 3.8).

3.3.6 Analysis of leukocyte spreading on smooth and nanotube-coated surfaces

The area of cell membrane in contact with a smooth or nanotube-coated surface functionalized with E-selectin was measured using confocal microscopy. A significantly larger contact area was formed on the smooth surface compare to nanotube-coated (216 ± 60 μm^2 and 110 ± 40 μm^2, respectively, N=3, pooled mean ± SD) (Figure 3.9). The perimeter of the contact area was also compared on either surface and a significant difference found as well (77.0 ± 21.8 μm smooth versus 43.5 ± 10.1 μm, pooled mean ± SD).

3.4 Discussion

In this study, I demonstrated a straightforward microscale flow device that was able to isolate cancer cells from blood with high specificity and purity at clinically relevant concentrations in blood (Figure 3.2), and primary CTC from patients diagnosed with metastatic breast, prostate, lung, and ovarian cancers (Figures 3.3 and 3.5). CTC capture was facilitated by E-selectin and CTC-specific antibodies and high purities were accomplished with a halloysite nanotube coating. A notable feature of the device is that it mimics the natural process by which CTC could adhere to the endothelium, thus the separation process may tend to select for those CTC that are more able to metastasize (*152, 158, 159*), and does not inflict cellular damage (*160*).

We recently reported methods for enhancing cell capture in which the nanoscale topography of a capture surface was altered using immobilized nanoparticles (*157, 161*). The halloysite nanoparticle coating was found to increase the surface area onto which molecules could adsorb, as well as present molecules into the hydrodynamic lubrication

layer that slows the sedimentation of cells to the device surface (*157*). Here, I show that the incorporation of the nanotube coating consistently captures primary CTC at high purities (Figure 3.6).

Cell response to nanostructured surfaces varies widely, depending on cell type, surface composition, surface feature dimensions, orientation, and organization. The modes of action are unclear (*162, 163*). Studies into the behavior of macrophages on microstructured surfaces have shown both increased spreading (*164*) and decreased spreading (*165*). A review of studies into the interaction of immune cells and nanostructured surfaces has concluded that materials with altered nanotopographies can generally be less inflammatory than planar surfaces (*166*). In the present study I showed that there was a significant reduction in leukocyte spreading on E-selectin coated halloysite nanotube surfaces (Figure 3.9). This behavior was also observed under flow conditions (data not shown). The presence of spread and activated leukocytes on the smooth surface exhibiting diameter approximately twice that of resting leukocytes on the nanotube-coated surface is indicative of greatly increased adhesion strength, and is a likely explanation for the increased capture purities obtained with nanotube-coated surfaces.

Cancer cells were successfully captured from two different types of samples, diluted blood (Figure 3.2) and buffy coat (Figures 3.3 and 3.5) to demonstrate the use of the device in clinical settings where the handling of patient samples varies. An advantage of using samples in which CTC are dispersed in blood is that the samples require only one step: a 1:1 dilution with buffered saline. This reduces potential target cell damage or loss due to minimal sample processing (*167*). In addition, the nature of blood flow in

microvessels promotes margination, which assists CTC capture. A drawback of using whole blood samples is that a sample typically must be analyzed within 24 hours of being drawn from the patient. Alternatively, buffy coat samples can be frozen, allowing samples to be shipped long distances and stored for extended periods of time. However, cell damage or loss in this process is possible.

Selectin binding is characterized by fast associations, which allows cells to be recruited from fast-moving blood flow to the endothelium (*168*). An important consequence of this behavior is that selectin-functionalized devices have the ability to process cells at high flow rates, a necessary feature for use in a clinical setting. As such, I report approximately 50% capture efficiency at a flow of 4.8 mL/h. Previously developed systems that rely entirely on antibody binding to capture CTC achieve similar capture efficiencies and purities, but require a flow rate of 1 mL/h. Subsequent advances to the CTC-chip geometry have resulted in greatly enhanced capture efficiency at low flow rate (~1 mL/h), and approximately 40% efficiency at flow rates near 4 mL/h (*169*). Several other microfluidic devices of varying geometry and orientation have been developed (*143, 170, 171*), however, because of their use of antibodies alone all require reduced flow rates to attain maximal capture purity levels.

The selectin-functionalized device has various parameters that impact capture efficiency and purity including protein density, flow rate, device length, and surface roughness. Previous work studied the effects of these parameters on cell capture (*144, 145, 157, 172*). Based on these studies it is clear that high concentrations of selectin molecules, ~ 20 μg/mL, result in increased leukocyte recruitment. It has also been observed that shear rate can affect cell capture rate, however shear stress does not have

much effect on adherent cells within the physiological range. As such, I chose a flow rate that allows all cells to settle to the surface before exiting the tube.

Of the eight healthy donor samples processed, three had positively stained cells (11.6, 7.75, and 3.87). Two out of these three samples were processed through tubes coated with anti-EpCAM while only one captured a small number of cells using anti-PSMA. These results represent the limit of specificity of the antigens targeted by the device. It is interesting to note that the combination of the nanotube coating with E-selectin and anti-PSMA antibodies resulted in zero positively stained cells detected in normal blood (N=3).

The only FDA-cleared method for quantification of CTC in patient blood, CellSearch®, was employed on identical samples as those processed in the selectin-functionalized device for comparison against this gold standard. There was substantial discord between CellSearch® and the selectin-functionalized device: 5 out of 12 samples processed by CellSearch® were negative for CTC, while these 5 patients were positive for CTC using the selectin-functionalized device. All together, 11 out of 12 samples were positive for CTC using the smooth selectin-functionalized device and 12 out of 12 were positive with the nanotube coating, using the most conservative threshold. Moreover, the CTC yield using the selectin-functionalized device was significantly higher (Figure 3.8).

In summary, this study reports on a novel system for isolating viable CTC from patient samples. This device is a straightforward system consisting of a polyurethane microtube functionalized with a bimolecular surface of selectin and antibody molecules that allow for the reproducible selection and retention of CTC in the device without inflicting cellular damage. I further report on the application of a halloysite nanotube

coating, which leads to enhanced device performance. I believe that this novel bimolecular device is a promising new tool for cancer treatment in the clinical setting.

3.5 Acknowledgements

This work was funded in part by the National Institutes of Health, Grant No. CA143876 (M.R.K.), and a National Science Foundation Graduate Research Fellowship (A.D.H).

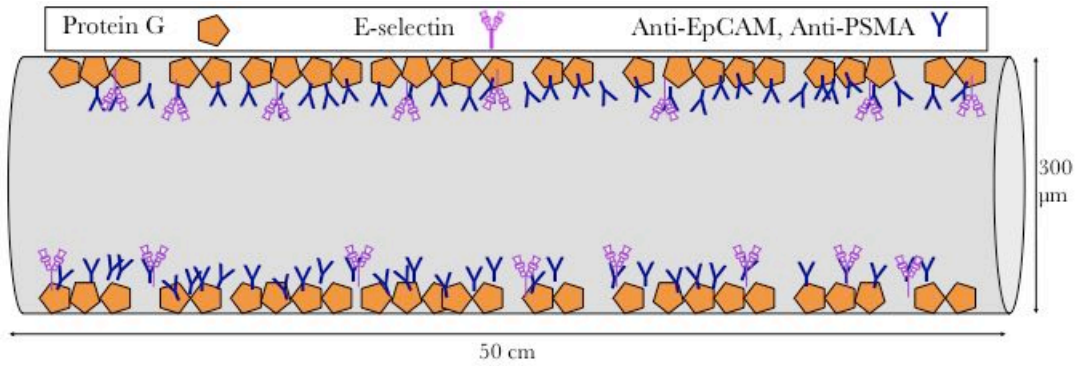

Figure 3.1. Schematic of a smooth MRE microtube functionalized for CTC capture.

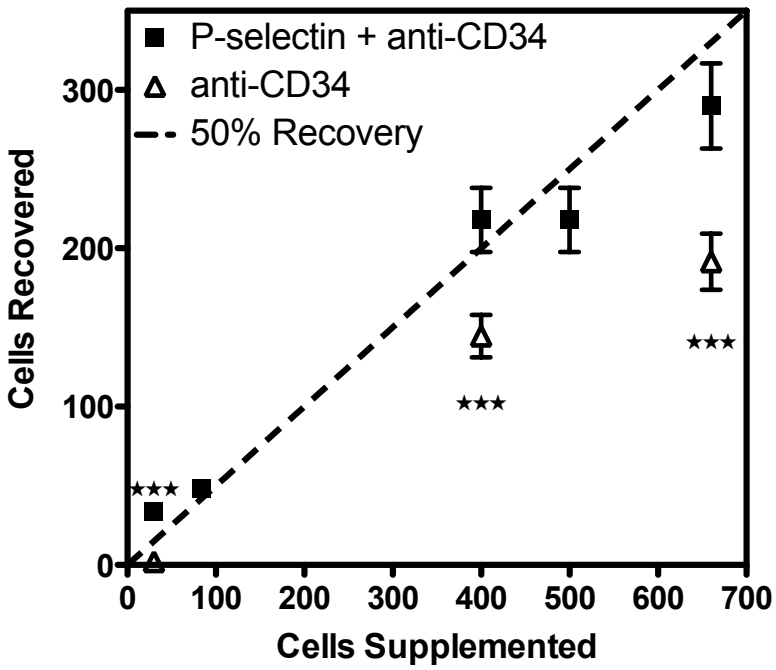

Figure 3.2. Relationship between numbers of KG1a acute myeloid leukemia cells supplemented into 4 mL diluted blood and the number of cells recovered.. Error bars represent the SEM determined from calibration experiments. *** $p < 0.001$.

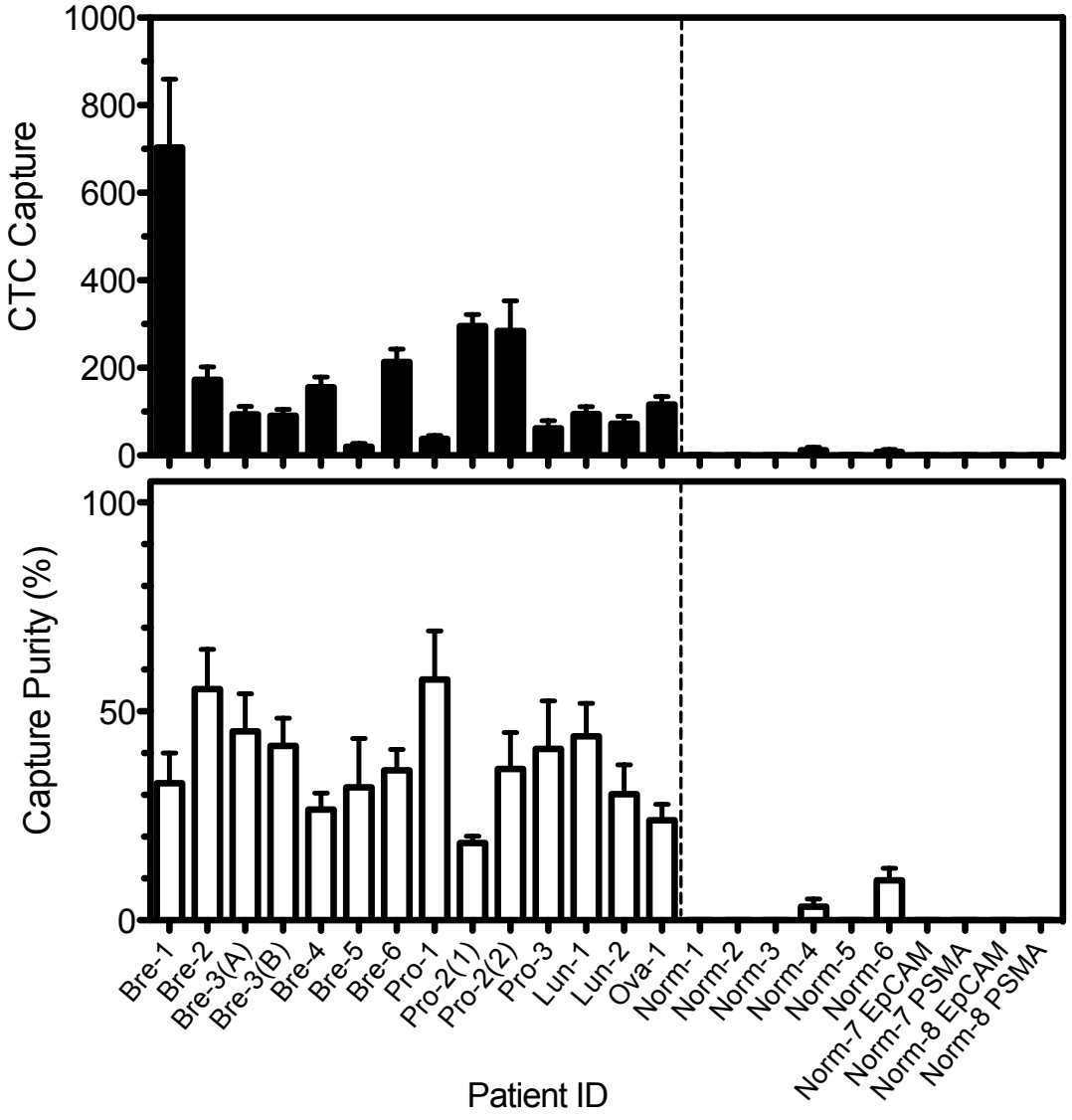

Figure 3.3. CTC were captured in the smooth device from blood samples from eleven cancer patients diagnosed with breast (Bre-1 through -6), prostate (Pro-1 and -2), lung (Lun-1 and -2), and ovarian (Ova-1) cancer. Blood samples drawn from eight healthy volunteers were processed in addition (Norm-1 through -8). Measureable numbers of cells that stained positively for epithelial markers were captured from each sample (top).

The fraction of total cells that were positive for epithelial markers shows the extent to which CTC were enriched in each patient sample (bottom).

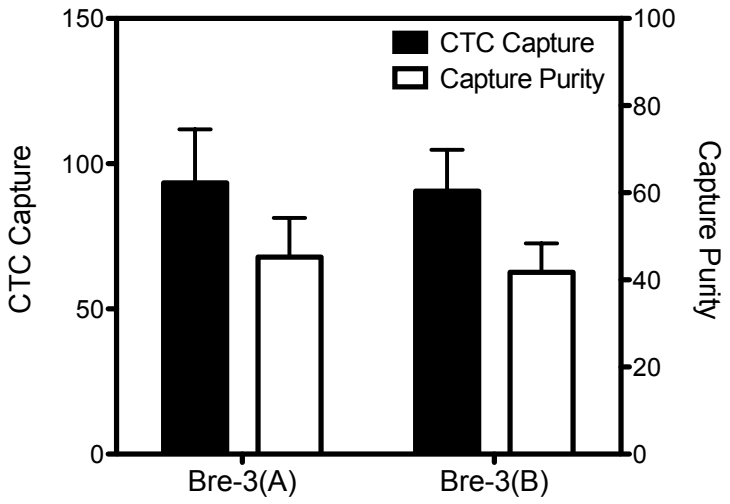

Figure 3.4. The reproducibility of the smooth device was determined by processing two identical samples from patient Bre-3 through two separate devices. The approximation of the number of CTC captured (filled bars) is plotted on the left ordinate, and the capture purity is plotted on the right ordinate. A high degree of congruity was observed.

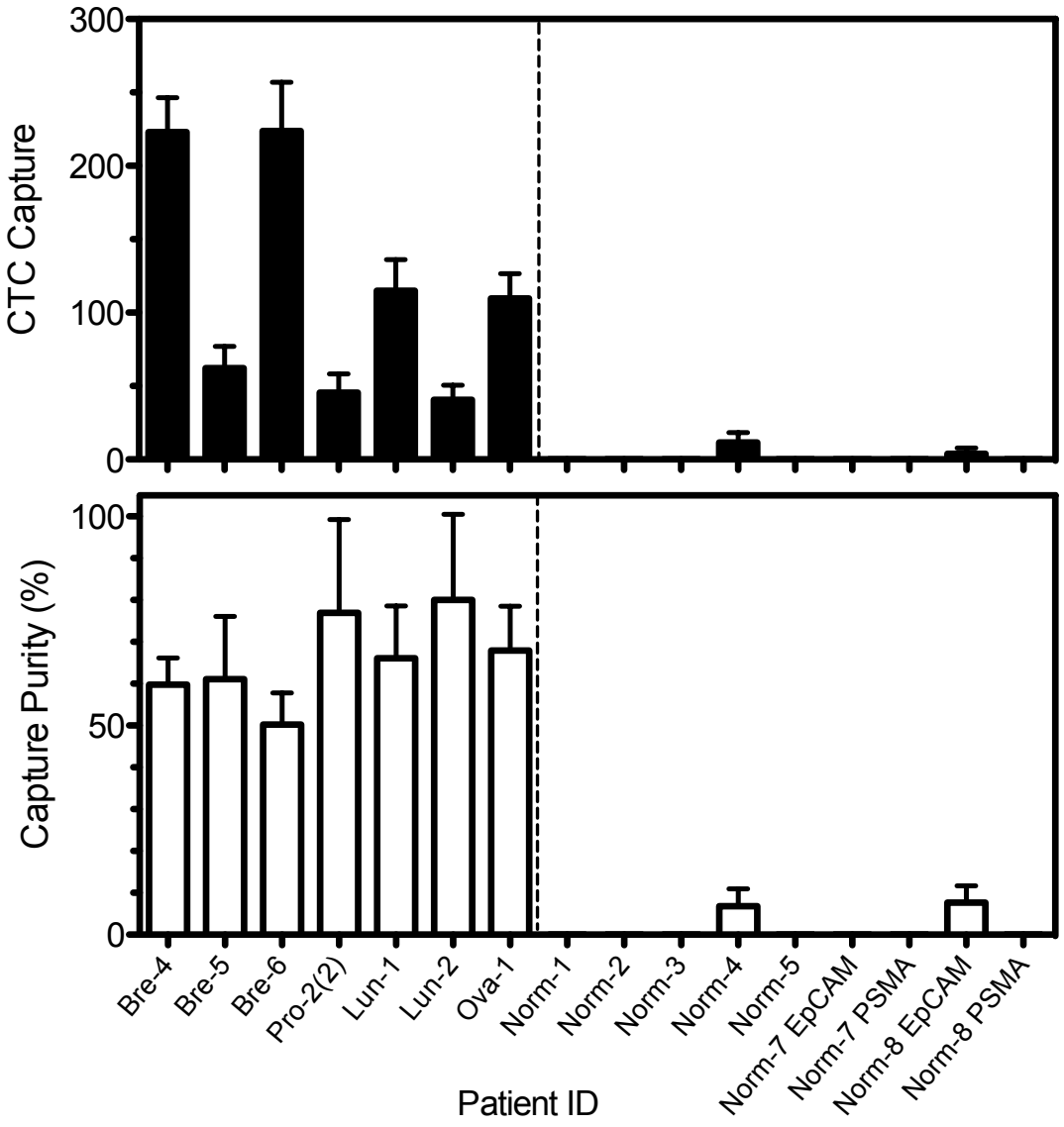

Figure 3.5. CTC were captured in the nanotube-coated device from several identical samples to those processed on the smooth device, for both cancer and healthy blood samples. An appreciable number of CTC-positive cells were captured from each cancer blood sample (top), and markedly high capture purities were achieved across cancer patient samples (bottom).

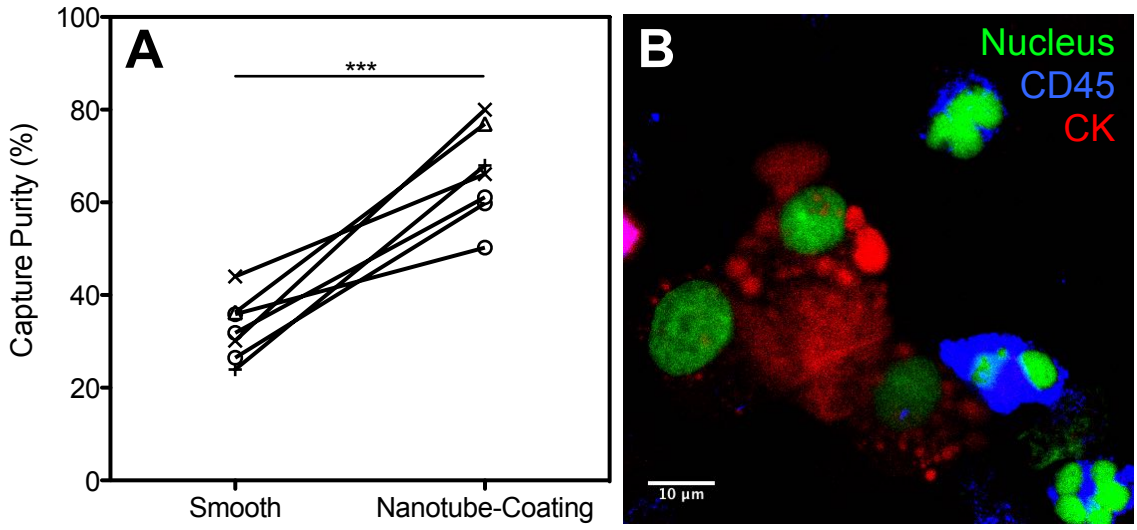

Figure 3.6. (A) The purity values of samples analyzed on both surfaces were compared and purity was significantly greater on the nanotube-coated surface. O's indicate breast cancer patients, Δ's indicate prostate cancer, X's indicate lung cancer, and +'s indicate ovarian cancer samples. *** $p < 0.001$ using paired nondirectional t-test. (B) Representative micrograph of CTC and contaminating leukocytes. Scale bar 10 µm.

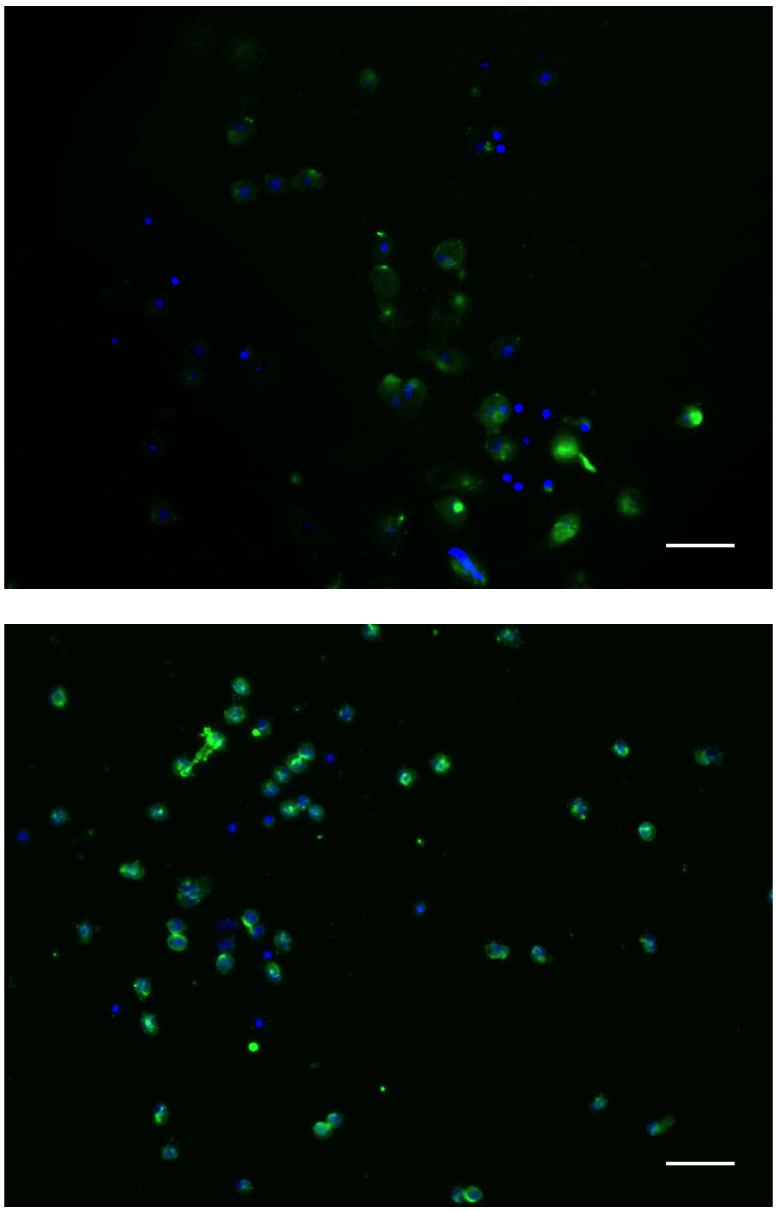

Figure 3.7. Primary CTC captured on the smooth (top) nanotube-coated surface (bottom) after 5 days in culture were stained for EpCAM (green) and DAPI (blue).

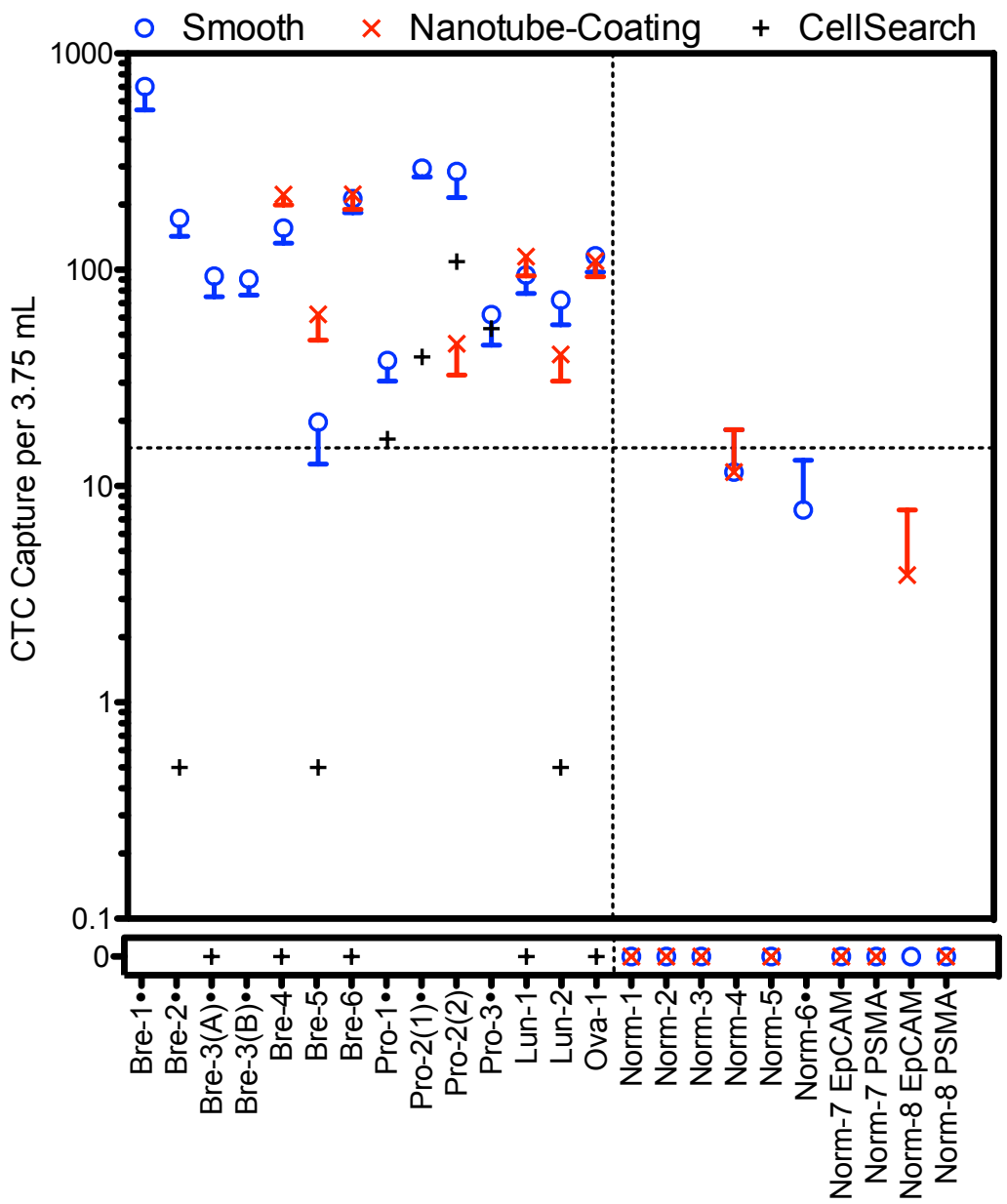

Figure 3.8. The number of CTC captured from the blood of all patients is compiled along with the results of samples collected from healthy participants. CTC counts from CellSearch® reported here were derived from 7.5 mL samples and renormalized for comparison. Participants Norm-1 through -5 were processed in tubes coated with EpCAM in addition to E-selectin. The ⊠ symbol indicates samples processed through smooth tubes only.

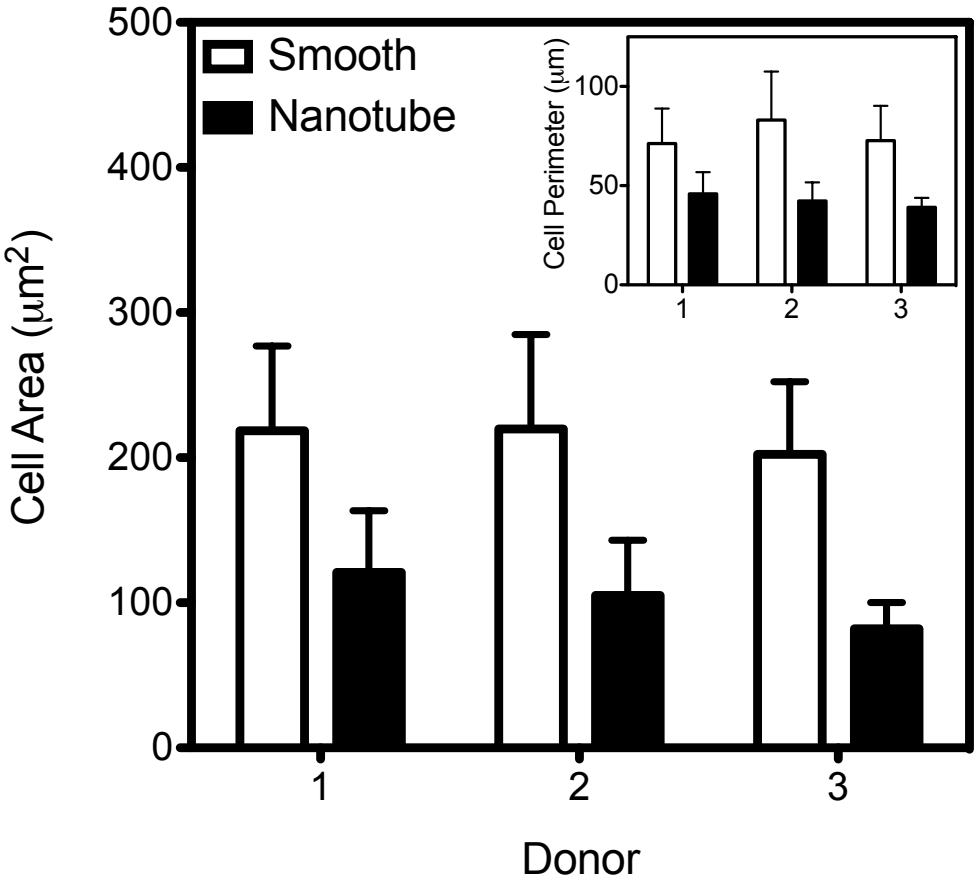

Figure 3.9. The contact area between adherent leukocytes and planar E-selectin-functionalized surfaces was measured on smooth and nanotube-coated surfaces. (A) Comparison of cell area on smooth versus nanotube-coated surfaces by two-tailed paired t test yielded $p = 0.0038$. (Insert) Cell spreading was also quantified based on cell perimeter on either surface. Paired t test yielded $p = 0.0175$. Error bars represent standard deviation.

3.6 References

136. U. De Giorgi *et al.*, 18F-FDG PET/CT findings and circulating tumor cell counts in the monitoring of systemic therapies for bone metastases from breast cancer. *J Nucl Med* **51**, 1213-1218 (2010).

137. S. Maheswaran, D. A. Haber, Circulating tumor cells: a window into cancer biology and metastasis. *Curr Opin Genet Dev* **20**, 96-99 (2010).

138. W. J. Allard *et al.*, Tumor cells circulate in the peripheral blood of all major carcinomas but not in healthy subjects or patients with nonmalignant diseases. *Clin Cancer Res* **10**, 6897-6904 (2004).

139. M. C. Miller, G. V. Doyle, L. W. Terstappen, Significance of Circulating Tumor Cells Detected by the CellSearch System in Patients with Metastatic Breast Colorectal and Prostate Cancer. *J Oncol* **2010**, 617421 (2010).

140. P. Paterlini-Brechot, N. L. Benali, Circulating tumor cells (CTC) detection: clinical impact and future directions. *Cancer Lett* **253**, 180-204 (2007).

141. P. C. Tong *et al.*, White blood cell count is associated with macro- and microvascular complications in chinese patients with type 2 diabetes. *Diabetes Care* **27**, 216-222 (2004).

142. S. Nagrath *et al.*, Isolation of rare circulating tumour cells in cancer patients by microchip technology. *Nature* **450**, 1235-1239 (2007).

143. J. P. Gleghorn *et al.*, Capture of circulating tumor cells from whole blood of prostate cancer patients using geometrically enhanced differential immunocapture (GEDI) and a prostate-specific antibody. *Lab Chip* **10**, 27-29 (2010).

144. S. D. Narasipura, J. C. Wojciechowski, N. Charles, J. L. Liesveld, M. R. King, P-Selectin coated microtube for enrichment of CD34+ hematopoietic stem and progenitor cells from human bone marrow. *Clin Chem* **54**, 77-85 (2008).

145. J. C. Wojciechowski *et al.*, Capture and enrichment of CD34-positive haematopoietic stem and progenitor cells from blood circulation using P-selectin in an implantable device. *Br J Haematol* **140**, 673-681 (2008).

146. N. Charles, J. L. Liesveld, M. R. King, Investigating the feasibility of stem cell enrichment mediated by immobilized selectins. *Biotechnol Prog* **23**, 1463-1472 (2007).

147. H. F. Langer, T. Chavakis, Leukocyte-endothelial interactions in inflammation. *J Cell Mol Med* **13**, 1211-1220 (2009).

148. S. Gout, P. L. Tremblay, J. Huot, Selectins and selectin ligands in extravasation of cancer cells and organ selectivity of metastasis. *Clinical & Experimental Metastasis* **25**, 335-344 (2008).

149. L. M. Coussens, Z. Werb, Inflammation and cancer. *Nature* **420**, 860-867 (2002).

150. D. J. Goetz, M. E. el-Sabban, D. A. Hammer, B. U. Pauli, Lu-ECAM-1-mediated adhesion of melanoma cells to endothelium under conditions of flow. *Int J Cancer* **65**, 192-199 (1996).

151. Y. J. Kim, L. Borsig, H. L. Han, N. M. Varki, A. Varki, Distinct selectin ligands on colon carcinoma mucins can mediate pathological interactions among platelets, leukocytes, and endothelium. *Am J Pathol* **155**, 461-472 (1999).

152. F. W. Orr, H. H. Wang, R. M. Lafrenie, S. Scherbarth, D. M. Nance, Interactions between cancer cells and the endothelium in metastasis. *J Pathol* **190**, 310-329 (2000).

153. F. W. Orr, H. H. Wang, Tumor cell interactions with the microvasculature: a rate-limiting step in metastasis. *Surg Oncol Clin N Am* **10**, 357-381, ix-x (2001).

154. G. Mannori *et al.*, Inhibition of colon carcinoma cell lung colony formation by a soluble form of E-selectin. *Am J Pathol* **151**, 233-243 (1997).

155. M. R. King, L. T. Western, K. Rana, J. L. Liesveld, Biomolecular Surfaces for the Capture and Reprogramming of Circulating Tumor Cells. *Journal of Bionic Engineering* **6**, 311-317 (2009).

156. S. R. Levis, P. B. Deasy, Characterisation of halloysite for use as a microtubular drug delivery system. *Int J Pharm* **243**, 125-134 (2002).

157. A. D. Hughes, M. R. King, Use of naturally occurring halloysite nanotubes for enhanced capture of flowing cells. *Langmuir* **26**, 12155-12164 (2010).

158. A. F. Chambers, A. C. Groom, I. C. MacDonald, Dissemination and growth of cancer cells in metastatic sites. *Nat Rev Cancer* **2**, 563-572 (2002).

159. S. Gout, P. L. Tremblay, J. Huot, Selectins and selectin ligands in extravasation of cancer cells and organ selectivity of metastasis. *Clin Exp Metastasis* **25**, 335-344 (2008).

160. K. Rana, J. L. Liesveld, M. R. King, Delivery of apoptotic signal to rolling cancer cells: a novel biomimetic technique using immobilized TRAIL and E-selectin. *Biotechnol Bioeng* **102**, 1692-1702 (2009).

161. W. Han, B. A. Allio, D. G. Foster, M. R. King, Nanoparticle coatings for enhanced capture of flowing cells in microtubes. *ACS Nano* **4**, 174-180 (2010).

162. E. K. Yim, K. W. Leong, Significance of synthetic nanostructures in dictating cellular response. *Nanomedicine* **1**, 10-21 (2005).

163. J. Y. Lim, H. J. Donahue, Cell sensing and response to micro- and nanostructured surfaces produced by chemical and topographic patterning. *Tissue Eng* **13**, 1879-1891 (2007).

164. B. Wojciak-Stothard, Z. Madeja, W. Korohoda, A. Curtis, C. Wilkinson, Activation of macrophage-like cells by multiple grooved substrata. Topographical control of cell behaviour. *Cell Biol Int* **19**, 485-490 (1995).

165. J. A. Schmidt, A. F. von Recum, Macrophage response to microtextured silicone. *Biomaterials* **13**, 1059-1069 (1992).

166. K. M. Ainslie *et al.*, In vitro inflammatory response of nanostructured titania, silicon oxide, and polycaprolactone. *J Biomed Mater Res A* **91**, 647-655 (2009).

167. K. Pachmann *et al.*, Standardized quantification of circulating peripheral tumor cells from lung and breast cancer. *Clin Chem Lab Med* **43**, 617-627 (2005).

168. R. Alon, D. A. Hammer, T. A. Springer, Lifetime of the P-selectin-carbohydrate bond and its response to tensile force in hydrodynamic flow. *Nature* **374**, 539-542 (1995).

169. S. L. Stott *et al.*, Isolation of circulating tumor cells using a microvortex-generating herringbone-chip. *Proc Natl Acad Sci U S A* **107**, 18392-18397 (2010).

170. A. A. Adams *et al.*, Highly efficient circulating tumor cell isolation from whole blood and label-free enumeration using polymer-based microfluidics with an integrated conductivity sensor. *J Am Chem Soc* **130**, 8633-8641 (2008).

171. U. Dharmasiri *et al.*, Highly efficient capture and enumeration of low abundance prostate cancer cells using prostate-specific membrane antigen aptamers immobilized to a polymeric microfluidic device. *Electrophoresis* **30**, 3289-3300 (2009).

172. D. Lee, M. R. King, Microcontact Printing of P-Selectin Increases the Rate of Neutrophil Recruitment Under Shear Flow. *Biotechnology Progress* **24**, 1052-1059 (2008).

CHAPTER 4 – HALLOYSITE NANOTUBE COATINGS SUPPRESS LEUKOCYTE SPREADING

This section is adapted from the following manuscript, submitted for publication to *Langmuir*: AD Hughes, G Marsh, RE Waugh, DG Foster, and MR King, Halloysite nanotube coatings suppress leukocyte spreading, Submitted to *Langmuir*

4.0 Abstract

The nanoscale topography of adhesive surfaces is known to be an important factor governing cellular behavior. Previous work has shown that surface coatings composed of halloysite nanotubes enhances the adhesion, and therefore capture, of rare target cells such as circulating tumor cells. Here, I demonstrate a unique feature of these coatings is its ability to reduce the adhesion of leukocytes and prevent leukocyte spreading. Surfaces were prepared with coatings of halloysite nanotubes and functionalized for leukocyte adhesion with E-selectin, and the dilution of nanotube concentration revealed a threshold concentration below which cell spreading became comparable smooth surfaces. Evaluation of surface roughness characteristics determined that the average distance between discrete surface features correlated with adhesion metrics, with a separation distance of approximately 2 μm identified as the critical threshold. Computational modeling of the interaction of leukocytes with halloysite nanotube coated surfaces of varying concentrations demonstrates that the geometry of the cell surface and adhesive counter-surface produce a significantly diminished effective contact area compared to a leukocyte interacting with a smooth surface.

Keywords:

Nanotopography, leukocyte, cell spreading, cell adhesion, E-selectin, nanotube

4.1 Introduction

The micro- and nanoscale topography of a biomaterial or tissue affect cell behavior independent of the chemistry of that surface (*173, 174*). This has been known for more than two decades, however no consensus for how a cell is likely to behave on surfaces of different roughness has been reached. This is because cell behavior has been found to be highly variable depending on cell type, material type, surface feature dimensions and arrangement, etc. (*175-177*). Nevertheless, the topographical nature of a surface has been shown to alter cell adhesion (*178-182*), motility (*183*), proliferation (*184*), activation (*185*), and differentiation (*186*). Micro- and nanostructured surfaces can additionally control the direction of movement of fibroblasts, epithelial cells, and macrophages as well as the degree of adhesion of different cell types, including leukocytes (*187*).

There are numerous stages in the adhesion of leukocytes as they home to sites of inflammation or infection. Selectin molecules are responsible for the first stage in adhesion within the bloodstream, in which cells tether and roll on the endothelial surface, followed by integrin activation and firm adhesion (*188*). What follows is a process of adhesion strengthening in which the cell flattens onto the surface and adhesion complexes are rearranged and the cytoskeleton is altered such that the cell is more firmly adhered to the surface and less likely to detach due to shear stress from the blood flow (*189*). These adhesion steps are followed by migration and extravasation. Adhesion strengthening is characterized by cell spreading, during which there is a marked increase in the contact area between the cell and the endothelium. The mechanical properties of the leukocyte

play a significant role during the adhesion strengthening stage, in that the compliance of the leukocyte can increase cell adhesion by greater than 10-fold in LFA-1/ICAM-1 mediated binding (*190*). Indeed, spreading is described as a distinct event in cell adhesion, and it is suggested that the kinetics and mechanisms required for adhesion and spreading are substantially different (*191, 192*).

Cell spreading has been characterized as a very active process, initiated by dramatic surface receptor rearrangement. In particular, it has been shown that neutrophils spreading onto a surface coated with IL-8 redistribute adhesion receptor LFA-1 and chemokine receptors CXCR1 and CXCR2 from troughs in the plasma membrane to peripheral regions most closely apposed to the IL-8-coated surface (*193*). Spreading has been associated with one of several integrins binding to their ligands, followed by the generation of outside-in signaling cascades resulting in activation, migration, release of cytokines, and degranulation (*194*). Nanostructured materials are therefore of great interest to the field of biomaterials if they are able to modulate leukocyte adhesion and subsequent activation to prevent biofouling and inflammatory foreign body responses (*195*).

Some of the innumerable applications of biomaterials lie in the field of cancer diagnostics. I have previously developed a device designed to positively select rare circulating tumor cells (CTC) from peripheral blood samples *in vitro* to facilitate downstream prognostic and drug susceptibility studies (*196, 197*). The device is modeled on an inflamed postcapillary venule, functionalized with recombinant human E-selectin and antibodies against target cell receptors. E-selectin has been implicated in the metastatic spread of cancer cells through the circulatory system (*198-200*), and as such is

used to rapidly capture flowing CTC within the sample. However, as E-selectin is primarily a physiological ligand for leukocyte adhesion, contamination of healthy leukocytes remains a challenge to device performance and acts to reduce the purity of isolated CTC samples. Purity can be improved with the incorporation of a coating of halloysite nanotubes (HNt), which was found to increase purity from 37% to 66% (*196*) and investigation of halloysite coatings as a bioactive material.

HNt are naturally occurring nanoparticles composed of aluminosilicate mineral having an outer diameter of 50 – 200 nm, net negative charge, and variable length that can approach 1 μm (Figure 4.1) (*201*). HNt have also been used to enhance the capture of cultured cancer cells, and mechanistic analyses revealed that increased protein absorption was accomplished on the rougher surface, and furthermore that the HNt coating overcame the innate physical limitation of microfluidic systems by penetrating the hydrodynamic lubrication layer (*202*).

In this study, I have carried out an investigation of the ability of HNt coatings to modulate the adhesivity of leukocytes, initially discovered in prior CTC capture studies. It is established that HNt coatings reduce leukocyte adhesion and prevent leukocyte spreading, and that these behaviors are associated with surface roughness, and correlate with one roughness parameter in particular: the average distance between features. The concentration of HNt is varied to control the material parameters of the surface, and with cell behavior as the output it is possible to identify critical parameters that drive leukocyte adhesion. I finally employ a dynamic computational model of leukocyte spreading that confirms and explains these findings.

4.2 Materials and Methods

4.2.1 Cells and reagents

Peripheral whole blood was drawn from healthy volunteers after informed consent. Blood was collected into heparinized tubes (BD Biosciences, San Jose, CA). 10X erythrocyte lysis buffer was prepared as a solution of 1.5M NH_4Cl, 0.1M $NaHCO_3$, 0.01M disodium EDTA in distilled water. Ammonium chloride and sodium bicarbonate were purchased from Sigma-Aldrich (St. Louis, MO). Halloysite nanotubes were provided as a gift from NaturalNano, Inc. (Rochester, NY). Recombinant human E-selectin-IgG chimera was purchased from R&D Systems (Minneapolis, MN). Paraformaldehyde was acquired from Electron Microscopy Sciences (Hatfield, PA). DAPI was purchased from Vector Laboratories (Burlingame, CA). Phosphate buffered saline (PBS), Hank's balanced salt solution (HBSS), and CellMask Deep Red plasma membrane stain were obtained from Life Technologies (Grand Island, NY). Blotting grade blocker nonfat dry milk was purchased from Quality Biological (Gaithersburg, MD). Calcium carbonate, poly-L-lysine (0.1% w/v), 8-well Flexiperm gaskets, and human serum albumin were obtained from Sigma-Aldrich. HEPES was purchased from ThermoFisher Scientific (Pittsburgh, PA).

4.2.2 Preparation of surfaces

Halloysite nanotube powder was dissolved in water to a concentration of 13.2% w/v and sonicated (Fisher Scientific) at 50% load for 1 min. Six serial 1:2 dilutions were then prepared with water, resulting in concentrations of 6.6, 3.3, 1.65, 0.825, 0.413, and 0.206%. Polystyrene microscope slides (VWR, Radnor, PA) were thoroughly cleaned

with detergent in a sonicator, then rinsed and cleaned with 75% ethanol. 8-well flexiperm gaskets were placed on the slides and 250μL 0.2% poly-L lysine was incubated in each well for 5 min. HNt solutions (250μL) were incubated within each well for 3 min, except for one that was filled with water to serve as a smooth surface. Each surface was gently rinsed twice with water, and then each well was filled with water and allowed to age for 24 h. 250 μL of 7.5 μg/mL E-selectin was incubated on each surface for 2 h followed by a blocking incubation of 5% milk protein for 1 h. Finally, the selectin was activated by incubating each surface with PBS saturated with calcium carbonate.

4.2.3 Preparation of leukocytes

10X erythrocyte lysis buffer (ELB) was prepared as a solution of 1.5M NH_4Cl, 0.1M $NaHCO_3$, 0.01M disodium EDTA in distilled water and sterilized by filtration. Working solutions of 1X ELB were prepared immediately prior to use using sterile distilled water and warmed to 37°C. Fresh whole blood was diluted 1:10 with 1X ELB and placed on a rocker for 5 min at 37°C. Cell suspensions were centrifuged at 1000 rpm for 5 min, washed once with HBSS, and resuspended in HBSS fortified with $CaCO_3$ (2mM), HEPES (10mM), and human serum albumin (5%). Cells were counted using a hemacytometer and diluted to a concentration of 800,000 cells/mL.

4.2.4 Leukocyte adhesion to HNt-coated surfaces

200,000 cells in 250μL were applied to each well and allowed to settle and adhere for 15 min. Surfaces were gently washed twice with fortified HBSS and remaining cells were subsequently fixed with 4% paraformaldehyde for 30 min. Cell membranes were

stained with CellMask Deep Red for 10 min at room temperature and washed twice with PBS. DAPI mounting medium was applied to the slides after carefully removing the flexiperm gaskets and cover slips were placed on each slide. Formyl-methionyl-leucyl-phenylalanine (fMLP) (R&D Systems, Minneapolis, MN) was added at a concentration of 1 nM to the fortified HBSS 15 min prior to introducing leukocytes to coated surface.

In a separate set of experiments, unprocessed and undiluted whole blood was applied directly to each surface for 15 min, followed by washing, fixing, and staining as before.

4.2.5 Analysis of cell spreading

Slides were analyzed by confocal microscopy in the Cornell University Institute of Biotechnology imaging facility. Micrographs were captured at the cell-slide interface at ten random locations on each surface and saved for offline analysis. Contact area was measured using the ImageJ software. Statistical analysis was performed by combining the area data from each donor at each HNt concentration, and these propagated errors were used to determine statistical significance between HNt concentrations via symmetric Student's t test in Graphpad Prism.

4.2.6 Quantification of adhering cells

Surfaces and cells were prepared as described above for analysis of contact area. Following fixation of cells, nuclei were stained with DAPI to aid in quantification. Brightfield and fluorescent micrographs were acquired at 100X magnification at ten

random locations on each surface. Cell count data was analyzed in the same way as that used for contact area data.

4.2.7 Surface roughness characterization

HNt-coated surfaces were prepared as described above, and then dried in a vacuum desiccator following the overnight aging step. Slides were analyzed using a Vecco DI-3000 atomic force microscope, managed by the Cornell University Nanobiotechnology Center. 10x10μm areas were scanned at three or more random locations on each surface. Image SXM was used to determine surface roughness (R_a) and area ratio (surface area ÷ planar area). Distance between peaks was determined by defining a peak as a surface feature that was distinct from its immediate surroundings by a height of ≥50nm. Line traces of topography were recorded at several random cross sections of each atomic force microscopy (AFM) image. Statistical comparisons were made via symmetric Student's t test in Graphpad Prism.

4.2.8 Computational modeling of leukocyte contact area

*This work was performed in a collaborative effort by Graham Marsh of the lab of Dr. Richard Waugh at the University of Rochester

A detailed description of the development of the model can be found in reference 17. Briefly, a cell surface was simulated with three microvilli of stochastic size within the range of 0-370nm and probability distribution determined to agree closely with previously published observations of microvillus heights. A random distribution of HNt

was populated in an area of 2x2μm and a leukocyte with three microvilli was compared to a smooth cell by calculating the separation distance at each point. From that contact region, the total area within 70nm of the surface was calculated as the contact area.

4.2.9 Leukocyte adhesion within microtube flow device

Microtube devices for cell capture were prepared as described previously (*202*). Briefly, 50 cm lengths of 300 μm i.d. Micro-renathane tubing (Braintree Scientific, Braintree, MA) were sterilized and coated with poly-L lysine and 6.6% HNt in a similar procedure as that used to coat slides, and as described previously (*196*). The smooth microtubes were coated with poly-L lysine with no HNt. Microtubes were incubated with 7.5 μg/mL E-selectin and blocked with 5% milk. Leukocytes at a concentration of 10^6/mL suspended in fortified HBSS were perfused through the microtubes at a flow rate that produced a wall shear stress of 2.5 dyn/cm^2 for 30 min. Microtube inlets were then transferred to cell-free buffer to wash off very loosely adherent cells, and then phase-contrast micrographs of 20 random locations along the length of each microtube were rapidly recorded with fluid flow maintained. Spread cells were identified visually by their spherical appearance and distinct edges. Statistical comparisons were carried out via symmetric Student's t test in Graphpad Prism.

4.2.10 Transmission electron microscopy of halloysite nanotubes

*This work was performed in a collaborative effort by Dr. David Foster at the University of Rochester

An aqueous dispersion of HNt was diluted with particle-free deionized water to a concentration suitable for well-dispersed particles in the electron microscope. A droplet of this dispersion (approximately 10 μL) was deposited on a commercial substrate (Ted Pella, P/N 1824) composed of an ultrathin amorphous carbon film supported by a lacey carbon net mounted on a 400 mesh Cu TEM grid. The substrate was soaked with acetone for 30 min prior to preparation to render the surface more hydrophilic.

Transmission electron micrographs were recorded from the dried specimen using a FEI CM20ST TEM operated at 200 kV. The images were recorded on a Gatan Model 894 Ultrascan CCD camera with a 2048x2048 pixel CCD. The magnification was calibrated using the 0.25 and 0.1 μm hole array from the "KMAG" standard manufactured for Kodak at Cornell University and certified by the National Physical Laboratory in Great Britain. The 2048x2048 pixel images were reduced to 1024x1024 pixel images with a bicubic interpolation.

4.3. RESULTS

4.3.1 Halloysite nanotubes

*This work was performed in a collaborative effort by Dr. David Foster at the University of Rochester

Electron microscope investigation of halloysite nanotubes revealed that they are not in large aggregates and exhibit a wide range of size (Figure 4.1). It is apparent, however, that the nanotubes are hollow and primarily longer on the longitudinal axis.

4.3.2 Halloysite nanotube coatings reduce leukocyte contact area

The contact area between adherent leukocytes, isolated by RBC lysis, and the surface was measured at varying concentrations of HNt coating. Confocal microscopy was used to focus on the plane of contact. It was observed that at high concentrations of HNt, contact area remained constant at approximately 100 μm^2, and when the concentration of HNt in the coating solution was decreased below 1% (w/v), the contact area increased to roughly twice the contact area on a smooth surface (Figure 4.2a). Variability in cell size was observed between patients, however a consistent trend in reduced contact area with increasing HNt concentration was observed for each donor. Analysis of the mean contact area of all leukocytes revealed that there was a significant reduction in the size of the contact region comparing 0.4% and 0.8% HNt. Serial micrographs captured in the Z plane demonstrate that leukocytes are flattened on the smooth surface (Figure 4.2b) and remain spherical on surfaces coated with higher concentrations of HNt (Figure 4.2c). Notably, identical adhesion of leukocytes was seen on smooth surfaces coated with E-selectin in the presence and absence of poly-L lysine, and negligible adhesion was observed when surfaces were coated with milk protein alone (data not shown).

4.3.3 Halloysite nanotube coating reduces number of adhering leukocytes

Surfaces prepared in an identical manner to those used to determine contact area were assessed for cell count following 15 min of settling time, gentle wash, and fixation. Nuclei were stained to facilitate counting. It was observed that the number of adherent cells decreased with increasing HNt surface concentration, a similar trend to that

observed for contact area (Figure 4.3a). The reduction in adherent cell number is quite dramatic, as can be directly observed in representative micrographs (Figure 4.3b and 4.3c). It is interesting to note that the most significant reduction in cell count was seen between 3.3% and 1.3%, which differs from the behavior observed for contact area in which the greatest change was seen between 0.8% and 0.4%.

4.3.4 Mean distance between surface peaks correlates with cellular behavior

Atomic force microscopy was used to determine the submicroscopic characteristics of the HNt coated surfaces. Surfaces were prepared in an identical manner to those used for studying cell behavior. Subsequent analysis of the HNt surfaces using the Image SXM software revealed that there were reductions in roughness (R_a) and area ratio at the lowest concentration of HNt compared to higher concentrations of HNt, however no discernable trend continued after the lowest concentration of HNt (Table 4.1). Numerous line traces of height were generated from AFM scans and evaluated for the average distance between distinct surface features to establish an alternate measure of surface roughness. The mean distance between peaks varied from approximately 1 to 4 μm and marked changes were measured at HNt concentrations below 1% (Figure 4.4). A separation distance of approximately 2 μm was found to correlate with the change in cell spreading that was seen between 0.4 and 0.8% HNT. Surface zeta potential of coated surfaces was analyzed by dynamic light scattering using a zetasizer and it was determined that the HNt coating did not impact charge appreciably: -43.5±1.5 mV on the 13.3% HNt surface versus -38.4±3.3 mV on the uncoated surface.

4.3.5 Leukocyte adhesive behavior is consistent in whole blood

To determine the behavior of leukocytes in more physiological applications, unprocessed heparinized whole blood was incubated on HNt-coated surfaces for 15 min. Following a gentle wash, adherent cells were imaged to quantify contact area as before. Despite inter-donor variability, it was determined that the adhesive behavior of leukocytes in the milieu of whole blood was very consistent with that seen for isolated cells in buffer as used in other experiments (Figure 4.5). Again, analysis of the mean contact area showed a significant increase in contact area at lower HNt concentrations, i.e., below 0.8%.

4.3.6 Computational modeling of leukocyte contact area is predictive of adhesive behavior

*This work was performed in a collaborative effort by Graham Marsh of the lab of Dr. Richard Waugh at the University of Rochester

Previous work by Bruel et al. identified a broad range of microvillus heights on leukocyte surfaces (*203*). Based on these data, Lomakina et al. developed a model of the leukocyte surface and the distribution of surface receptors in topographically-distinct regions, specifically on microvilli and intervening valleys (*193*). The inclusion of an adhesive surface with characteristic topography into this model (Figure 4.6b) allowed for computational inspection of leukocyte adhesion onto model HNt-coated surfaces with varying surface densities of HNt (Figure 4.6). For a smooth spherical cell, the maximum contact area occurred on a smooth surface and the contact area fell to a very low value

upon incorporation of a few HNt onto the adhesive surface. It should be noted that due to the scale of the plot, the large surface contact of a smooth cell and smooth surface is out of range. As expected, as the number of HNt on the adhesive surface was increased, thereby increasing the surface area, the contact area of the smooth cell increased as well. However, this was not the case for a cell that possessed three microvilli in the contact region of its surface. Using the distribution of microvilli heights measured by Bruel et al. a precipitous decrease in contact area was observed similar to that seen with a smooth surface, however due to the geometry of the three microvilli this contact area remained at the minimum contact area and did not increase with increasing numbers of HNt on the adhesive surface. This trend is consistent with what was seen in spreading experiments (Figure 4.1a) and provide a straightforward mechanism for this behavior.

4.3.7 Halloysite nanotube coatings improve performance of microtube flow device

A 300 μm (i.d.) flow device was assembled to test the adhesion behavior of leukocytes with and without the HNt coating in a model biomedical device. Following 30 min of perfusion through the microtube device at a flow rate producing 2.5 dyn/cm^2 of wall shear stress, it was observed that significantly more leukocytes adhered to the smooth surface regardless of the concentration of E-selectin used (Figure 4.7b). Furthermore, at higher concentrations of E-selectin virtually all of the adherent cells in the smooth tube had spread flat onto the surface, while a negligible number of leukocytes spread onto the HNt surface (Figure 4.7a). This is the case even at the highest concentrations of E-selectin studied. This indicates that the leukocytes are more firmly

adhered to the smooth surface, and that a greater total area of the smooth surface is covered with leukocytes than on the HNt surface.

4.4 Discussion

We demonstrate in this study that leukocytes spread on E-selectin coated substrates, and this behavior is largely abolished on nanostructured surfaces coated with halloysite nanotubes. The arrest of cell spreading occurred at a distinct concentration of HNt, namely between 0.4% and 0.8% HNt, and this was a robust observation in that it was consistent between isolated cells (Figure 4.2) and whole blood (Figure 4.5). Furthermore, it was observed that even in the presence of inflammatory signals such as fMLP leukocyte spreading was prevented (Figure 4.8). Usage of HNt was beneficial because it allowed for tuning of the surface roughness by simple dilution and is optically transparent when applied as a surface coating.

Previous work by the King lab has characterized the HNt coating as having an enhancing effect on cell adhesion, resulting in increased adhesion both in terms of number and strength of carcinoma and leukemic cells (*202*). It was determined that the effect of the HNt coating was to increase selectin adsorption in addition to projecting adhesive ligands into the hydrodynamic lubrication layer to enhance capture of flowing cells. Here, I present a wholly distinct phenomenon for normal blood cells, in which the adhesion behavior of normal leukocytes is diminished, rather than enhanced, by the HNt coating.

It is interesting to note that the trend in cell contact area, the measure used to quantify spreading, is also reflected in total cell adhesion counts (Figure 4.3), however

the shift in adhesion numbers occurs at a higher concentration of HNt. This is indicative of two simultaneous actions of the HNt coating, making it less likely that leukocytes will adhere and also preventing leukocyte spreading, with the threshold values for these activities not necessarily equivalent.

A key feature of the HNt surface coating that appears to play an important role in cellular adhesive behavior is the lateral spacing of surface features on the contact plane (Figure 4.4) rather than more conventional roughness measures. The roughness measurement R_a is more of a quantification of the height of surface roughness features rather than the spacing of features, and it follows that R_a is a gross evaluation of a surface and not necessarily representative of what an individual cell will experience when contacting a surface. I propose that it is the number of nanotubes on the surface and the geometry of these tubes that prevents leukocyte spreading. Computational modeling of a surface coated with variable numbers of nanotubes and a cell possessing physiologically-relevant microvilli supports this idea (Figure 4.6). Interestingly, the model also predicts that cells devoid of microvilli will experience increased surface contact with increasing HNt concentration, as was seen in previous studies (*202*).

Cell spreading on E-selectin alone is an interesting phenomenon and this may be one of the first examinations of such behavior. Selectins are well known as receptors responsible for cell tethering and rolling (*204*). Selectins bind sialylated and fucosylated carbohydrates (*205*) and it has recently been shown that core 1-derived o-glycans are required on ligands for E-selectin binding (*206*). Numerous leukocyte-bound ligands have been well described, including PSGL-1, ESL-1, CD44, CD43, Mac-1 ($\alpha_M\beta_2$), LFA-1 ($\alpha_L\beta_2$), and MUC1 (*200, 207-211*). Furthermore, E-selectin ligand binding is known to

activate leukocyte integrins, for example PSGL-1 and CD44 binding to E-selectin induce LFA-1 activation via tyrosine kinase Btk pathways (*212, 213*). Therefore it is likely that the effect of the HNt coating is to prevent leukocyte activation due to restricted access to E-selectin moieties as illustrated by the computational modeling, and the absence of activated integrins forgoes cell spreading. Spreading is an energy-expensive process that requires extensive receptor and cytoskeletal rearrangement (*193*), and it follows that this process would be restricted to productive settings such as when a leukocyte is already tethered or rolling on endothelium via selectin bonds. Such activity by the HNt coating has yet to be fully realized and should be the focus of future work.

There is a general lack of data in the literature concerning the topography of the endothelial surface *in vivo* (*214*), doubtless due in part to technical challenges, so the relevance of this study to cellular behavior *in vivo* is presently impossible to determine. Microplicae are ridge-like folds found on the surface of epithelial cells that are anisotropic but exhibit similar spatial dimensions to the HNt coating (*215*) and their biological function is not well understood. Microplicae have been identified on the surface of capillary endothelia in fowl (*216*), therefore it is possible to speculate on a role of nanotopography in leukocyte recruitment. It is also possible to consider the effect of inflammation on the topography of the endothelium, when vessels dilate and blood pressure increases. That leukocytes extravasate primarily in post-capillary venules is well known, and it is possible that endothelial smoothening aids this process. This too, however, is speculative at this time.

While the role of this study in the physiological setting is unclear, its utility *in vitro* is clear. I demonstrated this with the example of cell capture in a microfluidic

device (Figure 4.7). Microfluidic devices are very prevalent in research and increasingly so in the clinic, and here I propose an efficient and inexpensive way to significantly reduce biofouling by leukocyte adhesion. This phenomenon, in conjunction with previous reports by our group in which non-leukocyte cell types (such as circulating tumor cells) display enhanced adhesion to HNt coatings highlight the synergistic activity of HNt coatings.

4.5 Conclusions

In summary, I demonstrate a novel nanostructured coating that modulates the adhesive behavior of leukocytes in such as way that cell spreading is prevented. This is extended into a study of leukocyte spreading as a function of surface roughness by diluting the concentration of halloysite nanotubes on the surface and identifies a threshold concentration of HNt that precludes cell spreading. Surface roughness characterization identified a metric of surface roughness that correlates with cell behavior, the mean distance between distinct surface features. Computational modeling of leukocyte contact with simulated HNt-coated surfaces demonstrates that the geometry of the leukocyte and the HNt-coated surface restricts access of the leukocyte to the surface to a very small effective contact area and agrees with experimental findings presented both here and in previous works. Finally, I demonstrate the utility of this coating in preventing leukocyte spreading and reducing leukocyte adhesion in a microfluidic example device.

4.6 Acknowledgements

This work was supported by a National Science Foundation Graduate Research Fellowship to A.D.H. (DGE-0707428).

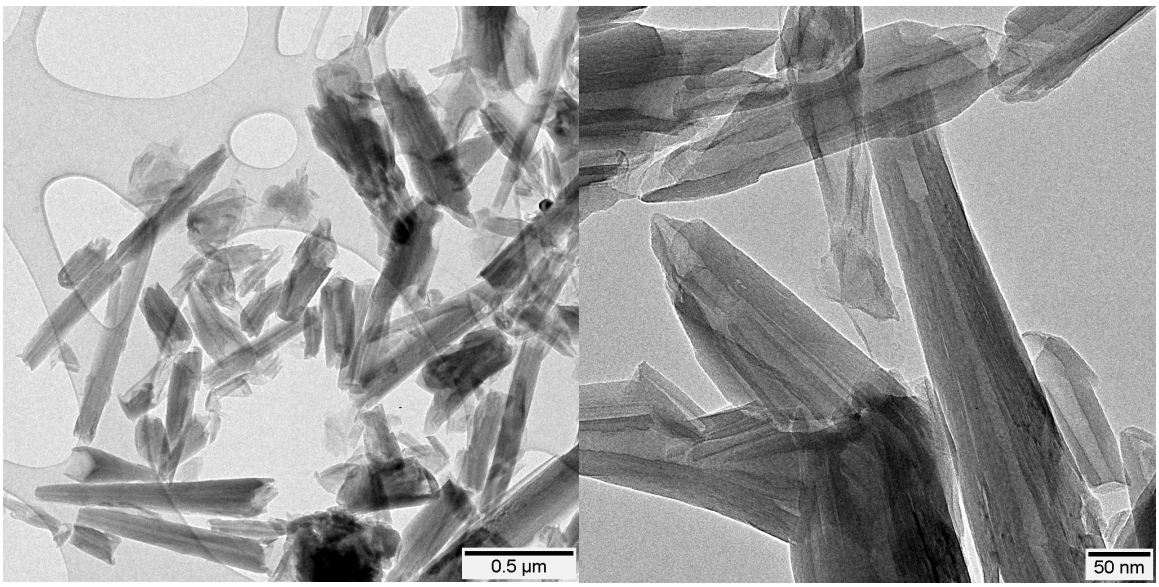

Figure 4.1. Transmission electron microscopy of halloysite nanotubes. Scale bars indicate 500 nm (left) and 50 nm (right).

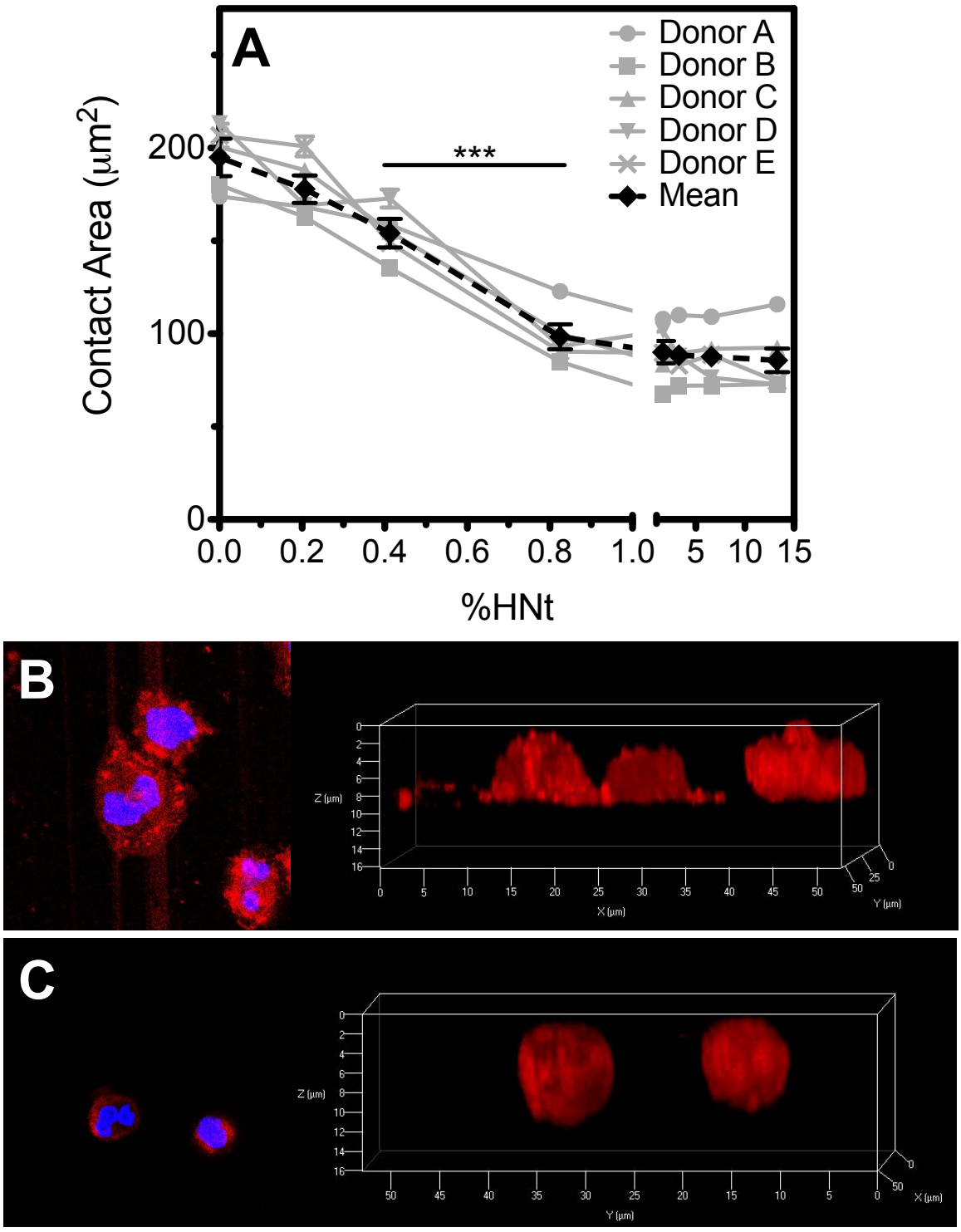

Figure 4.2. (A) Leukocyte contact area decreases with increasing HNt surface concentration, as identified by cell area at the plane of the surface (A). X-axis is broken at

1.0%. Cells on the smooth surface appear spread and flattened (B) compared to the more spherical cells bound to a surface coated with 13.3% HNt (C). In panels B and C the image on the right is the digital reconstruction of Z-stacks acquired by confocal microscopy and is the view of the image on the left as seen from the bottom. ***P<0.001.

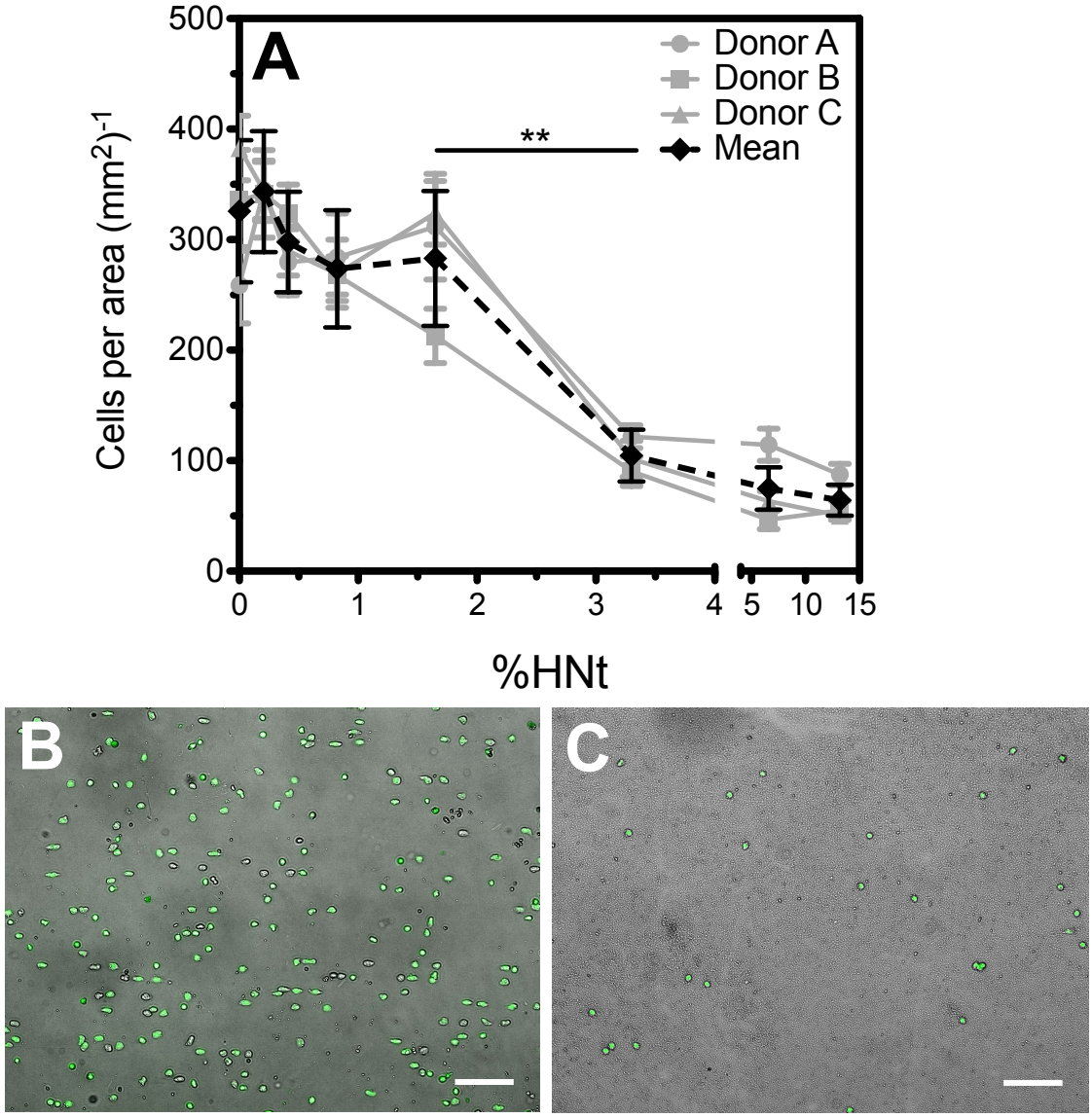

Figure 4.3. (A) The number of adherent leukocytes is reduced on high concentrations of HNt. X-axis is broken at 5.0%. Representative images demonstrate that there are more leukocytes bound to the smooth surface (B) than to the 13.3% HNt surface (C). Scale bars indicate 100 μm and cells are readily identified by DAPI staining of their nuclei (green). **P<0.01.

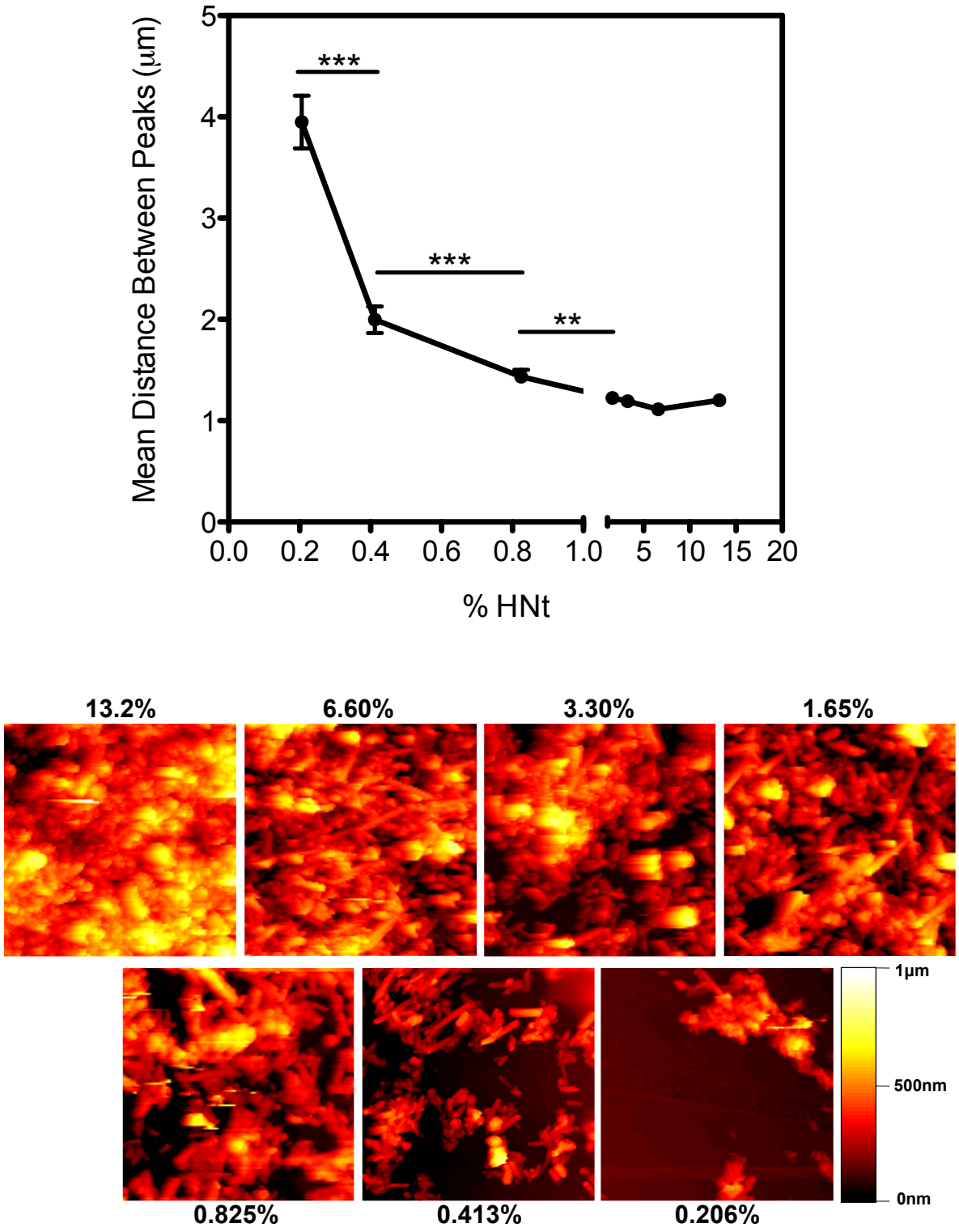

Figure 4.4. Analysis of the lateral spacing of surface features created by the HNt coating, obtained from atomic force microscopy (AFM) of the HNt coatings, reveals that there is a

significant reduction in spacing with increasing concentration of HNt (upper pane). All AFM images are 5x5μm. **P<0.01, ***P<0.001.

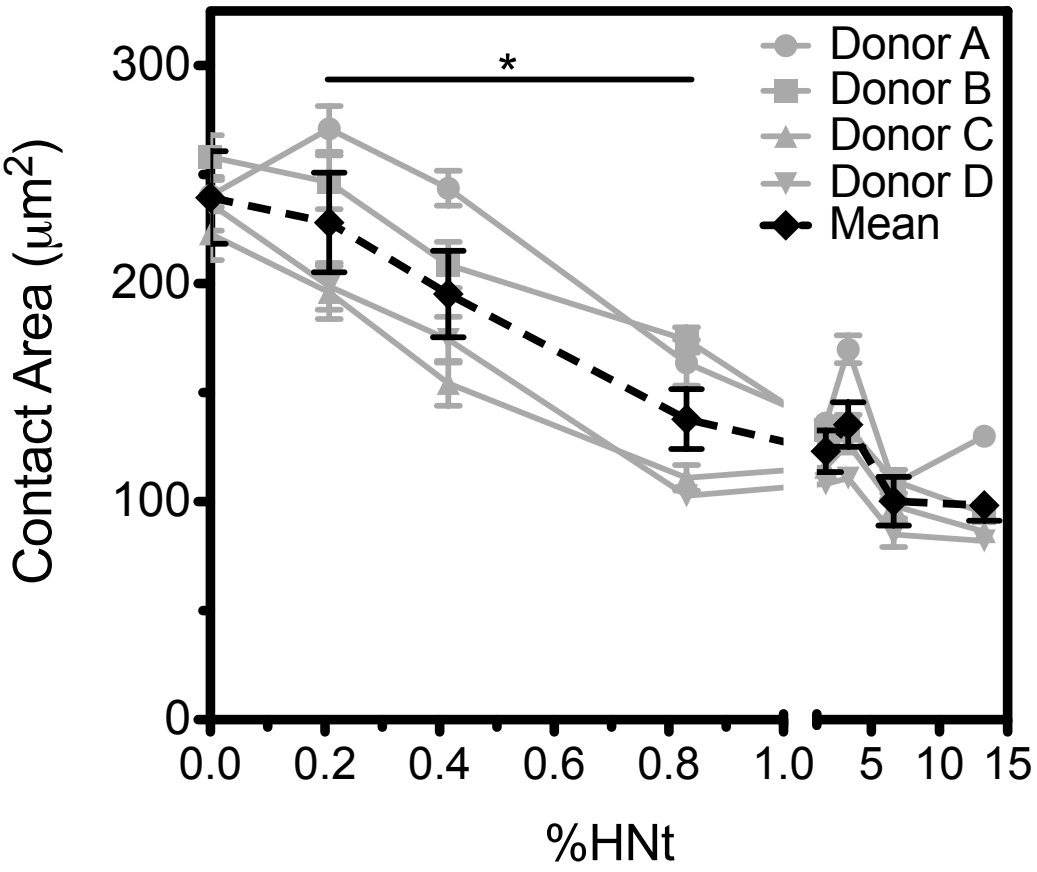

Figure 4.5. Leukocyte contact area decreases with increasing HNt surface concentration when incubated on surfaces in whole blood. *P<0.05.

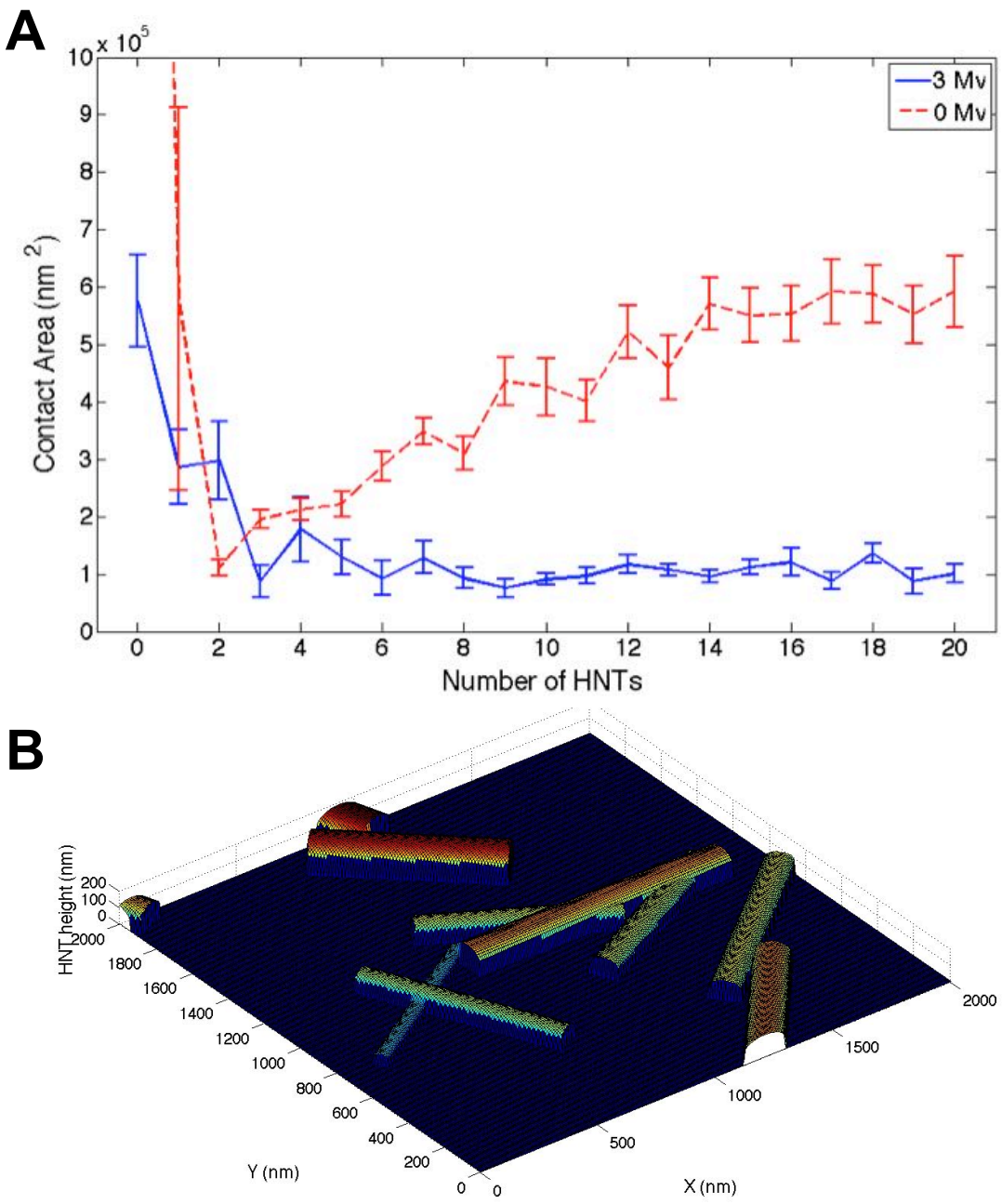

Figure 4.6. (A) Computational modeling of a leukocyte interacting with surfaces coated with different numbers of HNt demonstrates that leukocytes, distinct in their expression of microvilli (Mv) maintain a low molecular contact area with the surface (3 Mv, blue solid line) compared to a smooth cell (0 Mv, red dashed line) despite increasing numbers

of HNt. (B) HNt were generated based on random distributions of length, diameter, location, and orientation on the surface.

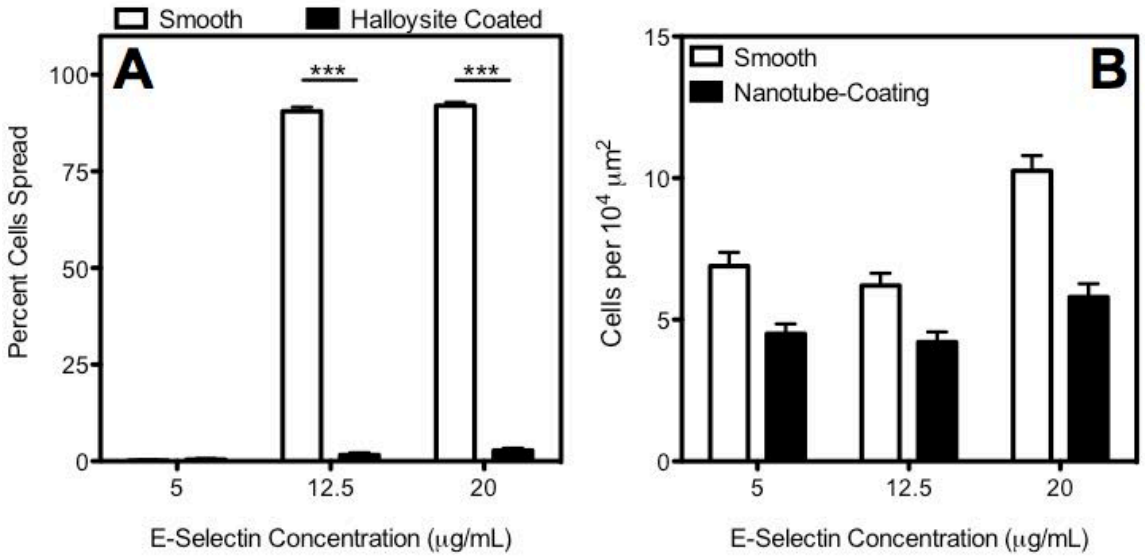

Figure 4.7. (A) Leukocyte spreading is absent within a microfluidic device at low surface concentrations of E-selectin and high concentrations of E-selectin in the presence of the HNt coating. (B) Additionally, total leukocyte adhesion is reduced on HNt coatings at all surface concentrations of E-selectin within the flow device.

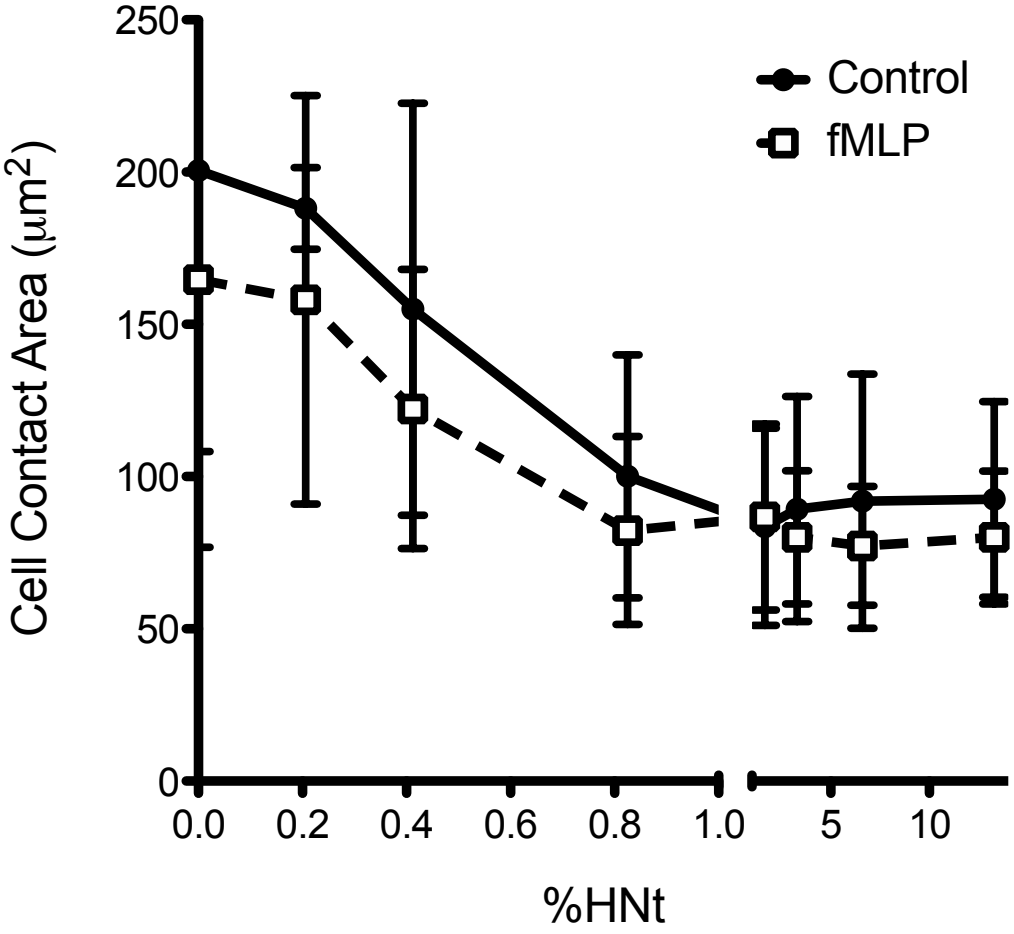

Figure 4.8. 1 nM formyl-methionyl-leucyl-phenylalanine (fMLP) was introduced to leukocytes 15 min prior to allowing cells to adhere to HNt-coated surfaces. Error bars represent standard deviation.

Table 4.1. Additional surface roughness characteristics of HNt coatings. The Area Ratio is a ratio of surface area to planar area.

% HNt	*R_a (nm)*	*Area Ratio*
13.2	146	1.267
6.60	119	1.321
3.30	131	1.251
1.65	166	1.264
0.825	137	1.288
0.413	101	1.265
0.206	81	1.163
0	5.3	1.00

4.7 References

173. B. Wojciak-Stothard, Z. Madeja, W. Korohoda, A. Curtis, C. Wilkinson, Activation of macrophage-like cells by multiple grooved substrata. Topographical control of cell behaviour. *Cell Biol Int* **19**, 485-490 (1995).

174. A. Curtis, C. Wilkinson, Topographical control of cells. *Biomaterials* **18**, 1573-1583 (1997).

175. R. G. Flemming, C. J. Murphy, G. A. Abrams, S. L. Goodman, P. F. Nealey, Effects of synthetic micro- and nano-structured surfaces on cell behavior. *Biomaterials* **20**, 573-588 (1999).

176. E. K. Yim, K. W. Leong, Significance of synthetic nanostructures in dictating cellular response. *Nanomedicine* **1**, 10-21 (2005).

177. J. Y. Lim, H. J. Donahue, Cell sensing and response to micro- and nanostructured surfaces produced by chemical and topographic patterning. *Tissue Eng* **13**, 1879-1891 (2007).

178. J. A. Schmidt, A. F. von Recum, Macrophage response to microtextured silicone. *Biomaterials* **13**, 1059-1069 (1992).

179. M. J. Dalby *et al.*, Rapid fibroblast adhesion to 27nm high polymer demixed nano-topography. *Biomaterials* **25**, 77-83 (2004).

180. N. W. Karuri *et al.*, Biological length scale topography enhances cell-substratum adhesion of human corneal epithelial cells. *J Cell Sci* **117**, 3153-3164 (2004).

181. A. S. Curtis *et al.*, Cells react to nanoscale order and symmetry in their surroundings. *IEEE Trans Nanobioscience* **3**, 61-65 (2004).

182. E. Martines, K. McGhee, C. Wilkinson, A. Curtis, A parallel-plate flow chamber to study initial cell adhesion on a nanofeatured surface. *IEEE Trans Nanobioscience* **3**, 90-95 (2004).

183. E. K. Yim *et al.*, Nanopattern-induced changes in morphology and motility of smooth muscle cells. *Biomaterials* **26**, 5405-5413 (2005).

184. E. T. den Braber, J. E. de Ruijter, L. A. Ginsel, A. F. von Recum, J. A. Jansen, Quantitative analysis of fibroblast morphology on microgrooved surfaces with various groove and ridge dimensions. *Biomaterials* **17**, 2037-2044 (1996).

185. K. M. Ainslie *et al.*, In vitro inflammatory response of nanostructured titania, silicon oxide, and polycaprolactone. *J Biomed Mater Res A* **91**, 647-655 (2009).

186. I. Wall, N. Donos, K. Carlqvist, F. Jones, P. Brett, Modified titanium surfaces promote accelerated osteogenic differentiation of mesenchymal stromal cells in vitro. *Bone* **45**, 17-26 (2009).

187. C. Eriksson, J. Lausmaa, H. Nygren, Interactions between human whole blood and modified TiO2-surfaces: influence of surface topography and oxide thickness on leukocyte adhesion and activation. *Biomaterials* **22**, 1987-1996 (2001).

188. H. F. Langer, T. Chavakis, Leukocyte-endothelial interactions in inflammation. *J Cell Mol Med* **13**, 1211-1220 (2009).

189. K. Ley, C. Laudanna, M. I. Cybulsky, S. Nourshargh, Getting to the site of inflammation: the leukocyte adhesion cascade updated. *Nat Rev Immunol* **7**, 678-689 (2007).

190. E. P. Wojcikiewicz, X. Zhang, A. Chen, V. T. Moy, Contributions of molecular binding events and cellular compliance to the modulation of leukocyte adhesion. *J Cell Sci* **116**, 2531-2539 (2003).

191. A. Pierres, A. M. Benoliel, P. Bongrand, Cell fitting to adhesive surfaces: A prerequisite to firm attachment and subsequent events. *Eur Cell Mater* **3**, 31-45 (2002).

192. P. Robert, D. Touchard, P. Bongrand, A. Pierres, Biophysical description of multiple events contributing blood leukocyte arrest on endothelium. *Front Immunol* **4**, 108 (2013).

193. E. B. Lomakina, G. Marsh, R. E. Waugh, Cell surface topography is a regulator of molecular interactions during chemokine-induced neutrophil spreading. *Biophys J* **107**, 1302-1312 (2014).

194. C. L. Abram, C. A. Lowell, The ins and outs of leukocyte integrin signaling. *Annu Rev Immunol* **27**, 339-362 (2009).

195. G. Voskerician *et al.*, Biocompatibility and biofouling of MEMS drug delivery devices. *Biomaterials* **24**, 1959-1967 (2003).

196. A. D. Hughes *et al.*, Microtube device for selectin-mediated capture of viable circulating tumor cells from blood. *Clin Chem* **58**, 846-853 (2012).

197. A. D. Hughes, J. Mattison, J. D. Powderly, B. T. Greene, M. R. King, Rapid isolation of viable circulating tumor cells from patient blood samples. *J Vis Exp*, e4248 (2012).

198. S. Hiratsuka *et al.*, Endothelial focal adhesion kinase mediates cancer cell homing to discrete regions of the lungs via E-selectin up-regulation. *Proc Natl Acad Sci U S A* **108**, 3725-3730 (2011).

199. F. W. Orr, J. Lee, W. C. Duivenvoorden, G. Singh, Pathophysiologic interactions in skeletal metastasis. *Cancer* **88**, 2912-2918 (2000).

200. Y. Geng, K. Yeh, T. Takatani, M. R. King, Three to Tango: MUC1 as a Ligand for Both E-Selectin and ICAM-1 in the Breast Cancer Metastatic Cascade. *Front Oncol* **2**, 76 (2012).

201. S. R. Levis, P. B. Deasy, Characterisation of halloysite for use as a microtubular drug delivery system. *Int J Pharm* **243**, 125-134 (2002).

202. A. D. Hughes, M. R. King, Use of naturally occurring halloysite nanotubes for enhanced capture of flowing cells. *Langmuir* **26**, 12155-12164 (2010).

203. R. E. Bruehl, T. A. Springer, D. F. Bainton, Quantitation of L-selectin distribution on human leukocyte microvilli by immunogold labeling and electron microscopy. *J Histochem Cytochem* **44**, 835-844 (1996).

204. T. A. Springer, Traffic signals for lymphocyte recirculation and leukocyte emigration: the multistep paradigm. *Cell* **76**, 301-314 (1994).

205. G. S. Kansas, Selectins and their ligands: current concepts and controversies. *Blood* **88**, 3259-3287 (1996).

206. T. Yago *et al.*, Core 1-derived O-glycans are essential E-selectin ligands on neutrophils. *Proc Natl Acad Sci U S A* **107**, 9204-9209 (2010).

207. Y. Katayama, A. Hidalgo, J. Chang, A. Peired, P. S. Frenette, CD44 is a physiological E-selectin ligand on neutrophils. *J Exp Med* **201**, 1183-1189 (2005).

208. L. Xia *et al.*, P-selectin glycoprotein ligand-1-deficient mice have impaired leukocyte tethering to E-selectin under flow. *J Clin Invest* **109**, 939-950 (2002).

209. M. Matsumoto, A. Shigeta, M. Miyasaka, T. Hirata, CD43 plays both antiadhesive and proadhesive roles in neutrophil rolling in a context-dependent manner. *J Immunol* **181**, 3628-3635 (2008).

210. A. Hidalgo, A. J. Peired, M. K. Wild, D. Vestweber, P. S. Frenette, Complete identification of E-selectin ligands on neutrophils reveals distinct functions of PSGL-1, ESL-1, and CD44. *Immunity* **26**, 477-489 (2007).

211. K. L. Crutchfield *et al.*, CD11b/CD18-coated microspheres attach to E-selectin under flow. *J Leukoc Biol* **67**, 196-205 (2000).

212. H. Mueller *et al.*, Tyrosine kinase Btk regulates E-selectin-mediated integrin activation and neutrophil recruitment by controlling phospholipase C (PLC) gamma2 and PI3Kgamma pathways. *Blood* **115**, 3118-3127 (2010).

213. T. Yago *et al.*, E-selectin engages PSGL-1 and CD44 through a common signaling pathway to induce integrin alphaLbeta2-mediated slow leukocyte rolling. *Blood* **116**, 485-494 (2010).

214. S. W. Park, M. Intaglietta, D. M. Tartakovsky, Impact of endothelium roughness on blood flow. *J Theor Biol* **300**, 152-160 (2012).

215. P. M. Andrews, Microplicae: characteristic ridge-like folds of the plasmalemma. *J Cell Biol* **68**, 420-429 (1976).

216. S. G. Kiama, J. Bhattacharjee, J. N. Maina, K. D. Weyrauch, Surface specialization of the capillary endothelium in the pecten oculi of the chicken, and

their overt roles in pectineal haemodynamics and nutrient transfer to the inner neural retina. *Acta Biol Hung* **48**, 473-483 (1997).

CHAPTER 5 – CONCLUSIONS & FUTURE DIRECTIONS

5.1 Conclusions from halloysite nanotube coating characterization

Much of this work has been conducted to demonstrate that halloysite nanotube coatings embody a novel technology for enhancing the capture of viable cells from flow. This has been accomplished by an alteration of the surface topography with immobilized nanotubes, as shown in Chapter 2. Specifically, enhancement in cell capture was established in terms of cell rolling velocity, indicative of increased adhesion strength, and the number of cells captured. Based on observations of these data, I developed a conceptual model of capture enhancement in which not only is the surface area increased, but individual surface features from the halloysite nanotube coating also span the hydrodynamic lubrication layer that exists close to the luminal surface of a tube through which flow is laminar. This model was underpinned by immunofluorescence measurements that quantified protein adsorption, atomic force microscopy analysis of the nanoscale surface features, and microscopic analysis of flowing tracer particles over the nanostructured surface. The result was the establishment of a technology that captured more cells with greater binding force. Cells are also captured with improved efficiency, in that less settling is required for surface contact, therefore decreasing the longitudinal distance that a flowing cells must travel through a device to interact with the biologically active surface.

A significant and remarkable additional feature of the halloysite nanotube coating was identified in its modulation of the adhesive behavior of leukocytes in such a way that cell spreading is prevented. The nanostructured roughness of the nanotube coating was identified as the essential factor that correlates with cell behavior, specifically the distance between distinct surface features. Computational modeling of leukocyte

adhesion to simulated halloysite nanotube coated surfaces supported experimental observations. This is highly useful in the capture of non-leukocyte target cells, as is very often the case, in that biofouling by leukocytes is a common limitation to the application of a wide array of biomedical devices.

5.2 Conclusions from circulating tumor cell (CTC) capture

*The following is adapted from the following publication: AD Hughes, J Mattison, JD Powderly, BT Greene, MR King, Rapid isolation of viable circulating tumor cells from patient blood samples, *Journal of Visualized Experiments*, **2012,** (64) e4248.

A major motivation for enhancing the capture of flowing target cells from a heterogeneous cell suspension is the capture of circulating tumor cells from samples of peripheral blood drawn from patients diagnosed with metastatic cancer. It is often the case that the early steps in the discovery of new cancer therapeutics utilize cancer cell lines, which bear questionable resemblance to primary cancer cells yet remain in use due to their ease of use in the laboratory. Research into the development of new cancer therapies would be expedited if primary human cancer cells were utilized early in novel research. CTC are the most easily accessible type of cancer cell, due to their presence in blood and the ease of a standard blood draw. In addition, circulating tumor cells represent a necessary step in the process of metastasis (*217, 218*), so their relevance to the disease and utility for targeting new drugs is clear. Isolation of CTC from blood in vitro is complicated by their low concentrations: on the order of one per million leukocytes or one per billion erythrocytes (*219*). The majority of current methods for detecting CTC in blood, including the only FDA-approved technique CellSearch® (Veridex), damage or destroy cells in the detection process, precluding use beyond enumeration. The method described above does not compromise cell viability and thus opens the door for future clinical research on cancer. As the recovery of intact cells is the goal of this technique, it is imperative that cells be handled with care, especially during blood separation steps.

There are a number of tunable parameters in this system that could be altered to achieve improved yield depending on critical characteristics such as cancer type. In the steps described in Chapter 3, I chose to use EpCAM as a CTC-specific antibody for all cancer types except when processing prostate cancer samples, wherein anti-PSMA was used. Further substitutions of cancer-specific antibodies can certainly be used to improve performance for individual patients. Furthermore, selectin and antibody concentrations can be altered to enhance capture (*220*).

An essential feature of the device is the incorporation of E-selectin molecules onto the surface. E-selectin is normally expressed on the luminal surface of endothelial cells and function to recruit fast moving leukocytes to sites of inflammation. Flowing leukocytes bind transiently to selectin molecules, resulting in a slower, rolling behavior that facilitates slower and stronger binding of the cell to the endothelium by integrins. Convincing experimental evidence exists that makes the case that CTC can extravasate by a similar mechanism (*221, 222*). The inclusion of selectin also allows the device to be operated at greater flow rates, rates that would otherwise prevent cells from binding to antibodies (*223*). Thus our device physiologically mimics a venule to biomimetically capture flowing CTC without inflicting cellular injury.

Enhanced device performance can be attributed to the addition of the halloysite nanotube coating to the luminal surface of the device. Previous studies have shown that there are three major components of the nanotube coating that allows for improved functionality. First, the nanotube coating provides increased surface area, allowing for greater protein deposition onto the surface (*224*). Second, in performing atomic force microscopy on the nanotube coating I have determined that individual nanotubes protrude

from the surface into the flow. This allows selectin molecules to be presented as much as one micron above the surface so that cells can be captured and recruited to the surface earlier in their trajectory through the tube (*224*). Finally, the halloysite nanotube coating is able to prevent leukocyte adhesion and spreading on the surface, allowing for a reduced number of leukocytes captured along with the CTC and thus greater subsequent CTC purities (*225*).

5.3 Personalized medicine driven by CTC characterization

Much current cancer research is focused on finding more effective targets for chemotherapeutic agents to better treat and kill tumors in the body. However, it is well known that cancer is a highly heterogeneous disease both inter-patient and intra-patient. For this reason, a growing trend in the treatment of cancer calls for personalized medicine, where diagnostic tests can be performed on each patient to tailor the best treatment cocktail available. For example, it has been shown that panitumumab can be effective therapy for colorectal cancer, but only in the presence of wild-type KRAS because KRAS mutation renders the treatment ineffective (*226*). Therefore colorectal cancer patients can be screened for KRAS mutations in order to choose a treatment regimen that is likely to be effective for them individually. As another example, a specific mutation of EGFR is sensitive to treatment with gefitnib, so individuals with non small cell lung cancer and this mutation are prescribed gefitnib and have a high likelihood of improved survival (*227*).

The traditional approach to predicting drug sensitivity when using a general chemotherapeutic (such as taxanes) that does not target a specific biomarker (such as Her2 for Herceptin) is to excise a small potion of a patient's tumor and treat the cancer cells *in vitro*. This methodology, however, has shown no statistically significant predictive capabilities (*228*). There are a number of potential reasons for this failure, including tumor heterogeneity (*229, 230*). In a typical punch biopsy only a small region of a tumor is tested for drug sensitivity, and while that small region may display a particular response to a drug this may not be indicative of the sensitivity of the overall tumor or the truly dangerous subsection of a tumor that may be the source of metastatic

cells. There is evidence that CTC reflect the breadth of tumor heterogeneity (*231*). CTC are believed to reflect in some way the breadth of tumor heterogeneity (*231*). Indeed, the case has been made that CTC are the relevant cancer cell subpopulation to target for therapy based on the fact that 90% of cancer deaths are due to metastasis (*232*). In addition, the circulatory system, within which cancer cells are termed CTC, is the primary route of metastasis (*233*), and thus it follows that the cells responsible for disease progression can be found in blood.

The device that was developed and evaluated in the preceding Chapters is ideally suited for the capture of CTC for personalized - or "precision" - medicine determination in that CTC can be captured in high numbers and purity without compromising the viability of captured cells. Furthermore, the CTC that are captured by the device are arguably the "most metastatic" of the CTC within the blood sample in that they are those most able to adhere to the device surface that is modeled after an inflamed postcapillary venule, and therefore the most important cells for which to determine drug sensitivity.

5.4 Circulating fetal cell capture from maternal peripheral blood

Fetal cells were first identified and captured from the blood of pregnant mothers in 1979 by Herzenberg et al. (*234*). To date, the gold standard techniques for sampling of fetal chromosomes are amniocentesis and chorionic venus sampling (CVS); invasive procedures that carry risks of harm to the fetus or miscarriage. The risks associated with amniocentesis and CVS are relatively small: studies disagree on actual fetal loss rates but they generally range from 0.2 to 2% (*235, 236*). Regardless of the true value of fetal losses the risk is significant compared to the zero risk associated with sampling of maternal peripheral blood. Isolation of fetal cells from maternal blood is nontrivial, in that their prevalence is blood is thought to be one fetal cell in every 10^6 to 10^8 nucleated maternal blood cells (*237*). Initial attempts at fetal cell isolation focused on fetal lymphocyte isolation by fluorescence-activated cell sorting (by its inventor no less) for paternally-inherited surface antigens (*234*). Subsequent generations of this technology evaluated the blood of mothers believed to be carrying male fetuses by fluorescence-activated cell sorting (FACS) for CD34 among other surface antigens followed by polymerase chain reaction (PCR) for the Y chromosome. Amazingly, male mononuclear cells were found in maternal blood up to 27 years postpartum (*238*). While this is a startling result, it has also shifted interest from fetal lymphocytes to other fetal cell types, specifically trophoblasts and erythroblasts, to reduce false positive results due to previous pregnancies.

Newer technologies have allowed for improved fetal cell capture and subsequent analyses. Fetal DNA has been identified using PCR for the Y chromosome in maternal blood serum and plasma (*239*). Magnetic-activated cell sorting (MACS) has provided the

ability to enrich for whole fetal erythroblasts, most commonly using anti-CD71 magnetic nanoparticles, followed by microdissection. These techniques have successfully identified fetal aneuploidies such as trisomy 18 and 21 in circulating fetal cells (*240, 241*). The National Institute of Child Health and Human Development Fetal Isolation Study (NIFTY) was created as a multi-center prospective study to assess the utility of circulating fetal cells for identifying fetal chromosome abnormalities. Results were to be compared to the gold standards amniocentesis and CVS. An early evaluation of the study found that MACS provided better results than FACS for fetal cell isolation, however different processing protocols used at different institutions caused inconsistent results and inferior results compared to metaphase karyotypes from amniocentesis or CVS (*242*).

Reliable capture of fetal cells from maternal blood would make the current procedures used to do genomic analysis on the fetus obsolete. This would be highly beneficial because the current procedures, namely amniocentesis and chorionic villus sampling, are invasive to the fetus and carry inherent risk of complications including miscarriage. The device previously developed to capture CTC from peripheral blood, as described in the previous Chapters, will be the starting point for a fetal cell capture device. For proof of purpose study, only peripheral blood samples from mothers carrying male fetuses should be used, allowing us to stain for the Y-chromosome for fetal cell identification as cells in the maternal circulation that contain a Y-chromosome must be from the male fetus.

5.4.1 Fetal trophoblast cell line surface marker expression

*****Work contributed by Y.Geng

To lay the groundwork for this study, two fetal trophoblast cell lines have been obtained and were analyzed by flow cytometry for surface marker expression. Selectin ligands include numerous molecules, so multiple ligands were tested for, namely sialyl lewis x (sLe^x), sialyl lewis a (sLe^a), and CD44. The cell line JAR was found to express sLe^x but not sLe^a or CD44, while the cell line HTR-8/SVneo expressed sLe^x and CD44, but not sLe^a (Figure 5.1). Thus both trophoblast cell line cells should be able to adhere to E-selectin in a similar manner as leukocytes and CTC.

The two trophoblast cells lines were investigated for surface expression of EpCAM, HLA-G, and L-selectin. It was found that JAR expressed EpCAM. In addition JAR were partially positive for L-selectin expression, meaning that a significant portion, but not all, of the cells expressed L-selectin (Figure 5.2a,b). HTR/SVneo cells were negative for all surface markers tested (Figure 5.2c,d).

To conclude, the summation of my doctoral work has been the construction of a selectin-functionalized microfluidic device designed for enhanced capture of rare cells from primary samples. I first developed a nanostructured coating composed of halloysite nanotubes that is able to increase the capture of target cells in terms of quantity of cells captured and the strength with which cells adhere to a selectin-functionalized surface. This nanotube coating was further investigated and found to project into the tubular lumen and project adhesion ligands across the hydrodynamic lubrication layer that opposes cellular interaction with the surface, without altering fluid dynamics within the microfluidic device. The enhanced capture technique was then applied to the clinical setting by demonstrating the ability to capture primary circulating tumor cells from patient blood samples. Comparison with today's gold standard CTC enumeration platform demonstrated the potential benefit to cancer diagnostics that is represented by this novel technology. Finally, further evaluation of leukocyte adhesion on the halloysite nanotube coating lead to the discovery that the nanotube coating prevents leukocyte adhesion, and critical surface concentrations were explored along with the mechanism of this rejection. In all, this technology embodies real potential for improved patient care in terms of diagnostics and the development of personalized therapeutic strategies

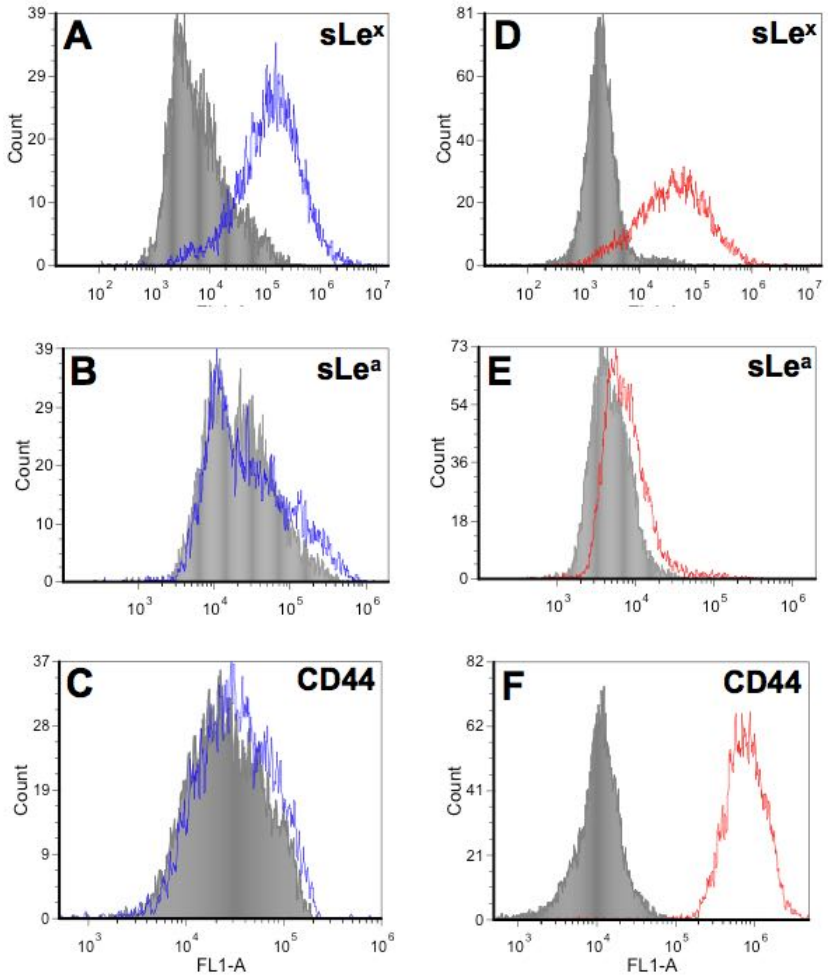

Figure 5.1. Surface expression flow cytometry of selectin ligands on fetal trophoblast cell lines JAR (A, B, C) and HTR-8/SVneo (D, E, F).

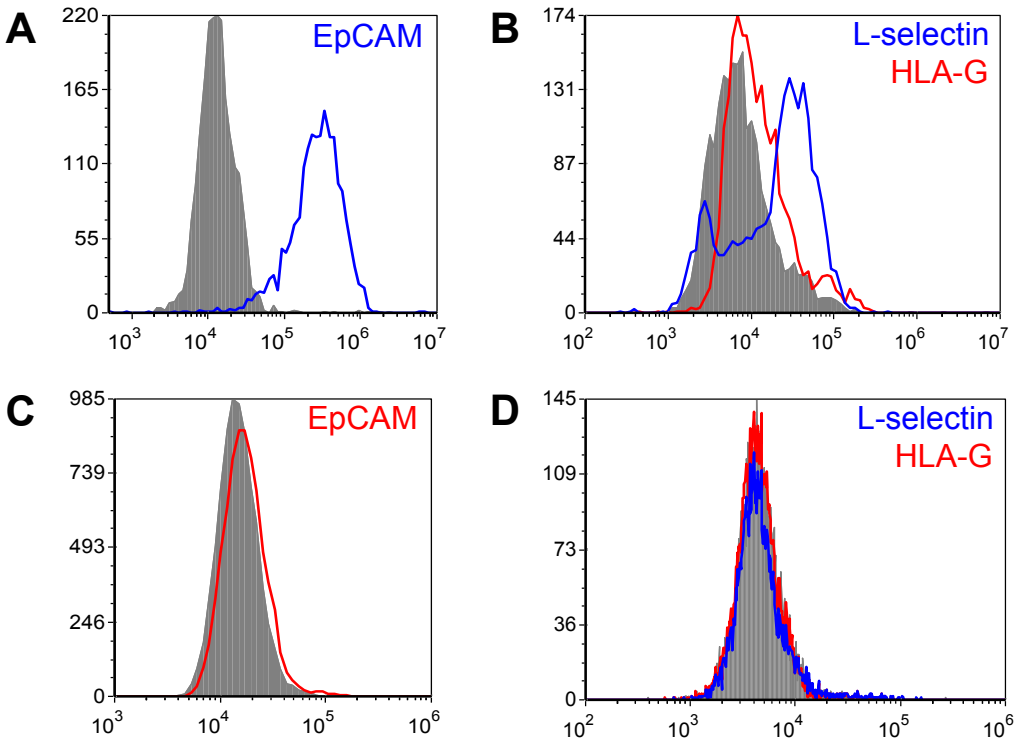

Figure 5.2. Surface expression of surface markers on fetal trophoblast cell lines. JAR cells were assessed for EpCAM expression (A) and for L-selectin and HLA-G expression (B) by flow cytometry. HTR-8/SVneo cells were assessed for EpCAM expression (C) and for L-selectin and HLA-G expression (D).

5.5 References

217. A. B. Al-Mehdi *et al.*, Intravascular origin of metastasis from the proliferation of endothelium-attached tumor cells: a new model for metastasis. *Nat Med* **6**, 100-102 (2000).

218. G. P. Gupta, J. Massague, Cancer metastasis: Building a framework. *Cell* **127**, 679-695 (2006).

219. S. Maheswaran, D. A. Haber, Circulating tumor cells: a window into cancer biology and metastasis. *Curr Opin Genet Dev* **20**, 96-99 (2010).

220. D. Lee, M. R. King, Microcontact Printing of P-Selectin Increases the Rate of Neutrophil Recruitment Under Shear Flow. *Biotechnology Progress* **24**, 1052-1059 (2008).

221. S. Gout, P. L. Tremblay, J. Huot, Selectins and selectin ligands in extravasation of cancer cells and organ selectivity of metastasis. *Clin Exp Metastasis* **25**, 335-344 (2008).

222. Y. Geng, J. Marshall, M. King, Glycomechanics of the Metastatic Cascade: Tumor Cell–Endothelial Cell Interactions in the Circulation. *Annals of Biomedical Engineering*, 1-16.

223. S. L. Stott *et al.*, Isolation of circulating tumor cells using a microvortex-generating herringbone-chip. *Proc Natl Acad Sci U S A* **107**, 18392-18397 (2010).

224. A. D. Hughes, M. R. King, Use of naturally occurring halloysite nanotubes for enhanced capture of flowing cells. *Langmuir* **26**, 12155-12164 (2010).

225. A. D. Hughes *et al.*, Microtube Device for Selectin-Mediated Capture of Viable Circulating Tumor Cells from Blood. *Clinical Chemistry* **In Press**, (2012).

226. R. G. Amado *et al.*, Wild-type KRAS is required for panitumumab efficacy in patients with metastatic colorectal cancer. *J Clin Oncol* **26**, 1626-1634 (2008).

227. M. Maemondo *et al.*, Gefitinib or chemotherapy for non-small-cell lung cancer with mutated EGFR. *N Engl J Med* **362**, 2380-2388 (2010).

228. D. J. Samson, J. Seidenfeld, K. Ziegler, N. Aronson, Chemotherapy sensitivity and resistance assays: A systematic review. *Journal of Clinical Oncology* **22**, 3618-3630 (2004).

229. M. Shipitsin *et al.*, Molecular definition of breast tumor heterogeneity. *Cancer Cell* **11**, 259-273 (2007).

230. I. Gonzalez-Garcia, R. V. Sole, J. Costa, Metapopulation dynamics and spatial heterogeneity in cancer. *Proc Natl Acad Sci U S A* **99**, 13085-13089 (2002).

231. F. Davnall *et al.*, Assessment of tumor heterogeneity: an emerging imaging tool for clinical practice? *Insights Imaging* **3**, 573-589 (2012).

232. C. Wittekind, M. Neid, Cancer invasion and metastasis. *Oncology* **69 Suppl 1**, 14-16 (2005).

233. A. F. Chambers, A. C. Groom, I. C. MacDonald, Dissemination and growth of cancer cells in metastatic sites. *Nat Rev Cancer* **2**, 563-572 (2002).

234. L. A. Herzenberg, D. W. Bianchi, J. Schroder, H. M. Cann, G. M. Iverson, Fetal cells in the blood of pregnant women: detection and enrichment by fluorescence-activated cell sorting. *Proc Natl Acad Sci U S A* **76**, 1453-1455 (1979).

235. A. H. Nassar *et al.*, Genetic amniocentesis complications: is the incidence overrated? *Gynecol Obstet Invest* **58**, 100-104 (2004).

236. F. Mujezinovic, Z. Alfirevic, Procedure-related complications of amniocentesis and chorionic villous sampling: a systematic review. *Obstet Gynecol* **110**, 687-694 (2007).

237. M. C. Cheung, J. D. Goldberg, Y. W. Kan, Prenatal diagnosis of sickle cell anaemia and thalassaemia by analysis of fetal cells in maternal blood. *Nat Genet* **14**, 264-268 (1996).

238. D. W. Bianchi, G. K. Zickwolf, G. J. Weil, S. Sylvester, M. A. DeMaria, Male fetal progenitor cells persist in maternal blood for as long as 27 years postpartum. *Proc Natl Acad Sci U S A* **93**, 705-708 (1996).

239. Y. M. Lo *et al.*, Presence of fetal DNA in maternal plasma and serum. *Lancet* **350**, 485-487 (1997).

240. D. GÄNshirt-Ahlert *et al.*, Detection of Fetal Trisomies 21 and 18 From Maternal Blood Using Triple Gradient and Magnetic Cell Sorting. *American Journal of Reproductive Immunology* **30**, 194-201 (1993).

241. Y. H. Yang, E. S. Yang, J. Y. Kwon, I. K. Kim, Y. W. Park, Prenatal diagnosis of trisomy 21 with fetal cells in maternal blood using comparative genomic hybridization. *Fetal Diagn Ther* **21**, 125-133 (2006).

242. D. W. Bianchi *et al.*, Fetal gender and aneuploidy detection using fetal cells in maternal blood: analysis of NIFTY I data. National Institute of Child Health and Development Fetal Cell Isolation Study. *Prenat Diagn* **22**, 609-615 (2002).

APPENDIX: PROTOCOL FOR DEVICE CONSTRUCTION

The following is adapted from the following publication: AD Hughes, J Mattison, JD Powderly, BT Greene, MR King, Rapid isolation of viable circulating tumor cells from patient blood samples, *Journal of Visualized Experiments*, **2012,** (64) e4248.

The following protocol is for the production of a single microtube device. A cartoon for the end product is shown in Figure A.1 and a catalog of products required is listed in Table A.1.

1. Preparation of Halloysite Nanotube Solution

1. Sonicate (10-13 W (rms)) 250 μL halloysite nanotube solution (6.6 wt% in water) 30 sec. Cool solution with cold water and repeat sonication once. Cool again.
2. Draw sonicated solution into a syringe, attach a 0.45 μm syringe filter, and filter solution into clean microfuge tube. Vortex the solution occasionally to maintain homogeneity.

2. Coating of Microtube Inner Surface with Halloysite Nanotubes

1. Obtain 50 cm long section of Micro-Renathane microtubing (300 μm inner diameter, 35.3 μL inner volume). Cut one end of the microtube at a diagonal and insert into a small IDEX adaptor piece. Insert the needle of a 3/10 cc 29G syringe into the other end of the microtube.
2. To clean the microtube, place the open end of microtube (the end with the adaptor) into 70% ethanol and draw ~50 μL ethanol into the syringe to fill microtube.
3. Rinse the ethanol out of the microtube by drawing a generous volume of distilled water into the syringe.

4. Detach the syringe from the microtube, empty the syringe, and then reattach to the microtube.
5. Prepare a solution of 0.02% w/v poly-L lysine in water. Draw 50 μL into the microtube and allow to sit for 5 min at room temperature (RT).
6. Draw 100 μL filtered nanotube solution into the microtube and allow to incubate for 3 min at RT.
7. Draw 100 μL water through the microtube to rinse out the nanotube solution. Allow coated microtube to sit, filled with water, overnight at RT.

3. Preparation of Microtubes for Cell Isolation

1. Prepare a solution of 10 μg/mL protein G in 1X Dulbecco's phosphate buffered saline (PBS, pH 7.0 - 7.2). Draw 50 μL PBS through microtube and then draw 50 μL of the protein-G solution and allow to incubate for 1.5 hr at RT.
2. Prepare a solution containing 5 μg/mL E-selectin-IgG and 50 μg/mL antibody (anti-EpCAM for most cancer samples, anti-PSMA for prostate cancer samples) in PBS. Draw 50 μL of the E-selectin and antibody solution into the microtube and allow to incubate for 2 hr at RT.
3. Nonspecific cellular adhesion is blocked with 5% milk protein. Prepare a solution of 5% (w/v) milk protein in PBS. Draw 50 μL milk protein solution into the microtube and allow to incubate for 1 hr at RT.
4. Draw 50 μL PBS into tube and leave at RT until blood or buffy coat samples are ready for processing.
5. 10 min prior to using the microtube for isolation, draw 50 μL PBS that has been saturated with Ca^{2+} ("PBS+") to activate the selectin molecules.

4. Preparation of samples for cell isolation

1. Draw or obtain 10 mL blood from patient into heparinized tube.
2. Place 10 mL Ficoll-Paque lymphocyte isolation solution into 50 mL centrifuge tube. Gently layer 10 mL whole blood on top of Ficoll so as not to mix the blood and Ficoll.
3. Centrifuge at 2000x *g* for 15 min at 4 °C with minimal deceleration.
4. Remove the buffy coat layer and place in new tube.
5. Wash buffy coat with PBS (centrifuge at 230x *g* for 10 min, discard the supernatant).
6. Gently resuspend cells with 1 mL RBC lysis buffer and incubate for 10 min at RT to lyse erythrocytes.
7. Add 10 mL PBS, mix gently, and centrifuge at 230x *g* for 10 min. Discard the supernatant and gently resuspend the pellet in 3 to 4 mL PBS+.

5. Cell isolation

1. Attach one end of the functionalized microtube to a 5 mL syringe using IDEX adaptors.
2. Insert the syringe onto a syringe pump.
3. Submerge the open end of the functionalized microtube into the cell suspension.
4. Process the cell suspension through the microtube at 1 to 4 mL/h.
5. Transfer the open end of the microtube to a tube containing PBS+ and draw 300 µL PBS+ into syringe at 0.016 mL/min to remove unbound and loosely bound cells from the microtube.
6. Place the open end of the microtube into a clean tube. Disconnect the syringe

from the microtube and attach a syringe prefilled with Accutase. Gently perfuse enough Accutase into the microtube to fill (~50 μL) and allow to incubate at RT for 10 min.

7. Attach a syringe prefilled with 1 mL of growth media (79% RPMI, 20% FBS, 1% penicillin streptomycin) and perfuse into microtube, collecting effluent into tissue culture treated well plate.
8. Culture cells at 37 °C and 5% CO_2 under humidified conditions.

6. Expected Results

The goal of this technique is to isolate viable cancer cells from the blood of cancer patients. Several methods exist to identify cancer cells in culture; a necessary verification of device success. We have chosen to stain cells in culture with antibodies against epithelial moieties such as EpCAM (epithelial cellular adhesion molecule) or PSMA (prostate specific membrane antigen), in addition to DAPI to identify intact cell nuclei. The number of cancer cells captured using this technique is necessarily a function of the number of CTCs in the starting sample, and patient variability can be high. In processing samples taken from patients diagnosed with stage IV cancers, we routinely capture between 100 and 500 cancer cells per tube of blood, at purities >40% (Figures A.2 and A.3). Immediately following isolation, greater numbers of contaminating leukocytes may be present. However these numbers will be depleted following incubation in culture medium for up to 5 days.

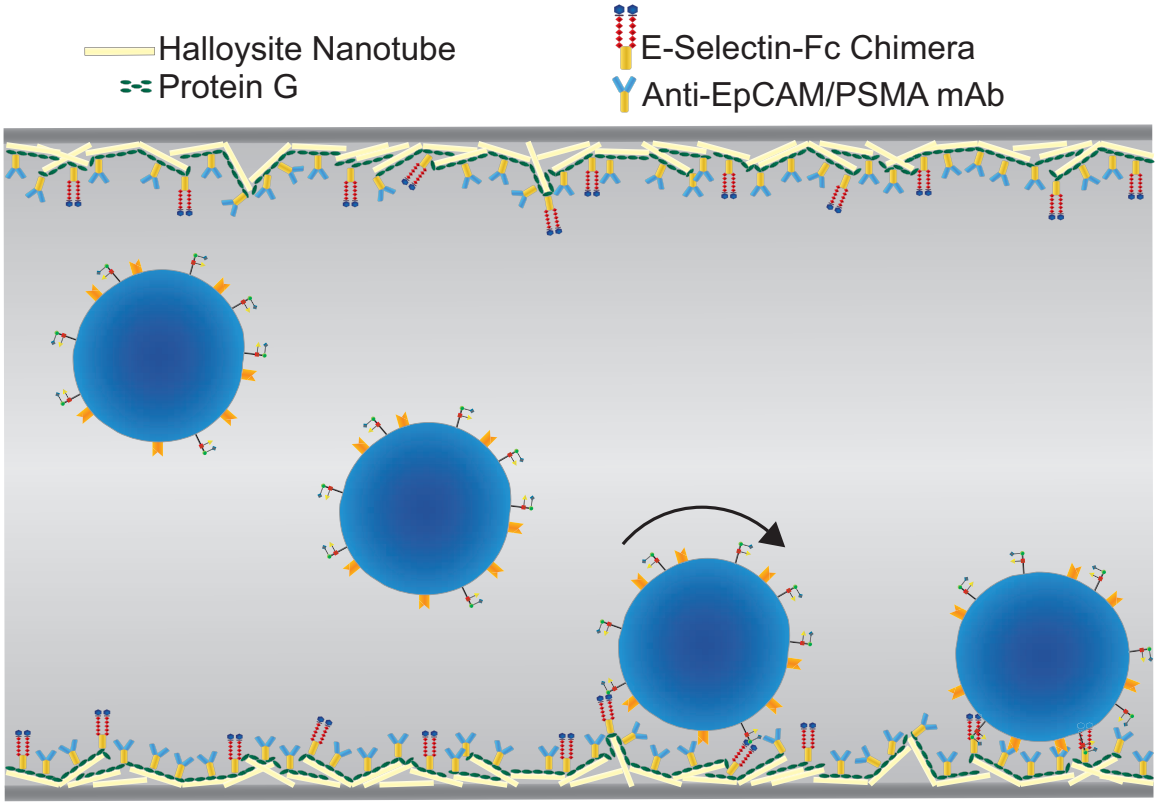

Figure A.1. Schematic of functionalized microtube for CTC isolation, showing a selectin-mediated rolling followed by antibody-mediated static adhesion.

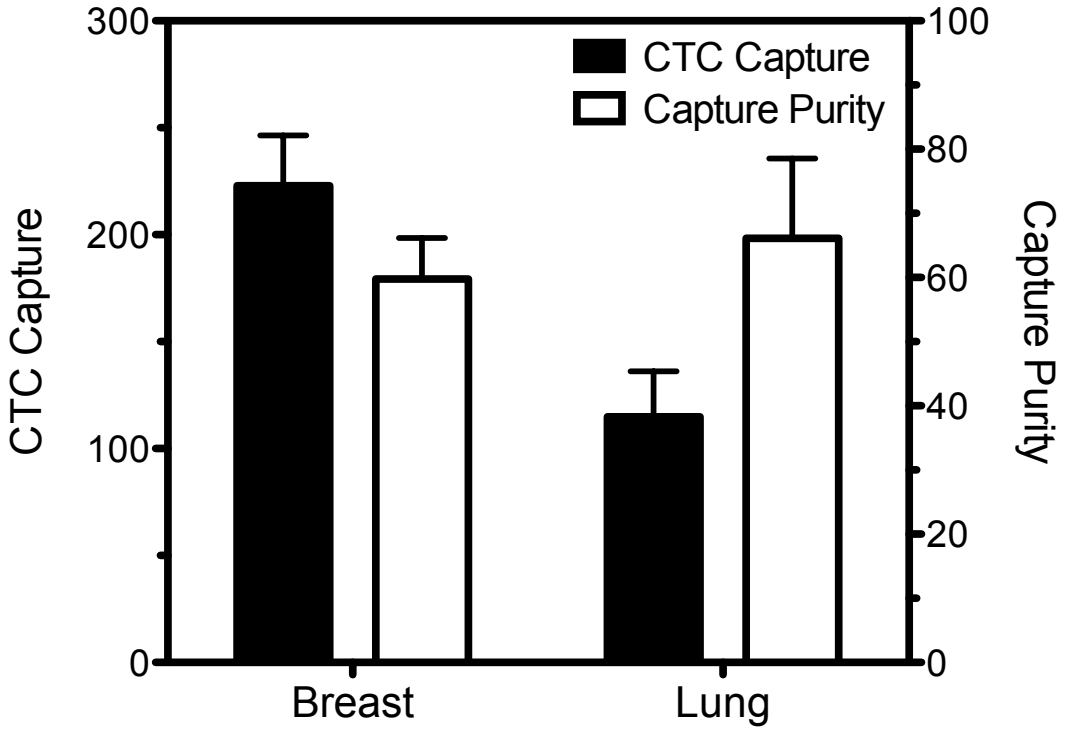

Figure A.2. Representative data of CTC isolation from blood samples drawn from a breast cancer patient and a lung caner patient. The number of viable cells positively identified as CTC based on EpCAM staining is represented by the filled in bars and pertain to the left ordinate and the percentage of cells that were identified as CTC compared to the total number of captured cells is represented by the empty bars and measured on the right ordinate. Results are following five days in culture.

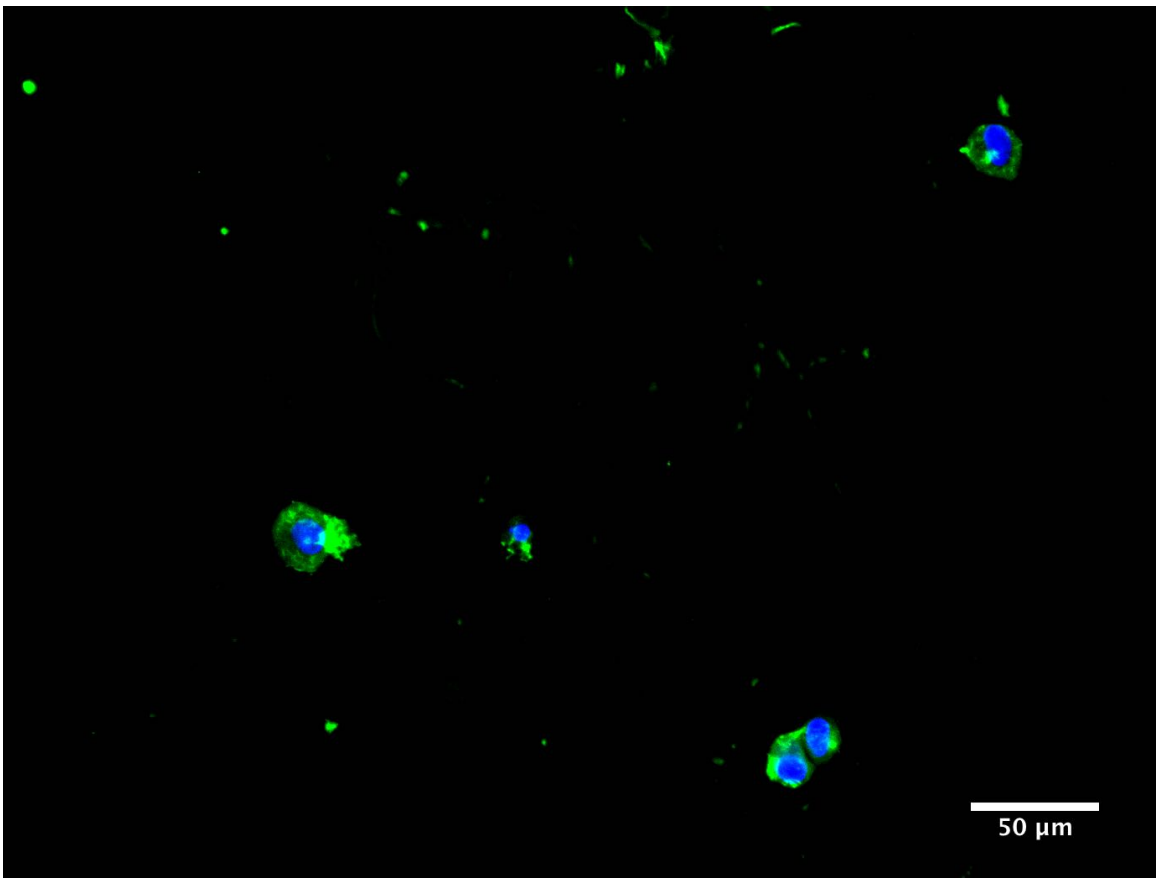

Figure A.3. Micrograph of CTC in culture 5 days subsequent to isolation from a cancer patient blood sample. Cells were stained for EpCAM (green) and DAPI (blue).

Table A.1 Specific reagents and equipment

Reagent	**Company**	**Catalog Number**
300 um ID tubing	Braintree Scientific	MRE025
Larger tubing for connection to syringe	IDEX Health & Science	1507L
5mL syringe for pump	BD	309603
Connector small to large tubing	IDEX Health & Science	P-770
Connector large tubing to syringe	IDEX Health & Science	F-120 and P-659
Syringe for microtube (3/10cc Insulin Syringe U-100 29G 1/2")	BD	309301
Accutase	MP Biomedicals LLC	1000449
Ficol-Paque Plus	GE Healthcare Bio-Sciences AB	17-1440-03
RBC Lysis Buffer (Buffer EL, 1000mL)	Qiagen	1014614
Protein G, 5 mg	CalBiochem (calbiochem.com)	539303
Human EpCAM/TROP-1 Antibody	R&D Systems	MAB960
PSMA Antibody (GCP-04)	abcam	ab66911
96 well plates (Microtest 96)	BD Falcon	35-3072
Blotting Grade Blocker Non-Fat Dry Milk, 300g	Bio-Rad Laboratories	216005508
Halloysite Nanotubes	NaturalNano	NN-HNT200
Calcium Carbonate, 5g	Aldrich Chemistry	481807
rhE-Selectin/Fc Chimera, 100 ug	R&D Systems	724-ES
RPMI Medium 1640	Gibco	22400-089
DPBS	Gibco	14190-095
Fetal Bovine Serum	Atlanta Biochemicals	S11056H
Pennicilin Streptomycin	Sigma Life Siiences	P0781